Characterizing Groundwater Flow Across the Barrier Island-High Marsh Interface

By
Dean M. Wrobel

A Thesis submitted
in Partial Fulfillment of the Requirements for the
Degree of Master of Science in
Coastal Marine and Wetland Studies

Gupta College of Science

Coastal Carolina University

2024

Dr. Richard Viso
Graduate Faculty Advisor, Coastal Carolina Univ.

Dr. Angelos Hannides
Committee Member, Coastal Carolina Univ.

Dr. Bret Jarett
Committee Member, Coastal Carolina Univ.

Dr. Shaowu Bao
Committee Member, Coastal Carolina Univ.

Dr. Zhixiong Shen
Committee Member, Coastal Carolina Univ.

Dr. Zhixiong Shen
MSCI Associate Chair of Graduate Programs

Dr. Chad Leverette
Dean, Gupta College of Science

© Copyright 2024

Dean M. Wrobel

All Rights Reserved

Acknowledgements

I would like to extend my sincere gratitude to Dr. Richard Viso, for his unwavering enthusiasm, support and mentorship throughout this project and my academic journey. He has allowed me to pursue and engage in independent research, contemplation, and at times execution of this project, all the while providing a steady hand of guidance and allowing me to cultivate a skillset that undoubtedly serve me for a lifetime to come. Outside of this study he has provided me countless professional and networking opportunities, allowing me to engage with once in a lifetime scientific opportunities and adventures. It is no understatement that the years I've spent under his counsel have allowed me to grow and develop in ways I would have found incomprehensible upon starting this project. I am certain that I will look back on the past six years with great fondness for the rest of my life, and I owe him my deepest gratitude for that.

I would like to recognize my fiancé Morgan, for her perpetual encouragement, guidance, and seemingly endless time for editorial support and presentation practice. You have been unwavering in your commitment to helping me see this project through and keeping me grounded, words alone cannot express my gratitude to you.

This endeavor would not have been possible without the guidance and expertise of my committee members: Dr. Angelos Hannides, Dr. Shaowu Bao, Dr. Zhixiong Shen, and Dr. Bret Jarrett, who each imparted their own knowledge and wisdom into this study and in doing so allowed me to expand my technical skills and knowledge, thank you.

I would like to thank the Geological Society of America and Coastal Carolina University for providing me the funding to complete this study, in addition to various

peers and scientists who joined me in the field during data collection and helped troubleshoot through technical challenges.

Finally, I would like to recognize my family and friends who provided unique support and perspective to me throughout this project and my two cats, Butters and Noofy who remained literally by my side through the writing of this manuscript.

Abstract

The freshwater resources of barrier islands are influenced by a variety of hydrogeologic factors, which create unique regions of groundwater composition. Factors including evapotranspiration, geologic constraints, tidal forcing, and meteoric inputs influence subterranean flow creating a groundwater salinity gradient throughout the island-marsh setting which directly influences the spatial distribution of dominant vegetation on the island. Rising sea levels and variation in local climate may alter the hydrologic balance on barrier islands, potentially shifting salinity gradients and ecological baselines on short timescales. The intrusion of saltwater into the barrier island freshwater system could result in the shifting of ecotones and potential destabilization of barrier sediments.

Over three years, multiple methods were adopted to characterize the groundwaters of Waties Island, a barrier island located in northeastern South Carolina. Three study transects located on the sound side of the island encompassed the ecological shift between maritime forest and salt marsh. Shallow groundwater monitoring wells were installed along the transects to observe mixing between fresh island-derived groundwaters and more saline groundwaters from the estuary. Water table elevation, temperature, and salinity measurements were recorded at 20-minute intervals over an 11-month period (n = 24,332). Modal analysis of the data revealed tidal and meteorological drivers of groundwater level across the transect. Twenty-nine time-series electrical resistivity (ER) surveys along the transition from forest to marsh revealed horizontal mixing of groundwater within highly permeable sediment layers. Geologic analyses of sediments along the transition elucidated a geologic framework with distinct zones of

permeability bounded by impermeable muddy sediment layers. The primary movement and transport of porewaters from the island into the marsh platform was determined to be horizontal with sandy overwash and erosional fans serving as conduits. No tidal signal influence was observed within the surficial aquifer in the maritime forest, however at the forest-high marsh boundary, precipitation was the principal driver of subterranean flow with spring and storm tides periodically raising the water table and reversing flow towards the island. Within the low marsh, groundwater elevation and flow direction was directly linked to the tidal stage of Dunn Sound.

The results presented here highlight the dynamic nature of shallow hydrogeologic interactions between barrier islands and back barrier environments with implications for shifting ecological baselines, understanding the subterranean estuary of biogeochemical reactions, and determining barrier island stability in an uncertain climatic future.

Table of Contents

Copyright ii

Acknowledgements iii

Abstract v

Table of Contents vii

List of Tables ix

List of Figures x

List of Symbols and Abbreviations xvi

1. Introduction 1

2. Study Goals 6

3. Methods 8

3.1 Study Site 8

3.2 Electrical Resistivity 13

3.3 Monitoring Wells 18

3.4 Water Level Signal Decomposition 22

3.5 Estimations of Darcy Flow 25

3.6 Sediment Description and Analysis 26

4. Results 27

4.1 Geologic Description 27

4.2 Electrical Resistivity 37

4.3 Groundwater Level, Temperature, and Salinity 42

4.4 Groundwater Level Signal Analysis 52

4.5 Cross-Correlation Analysis 62

4.6 Darcy Flow Calculations 66

5. Discussion 69

5.1 Electrical Resistivity 69

5.2 Groundwater Level Signal Analysis 78

5.3 Sediment Analysis and Darcy Flow 86

6. Conclusion 90

7. References 93

List of Tables

Table 1. Locations and elevations groundwater wells. ……... 20

Table 2. Description and hydraulic conductivity of sediment at each well point along transect Z. ……. 29

Table 3. Soil resistivity extrema observed throughout the 29 electrical resistivity surveys. 48-hour precipitation prior to the survey indicates the general saturation of the system before measurement. ……...……. 38

Table 4. Principal harmonic constituents in tidal signals, adapted from Chen et al. 2013. ……..……. 53

Table 5. eIMF periodicity, frequencies, and variance ratios from EEMD analysis on well LM water table elevation. ……..…….. 54

Table 6. eIMF periodicity, frequencies, and variance ratios from EEMD analysis on well HM water table elevation. ……..….. 55

Table 7. eIMF periodicity, frequencies, and variance ratios from EEMD analysis on water table elevation subset 1 from the MF well. ……..…….. 56

Table 8. eIMF periodicity, frequencies, and variance ratios from EEMD analysis on water table elevation subset 2 from the MF well. ……...……. 57

Table 9. Water samples of various salinity and representative electrical resistance at 25°C. Table adapted from Wiater 2012. …….. 72

Table 10. Frequency and description of rainfall events from Sunset Beach, NC. …..… 80

Table 11. Comparison of calculated groundwater fluxes from regional sites. …… 88

List of Figures

Figure 1. Conceptual model of barrier island hydrogeologic components where groundwaters are confined by mud and silt aquitards. Single arrows represent freshwater inputs into the system through precipitation and groundwater from the mainland, double arrows represent exchange and mixing interfaces at estuarine and ocean boundaries. …. 5

Figure 2. Waties Island, South Carolina is typical of tidally dominated barrier islands of the southeastern United States and supports an extensive salt marsh complex with a diversity of ecotones. ……...… 10

Figure 3. A) Orthoimage of Waties Island. B) Aerial Topo-Bathy LiDAR-derived elevation of Waties Island and surrounding waters. Island elevation maxima is located near the center of the maritime forest, reaching heights of 8.41 meters atop a relic dune field. ……. 11

Figure 4. A) Orthoimage of the study site, transect termini are denoted with a prime symbol, groundwater well locations are marked with a red ‘x’, and vibracore locations are marked with a white circle. B) Aerial LiDAR-derived elevation of the study site, a ridge of maritime forest sediment marks the transition from high marsh to forest. …… 12

Figure 5. Diagram of an electrical resistivity survey to collect data in a dipole-dipole array. The degree and depth for which apparent resistivity can be resolved is a function of electrode spacing. ……. 15

Figure 6. Cross section schematic of transects X and Y. Transect X resolved apparent resistivity to a depth of 26 meters while transect Y resolved to a depth of 4 meters. …. 16

Figure 7. Cross section schematic of Transect Z, the ER survey centered on the well HM, where significant mixing and change in soil resistivity were expected. Data was resolved to a depth of 4 meters. ……..... 17

Figure 8. Comparison of the raw signal recorded by the level logger in well LM (blue) with the atmospheric pressure corrected signal (solid black) and the atmospheric pressure from NOAA Springmaid pier station (dashed black). ……. 21

Figure 9. A visual example of EEMD signal decomposition. A) A simple two-function signal represents the original signal. B) Repeated decomposition of the original signal yields oscillatory components or intrinsic mode function. …….. 24

Figure 10. Geologic cross-sectional diagram of transect Y. Surface derived from topo-bathy LiDAR elevation. ……...… 30

Figure 11. Geologic cross-sectional diagram of transect Z and wells LM and MF. Surface derived from topo-bathy LiDAR elevation. ……...……. 31

Figure 12. Geologic description and sedimentary analysis of core C1, taken from the low marsh. ……..….. 32

Figure 13. Geologic description and sedimentary analysis of core C2, taken from the low marsh, high marsh transition. ……...…… 33

Figure 14. Geologic description and sedimentary analysis of core C3, taken adjacent to well HM. ……..……. 34

Figure 15. Geologic description and sedimentary analysis of core C4, taken adjacent to well MF. ……...…… 35

Figure 16. Geologic description and sedimentary analysis of core C5, taken from the high marsh adjacent to the nested wells series. …… 36

Figure 17. ER tomograms from transect X, Waties Island's headlands are towards the right of each tomogram while Dunn Sound is towards the left. …….. 39

Figure 18. ER tomograms from transect Y, Waties Island's headlands are towards the right of each tomogram while Dunn Sound is towards the left. ……..… 40

Figure 19. ER tomograms from transect Z, Waties Island's headlands are towards the right of each tomogram while Dunn Sound is towards the left. …….……. 41

Figure 20. Groundwater level, temperature, and salinity from well LM, water table elevations are tightly coupled with tidal fluctuations. …….…… 44

Figure 21. Groundwater level, temperature, and salinity from well HM, water table elevations are driven primarily by major precipitation events and periodically by spring tides. ……. 45

Figure 22. Groundwater level, temperature, and salinity from well MF, water table elevations reflect recharge from precipitation events. ……...…….. 46

Figure 23. Boxplots of groundwater salinity and temperature observed in study wells. Whiskers represent data extents three standard deviations from the median. …...…….. 47

Figure 24. Tide predictions at Dunn Sound West, station 8660195, derived from water levels at the NOAA Springmaid Pier station 8661070 by applying high-low offsets and time corrections. Mean tidal range is 1.53 meters. ……..…… 48

Figure 25. Daily precipitation totals from CoCoRaHS station US1NCBR0006, Sunset Beach. Local station precipitation totals verified against daily precipitation data from NOAA Springmaid Pier station and NWS North Myrtle Beach Airport station. Major meteorological events are highlighted. ……..…….. 49

Figure 26. Daily precipitation totals from Sunset Beach. Dates of ER surveys are indicated with vertical red lines. ……. 50

Figure 27. Sunset Beach, NC daily precipitation totals and atmospheric pressure from Springmaid Pier, SC. Major meteorological events corresponding with high precipitation totals are well correlated with drops in barometric pressure. ……..…… 51

Figure 28. Water table elevation and eIMFs from the low marsh, well LM. …...…….. 58

Figure 29. Water table elevation and eIMFs from the high marsh, well HM. ……...…. 59

Figure 30. Water table elevation and eIMFs from the maritime forest, well MF, subset 1. …….…….. 60

Figure 31. Water table elevation and eIMFs from the maritime forest, well MF, subset 2. ……..…….. 61

Figure 32. Cross correlation of Dunn Sound West tides and daily precipitation with low marsh groundwater level. ……...…….. 63

Figure 33. Cross correlation of Dunn Sound West tides and daily precipitation with high marsh groundwater level. ……. 64

Figure 34. Cross correlation of Dunn Sound West tides and daily precipitation with maritime forest groundwater level. …….……. 65

Figure 35. Calculated groundwater flow between wells MF and HM. Large precipitation enhanced the transport of waters off the island, while spring tides and storm tides reversed transport, pushing salt marsh porewaters towards the island. …….…….. 67

Figure 36. Calculated groundwater flow between wells LM and HM. Precipitation exerted less influence on groundwater transport between wells. Frequent excursions of

flow rates to negative values indicate the tidal nature of transport between these wells. ……..….. 68

Figure 37. ER tomogram from transect Y with nested well series and core C5 imposed to show relative depths. ……..…….. 73

Figure 38. ER tomogram from transect Z with well HM and core C3 imposed to show relative depths. ……...…….. 74

Figure 39. Timeseries comparison of average electrical resistance across all ER surveys with precipitation totals from Sunset Beach, NC 48 hours prior to surveying date. …... 75

Figure 40. Linear regression results between precipitation, average survey resisitivty, and observed groundwater salinity on transects X and Y. …….……. 76

Figure 41. Linear regression results of average tomogram resistivity and precipitation totals from Sunset Beach, NC 48 hours prior to survey date. Results indicate the saturation of back barrier sediments is not resolvable by comparing soil resistance. …. 77

Figure 42. Water table elevation in wells LM, HM, MF, and water levels in Dunn Sound West. Correlation with tidal water level decreases with increasing distance from the sound. …….…….. 81

Figure 43. Water table elevation in wells LM, HM, MF, and daily precipitation totals from Sunset Beach, NC. Major precipitation events were observed as pulses in water table elevation throughout each well. …….. 82

Figure 44. Groundwater salinity in wells LM, HM, MF and Sunset Beach, NC daily precipitation totals. ……..……. 83

Figure 45. Linear regression models of groundwater level and salinity within each well located along transect Z. Rows containing missing values from either level or salinity

were removed prior to analysis. The line of best fit is indicated in red and the Pearson correlation coefficient R is listed in each figure. ……...…….. 84

Figure 46. Recorded groundwater parameters following Hurricane Idalia, which passed approximately 25 nautical miles southeast of Waties Island, SC as a tropical storm on August 30th, 2023. ……...……. 85

Figure 47. Comparison of groundwater flow rates within and between estuarine and upland systems. Markers represent average values or reported value of study, whiskers indicate total reported range. …… 89

List of Symbols and Abbreviations

A	Two-Dimensional Area of Well Screen
ASTM	American Society for Testing and Materials
dH	Difference in Water Table Elevation Between Measurements
dL	Horizontal Distance Between Well Locations
EEMD	Ensemble Empirical Mode Decomposition
eIMF	Ensemble Intrinsic Mode Function
EMD	Empirical Mode Decomposition
ER	Electrical Resistivity
ERT	Electrical Resistivity Tomography
g	Gravitational Constant
GRADISTAT	Program developed for analysis of laser grain size output
GDP	Gross Domestic Product
K	Hydraulic Conductivity
k	Permeability
L2	Euclidean Normalization Statistic
n	Sample Size
NAVD88	North American Vertical Datum of 1988

NOAA	National Oceanic and Atmospheric Administration
ρ	Fluid Density
PVC	Polyvinyl Chloride
Q	Volumetric Flow
μ	Specific Viscosity
YSI	Yellow Springs Instruments

1. Introduction

The coastal margins of the United States are regions of immense natural resource and dense population. Approximately 40.7% of total U.S. GDP is derived from coastal counties in addition to housing 128 million Americans in cities adjacent to the coast (NOAA 2013). Estuarine ecosystems span the boundary between land and sea and support societal and economic interests, serving as transportation routes, pollution sinks, water resources, and pillars of regional culture and identity. As land usage within estuarine watersheds shifts and becomes increasingly urban, the demand for coastal resources and ecosystem services continues to grow.

Faced with the pressures of increasing utilization and extraction, coastal ecosystems have become more susceptible to stressors associated with climate change. Rising sea levels, tropical and extra-tropical storms of changing frequency and intensity are ushering in a new hydrologic regime at the coast, threatening coastal environments and resources such as barrier islands and coastal aquifers. The severity and large spatial impact of these events have the potential to rapidly shift ecological baselines in coastal environments on short timescales. Barrier island systems along the southeastern Atlantic coast of the United States are highly susceptible to these ecological shifts due to their delicate hydrogeologic balance.

The dynamic hydrogeologic cycle on barrier islands represents a multitude of factors which affect subsurface flow, as seen in a simplified model of barrier island

hydrogeology (Figure 1). Unconfined porewaters near the surface comprise a freshwater lens containing a salinity gradient ranging from low salinity freshwaters to brackish-estuarine, and full salinity seawater. Shallow transport is largely lateral through sandy sediment layers separated by aquitards of low permeability soils, with larger, regional-scale aquifers below.

Processes controlling groundwater flow at a given barrier island vary greatly due to the geologic setting, tidal range, local meteorology, ecology, and anthropogenic modification. Regional freshwater aquifers in the coastal environment have garnered research interest due to their importance to coastal communities as a utility resource and their susceptibility to saltwater intrusion after significant withdrawal (Anderson, 2002; Payne, 2010). Shallow freshwater lens systems have been recognized as an important vector for nutrient transport and exchange between porewaters of the salt marsh and surface waters of the surrounding estuary and coastal ocean (Valiela et al. 1978; Howes and Goehringer 1994; Seffereth et al. 2020). Analyzing the local drivers of groundwater flow through the barrier provides insight into how salt marsh and estuarine nutrient budgets interact.

The highly permeable sands associated with dune complexes have been implicated as the primary recharge zones of the freshwater lens, where dune field characteristics such as elevation and area define the spatial extent of the freshwater lens (Holt et al. 2019). Once meteoric waters enter the freshwater lens, they acquire unique chemical profiles, traversing ecotones with extensive biogeochemical activity such as salt marshes, freshwater swales, and maritime forests.

The freshwater lens on a barrier island exists between tidal bodies of water which impact horizontal groundwater flow, often reversing the hydraulic gradient during high tides. Tidal forcing is a major component controlling groundwater flow and mixing within the low marsh platform (Ledoux et al. 2013). Local variations in sea level due to storm surge and wave setup can amplify tidal forcing and mixing of waters surrounding the freshwater lens (Anderson, 2002; Wilson et al., 2011; Housego et al., 2021). The major freshwater input in the hydrologic balance is from precipitation. Evapotranspiration, varying with ecotone, removes a significant portion of freshwaters within the vadose zone (Gardner and Reeves, 2002; Ursino et al., 2004; Moffett et al., 2012; Wilson et al., 2015).

The unique geomorphology of barrier island systems directly affects subterranean flow with small-scale changes in stratigraphy resulting in distinct layers of varying porosity and permeability. Sandy deposits, typical of tempestites, and overwash fans act as conduits for groundwaters to flow through the surrounding less porous, muddy matrix. (Moore, 1990; Gardner, 2007). The interlayering of sediments within the marsh platform creates specific regions of porosity and permeability resulting in heterogenous porewater mixing and transport. Spatial variability in porewater composition is reflected at the surface through ecozonation (Pennings et al., 2004; Crain et al., 2004; Moffett et al., 2012).

Characterizing how groundwaters flow within barrier island systems is essential to understanding how hydrogeologic shifts will affect barrier islands. Sea level rise and meteorological events such as hurricanes and extratropical storms may drastically alter barrier island environments on short time scales by shifting the freshwater–saltwater

mixing interface in both surface and groundwaters. Recognizing the governing capacity that groundwater composition and abundance exert on the stability of barrier island environments is key to ensuring the future resiliency of these systems so that their ecological and societal value remains.

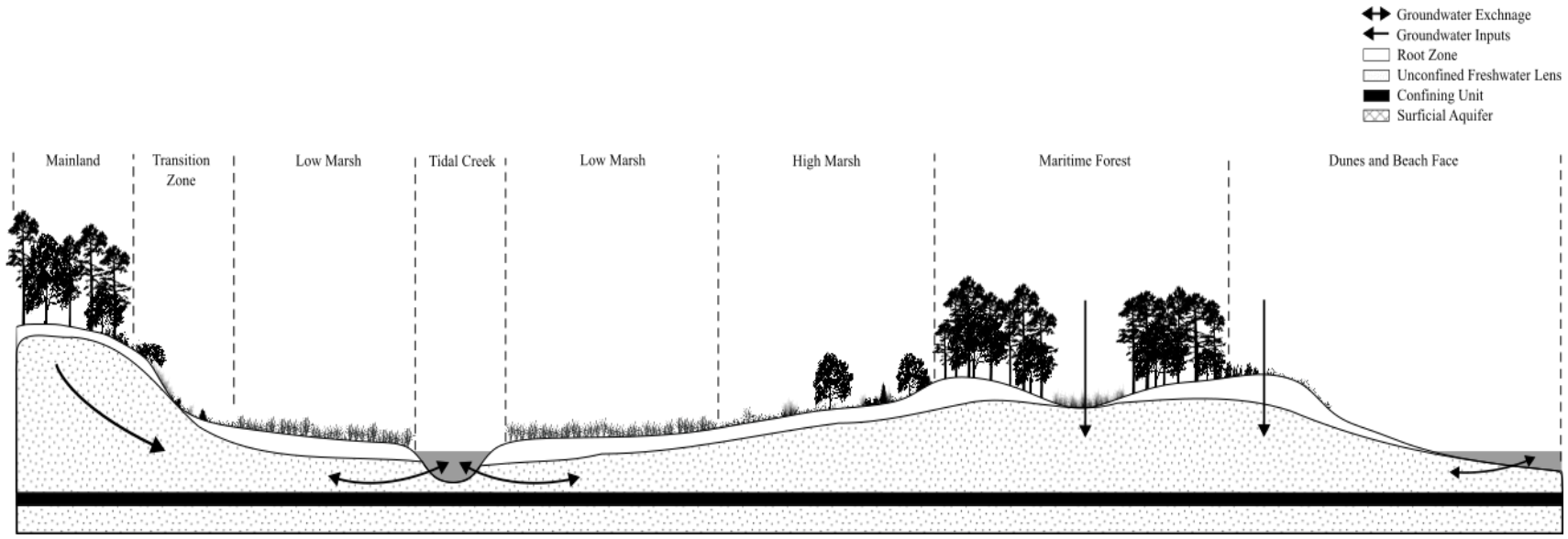


Figure 1. Conceptual model of barrier island hydrogeologic components where groundwaters are confined by mud and silt aquitards. Single arrows represent freshwater inputs into the system through precipitation and groundwater from the mainland, double arrows represent exchange and mixing interfaces at estuarine and ocean boundaries.

2. Study Goals

Recent research on porewater mixing and transport within the unconfined freshwater lens on barrier islands has focused on model-based approaches (Xin et al., 2022; Holt et al., 2019). This method is ideal for describing flow through time, predicting how hydrologic events will impact the system, and for extrapolating results from field experiments. However, the parameterization requirements of model-based approaches struggle to incorporate nuances in formation geology, anthropogenic modification, and study site geography. Identifying and quantifying these site-specific variables is critical to improving modeling efforts and creating system-specific predictions for groundwater abundance and salinity into the future.

This project seeks to identify detailed hydrogeologic variability in a salt marsh – barrier island system. In addition, the viability of coupling traditional hydrogeologic field methods with a geophysical imaging approach as techniques to better characterize porewater mixing through time is explored. By resolving fine-scale geologic changes and the resulting effect on groundwater flow, the boundaries and mixing zones of porewaters can be better understood in a manner that reflects the reality of these dynamic environments. We postulate that with high-resolution geologic analyses, time-series electrical resistivity surveys, and statistical decomposition of water table elevation time-series data, the factors that influence groundwater flow and mixing across this transition can be better understood. The major objectives of this study are as follows:

Objective 1. Utilize time-series electrical resistivity surveys to spatially characterize the contribution of pore water salinity to the resistivity of shallow sediments present along the barrier island-salt marsh interface.

Objective 2. Apply signal decomposition techniques to water table time-series data from monitoring wells to evaluate and quantify the local drivers of subterranean flow.

Objective 3. Describe the hydraulic properties of sediment along the maritime forest–salt marsh transition, including grain size, permeability, and stratigraphy to support the interpretation of electrical resistivity tomograms.

Objective 4. Utilize hydrogeologic data to estimate groundwater flow between the barrier island and salt marsh using Darcy's Law.

Objective 5. Describe the local geology and structure of the surficial aquifer along the study site at Waties Island.

3. Methods

3.1 Study Site

Waties Island is an undeveloped barrier island in Long Bay, located in northeastern South Carolina. Bound by tidal inlets to the northeast and southwest, the island supports a back barrier salt marsh system known as Dunn Sound (Figure 2). Northeast of the island, barriers are similar in character to Waties, punctuated by inlets on each end and supporting a narrow back barrier marsh system. Southwest, an approximately 30-mile expanse of coastline is interrupted only by small swashes on the beach face, absent of large barriers.

Waties Island is a Holocene feature consisting of sands from relic dunes and beach ridges (Figure 3). Elevation maxima on the island exist on the modern beach ridge and a relic dune field in the maritime forest on the northeast of the island. Waters from the Atlantic Intracoastal Waterway, Atlantic Ocean, Calabash River and Little River mix to form saline to brackish conditions within Dunn Sound. The average tidal range is 1.7 meters. The island contains a diversity of ecological environments including maritime forest, interdunal swale, saltpans, low and high elevation salt marshes and intra marsh hammocks (Luken 2012).

Three transects on the sound side of the island extend from maritime forest and high marsh into the low marsh (Figure 4). Transects X and Y are co-located originating at the base of an access road in the high marsh and extend into the salt marsh 108 meters

and 16.8 meters northwest, respectively. Transect Z originates within the maritime forest and extends 120 meters northwest, terminating in the low marsh.

The geologic setting of the site is similar to barrier-marsh complexes in the region (Riggs et al. 1995; Gardner and Porter 2000). The upper sediments of the maritime forest are sandy with a surficial mat of organic material. The high marsh is composed of sands similar to those found on the barrier's mainland, with various amounts of silts and muds incorporated from salt marsh sediment trapping. Low marsh surficial sediments are characterized by increased fines resulting in muddy sands and silts. Sandy mud and clays underly the low and high marsh sediments with intercalated sands consistent with overwash fan and tempestite deposition.

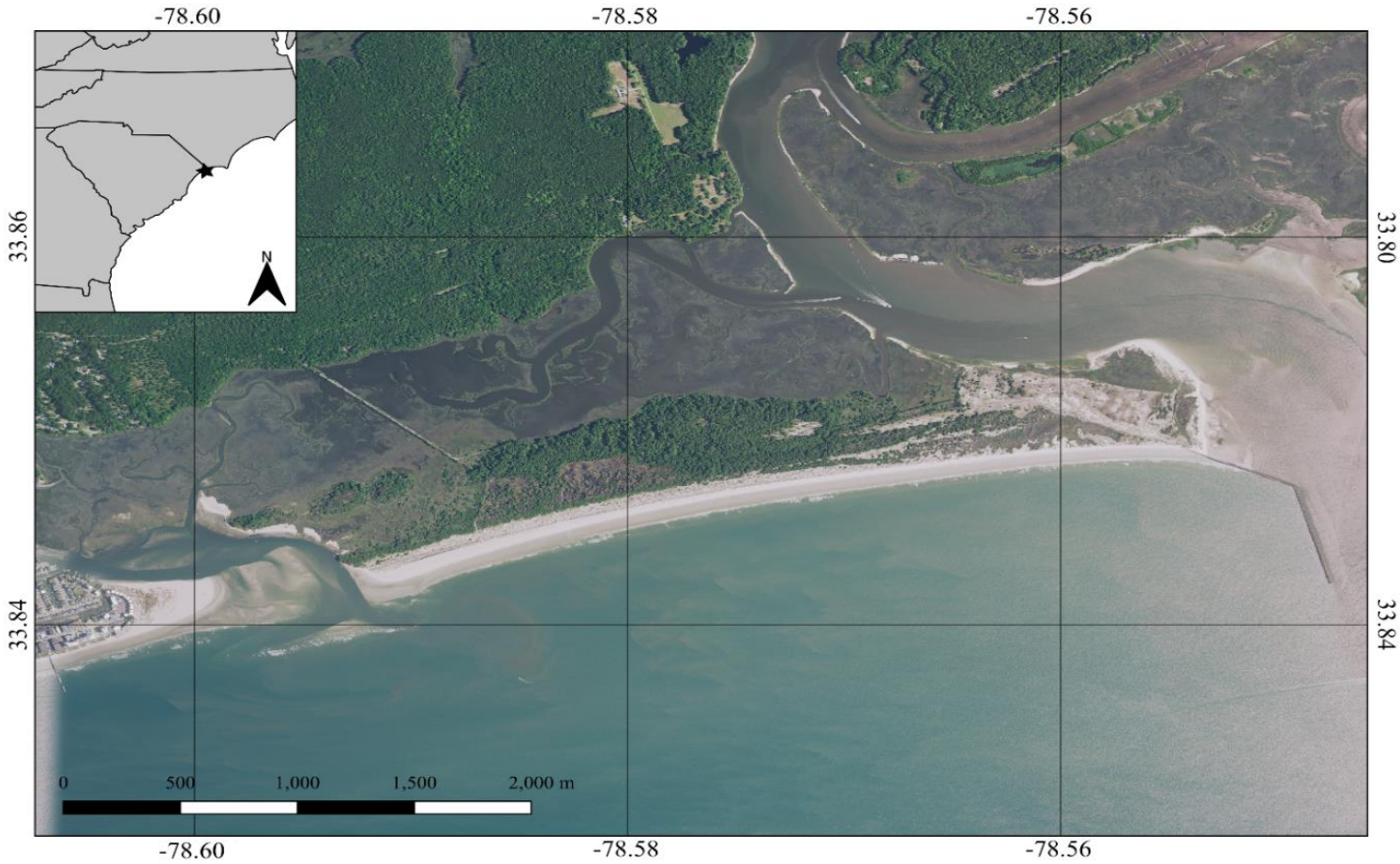


Figure 2. Waties Island, South Carolina is typical of tidally dominated barrier islands of the southeastern United States and supports an extensive salt marsh complex with a diversity of ecotones.

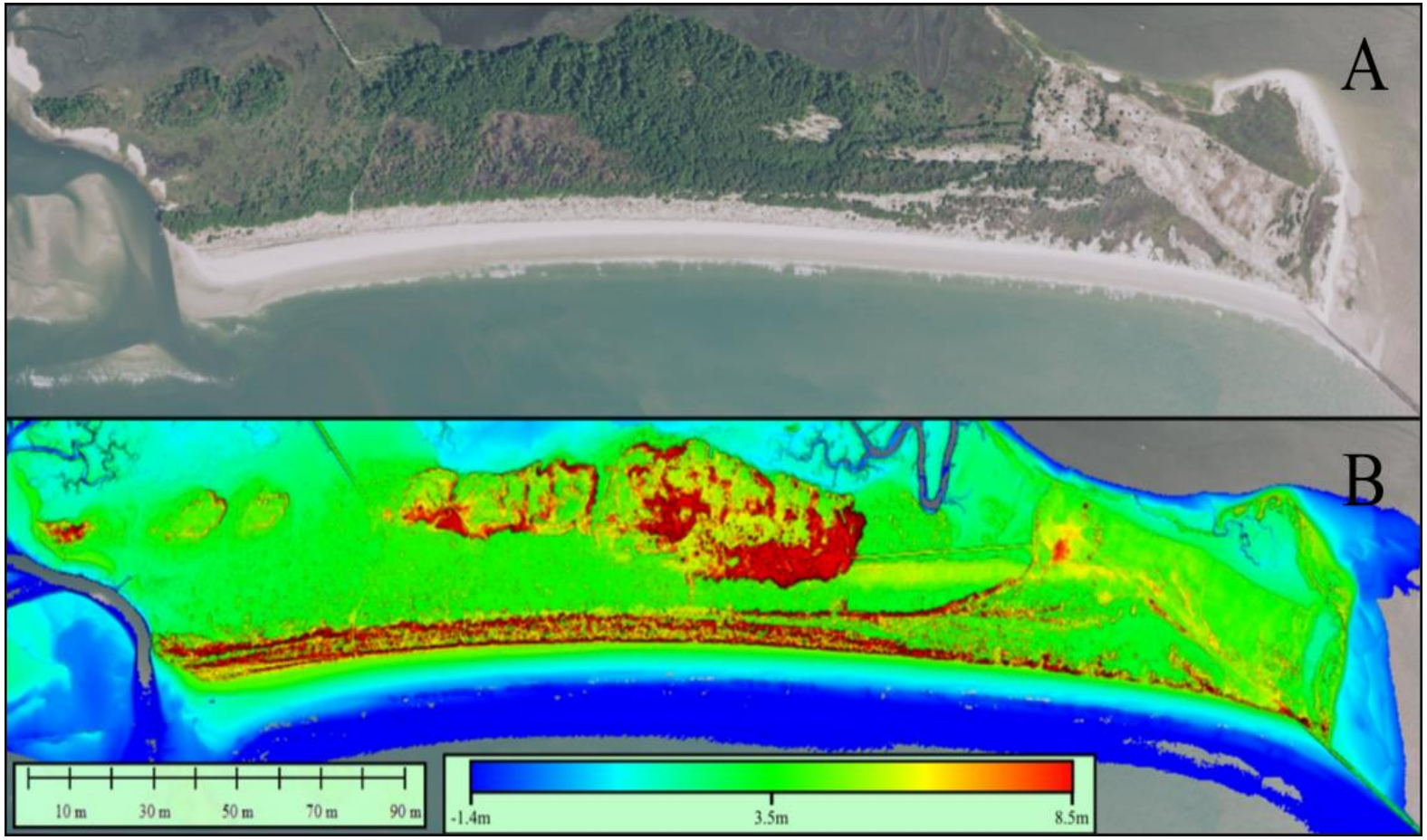


Figure 3. A) Orthoimage of Waties Island. B) Aerial Topo-Bathy LiDAR-derived elevation of Waties Island and surrounding waters. Island elevation maxima is located near the center of the maritime forest, reaching heights of 8.41 meters atop a relic dune field.

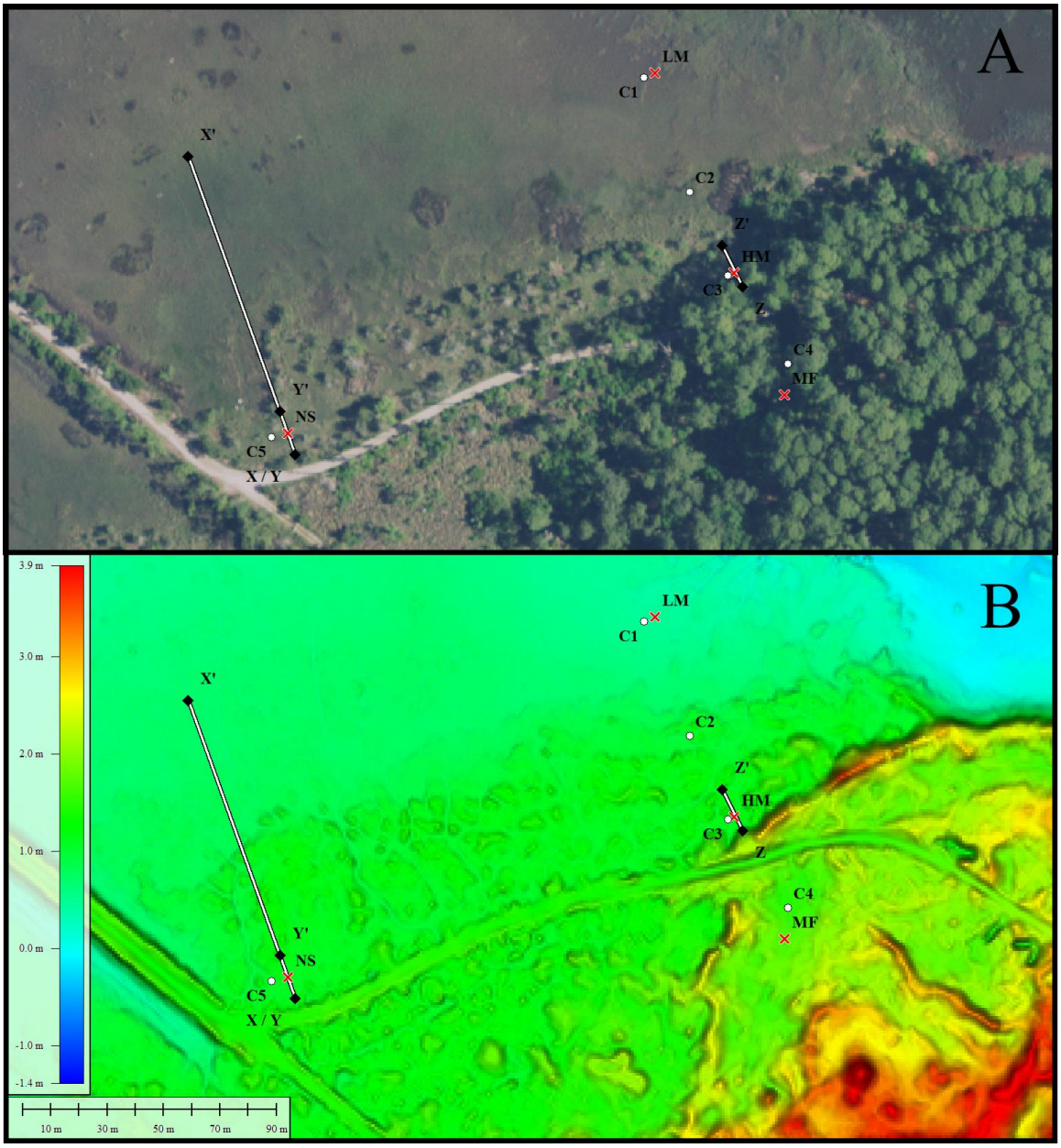


Figure 4. A) Orthoimage of the study site, transect termini are denoted with a prime symbol, groundwater well locations are marked with a red 'x', and vibracore locations are marked with a white circle. B) Aerial LiDAR-derived elevation of the study site, a ridge of maritime forest sediment marks the transition from high marsh to forest**.**

3.2 Electrical Resistivity

Electrical resistivity (ER) is a geophysical method which determines the resistive properties of bulk earth materials along a transect line. An array of electrodes placed into the soil receive an electric current. The current travels through the soil, which acts as a resistor. The ER instrumentation measures the electrical potential drop between electrode pairs of varying offset distances. As the offset distance of electrode pairs changes, a matrix of apparent resistivities beneath the transect line is created, with increasing distance resulting in deeper measurements (Figure 5). Full penetration depth is approximately one-third of the horizontal array length. The electrical resistivity of marsh sediments varies with groundwater salinity and geologic characteristics, such as porosity, sediment texture, and percent organic material (Griffiths and Barker, 1993; Carter et al., 2008). Interpretation of individual ER surveys from salt marsh environments is difficult due to the multitude of factors creating the observed signal. However, time-series surveys along fixed transect lines allow for interpretation of the signal as a result of varying porewater salinity since a constant geology through time can be assumed.

The resistivity array consists of a SuperSting R8 resistivity meter (Advanced Geosciences, Inc, Austin Texas) with a 56 passive electrode array built into a cable. ER surveys along transects X and Y were co-located, with electrode spacing of 2 and 0.3 meters, respectively. Co-location allowed for imaging the subsurface at shallower, higher resolution in transect Y and at a deeper but coarser resolution along transect X (Figure 6). Electrodes were spaced at 0.3 meters along transect Z, which was conducted directly adjacent to well HM to obtain the highest resolution image of groundwaters (Figure 7).

Apparent resistivity data were processed using Earth Imager 2D (Advanced Geosciences, Inc, Austin Texas) inversion software. A forward finite difference modeling method generated a color-contoured resistivity cross-section that can be interpreted within known geological and hydrological constraints. Root-mean-square and L2 statistics assessed the goodness of fit between actual data and pseudo-data generated from the resistivity model. The model was adjusted until the best statistical fit was achieved. The resistivity section was then adjusted to a standard color palette for comparison to other surveys and a terrain file of the survey transect applied. Low confidence regions at the edges of the tomogram were excluded, resulting in a trapezoidal shape. Eleven ER surveys were conducted between April 2021 and January 2022 on transects X and Y, and eight surveys were recorded on transect Z between August 2023 and March 2024.

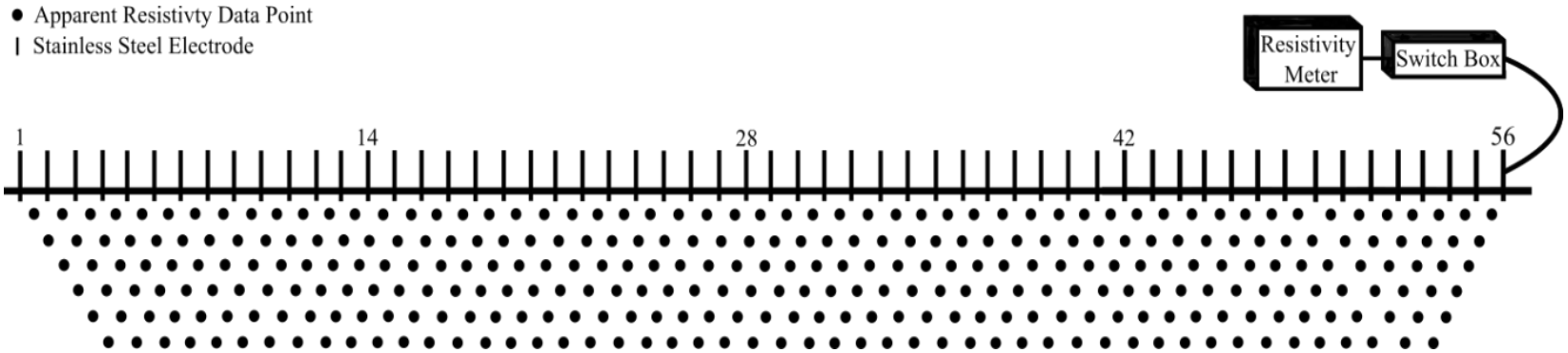


Figure 5. Diagram of an electrical resistivity survey to collect data in a dipole-dipole array. The degree and depth for which apparent resistivity can be resolved is a function of electrode spacing.

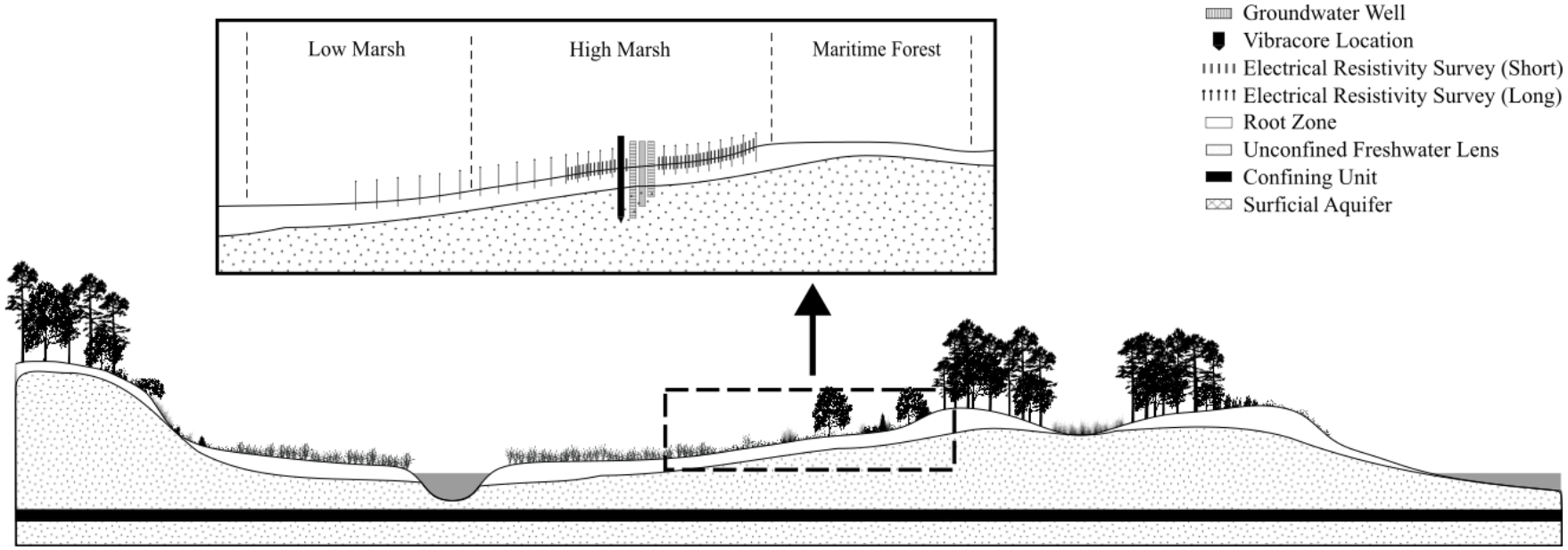


Figure 6. Cross section schematic of transects X and Y. Transect X resolved apparent resistivity to a depth of 26 meters while transect Y resolved to a depth of 4 meters.

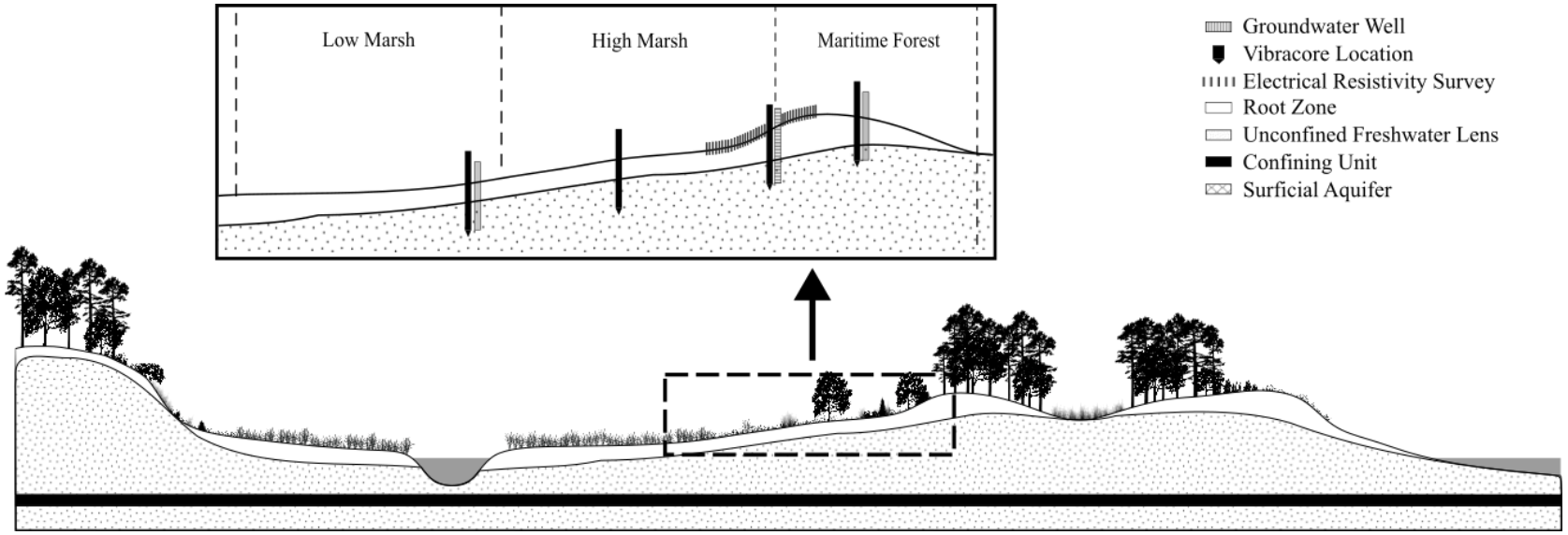


Figure 7. Cross section schematic of Transect Z, the ER survey centered on the well HM, where significant mixing and change in soil resistivity were expected. Data was resolved to a depth of 4 meters.

3.3 Monitoring Wells

Three nested groundwater wells (NS) were installed at the center of transect Y (Figure 4). Each well was constructed of 2-inch diameter schedule 40 PVC pipe with variable length, terminating in a 2.5-inch screened interval. Installation included manual excavation until surrounding sediment showed sign of collapse upon which a temporary 6-inch diameter PVC well casing was inserted. Excavation continued by hand auger until the water table was reached. The well point was then inserted into the hole and backfilled with local dune sand until the screened interval was covered on all sides. The temporary casing was then removed, allowing the sediment to collapse and infill the excavation. The nested wells reached depths of 0.75 (NS 0.75), 1.2 (NS 1.2), and 2 meters (NS 2) depth at the bottom of the screened interval. Peristaltic pumps were used to clear the well volume of stratified fluid and allow for recharge prior to monthly sampling using a handheld YSI (YSI Inc., Yellow Springs, Ohio).

Similarly, three wells were installed along transect Z within maritime forest (MF), high marsh (HM), and low marsh (LM) regions (Figure 4). Wells were constructed of 2-inch diameter schedule 40 PVC pipe with a 4-inch screened interval at the terminus of the well. Well depths reached 74.68, 40.31, and -22.93 centimeters relative to NAVD88 in wells MF, HM, and LM respectively. Solinst LTC 5 (Solinst Canada, Georgetown, Ontario) leveloggers were installed in each well to record conductivity, temperature, and water level data. Leveloggers were retrieved monthly for data download and to clear any biofouling. Prior to redeployment, well fluid was purged by peristaltic pump and resampled with a YSI instrument to ensure quality control of datalogger measurements and to mitigate the influence of well volume stratification. Throughout all well

installations well recharge after pumping was rapid, in low and high marsh sites, recharge of well fluid outpaced pumping rates of 375 milliliters per minute.

Temperature, specific conductivity, and pressure were recorded in wells HM, LM, and MF at 20-minute intervals over a 338-day duration to detect seasonal and tidal variations in groundwater properties. The effect of atmospheric pressure was removed by subtracting atmospheric pressure measurements taken from NOAA station 8661070 (Springmaid Pier, SC), from the total recorded pressure at the leveloggers within each well (Figure 8). The resulting total water column pressure was converted to the length of the water column above the sensor using Equation 1, then used to calculate the elevation of the water table surface relative to the NAVD88 datum.

$$Elevation\ (cm) = (Raw\ Pressure\ from\ Levelogger\ (mbar) - Barometric\ Pressure\ (mbar))\ x\ \frac{0.0101972\ (m)}{(1\ mbar)}\ x\ 0.01\ (m) \quad 1)$$

Data were preprocessed by filtering outliers beyond 3 standard deviations along a moving block average of 300 measurements. Groundwater level signals were then decomposed, as described in section 3.5, to further resolve hydrological drivers. Specific conductivity was converted to salinity (parts per thousand), using Equation 2.

$$Salinity\ (ppt) = 0.0080\ x\ Conductivity_{35}\ \ (mS\ cm^{-1}) - 0.1692 \quad 2)$$

Cross-correlation analyses between water table elevations, water level in Dunn sound, and daily precipitation assessed the lag time for hydrologic events to reach each well.

Table 1. Locations and elevations groundwater wells.

Well Name	Surface Elevation (m)	Instrument Elevation (m)	Well Point Elevation (m)	Latitude	Longitude
LM	0.48	-0.16	-0.21	33.849722	78.586389
HM	1.139	0.49	0.40	33.849167	78.585833
MF	1.521	0.96	0.51	33.848889	78.58556
NS – 0.8	1.058	-	0.26	33.848758	78.587653
NS – 1.2	1.058	-	-0.14	33.848758	78.587653
NS - 2	1.058	-	-0.94	33.848758	78.587653

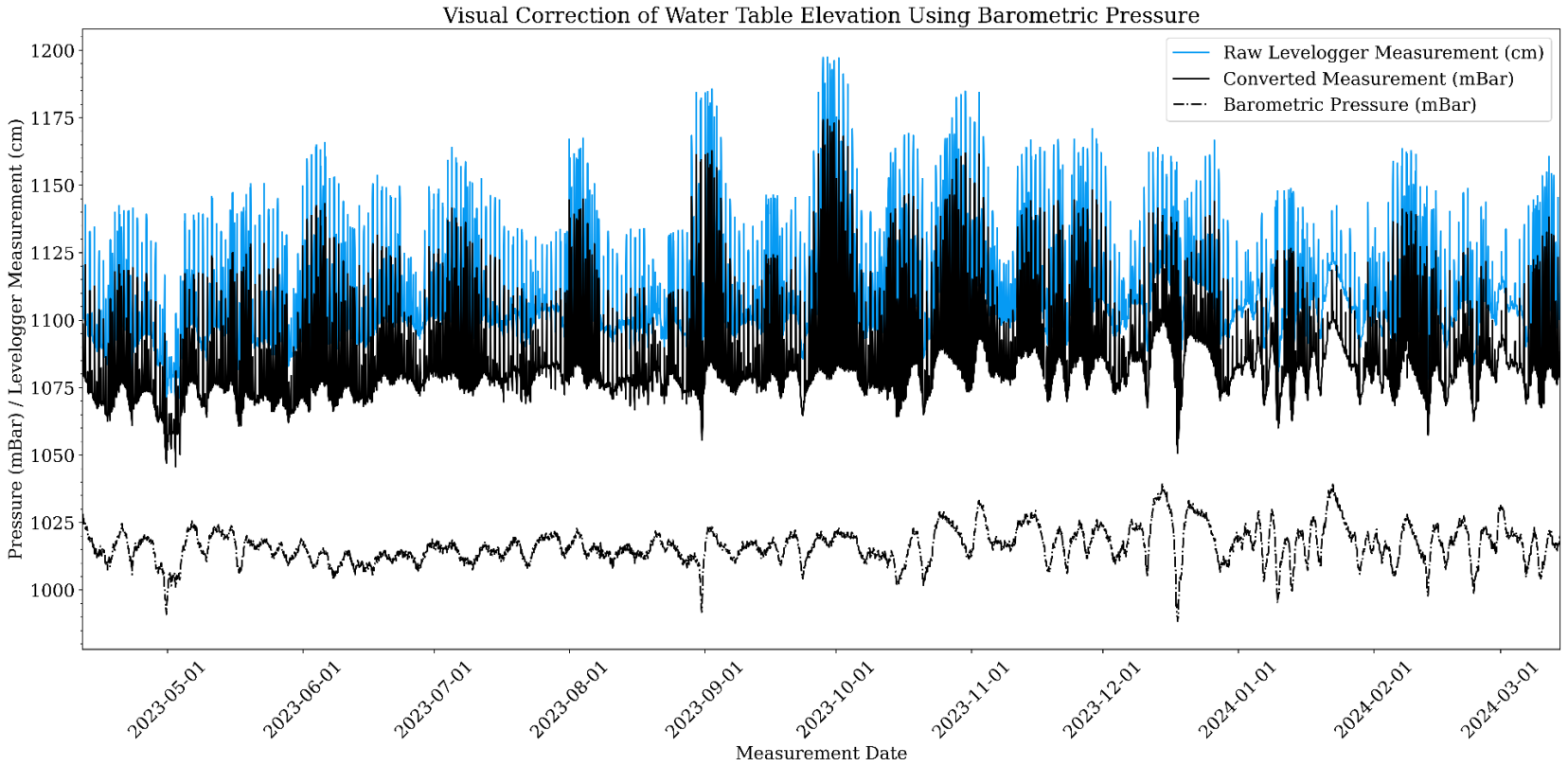


Figure 8. Comparison of the raw signal recorded by the level logger in well LM (blue) with the atmospheric pressure corrected signal (solid black) and the atmospheric pressure from NOAA Springmaid pier station (dashed black).

3.4 Water Level Signal Decomposition

Ensemble empirical mode decomposition (EEMD) is a statistical method that decomposes complex signals into principal harmonic components known as ensemble intrinsic mode functions (eIMFs). EEMD is an enhancement of empirical mode decomposition (EMD), as a level of artificial noise is added to the original signal to reduce the mixing of modes, and errors which arise at the tails of the dataset (Wu and Huang 2009; Huang et al. 1998). The process of decomposition includes identifying extrema in the dataset, creating an upper and lower envelope around the extrema, and identifying the mode between envelopes. The resulting mode is a principal oscillatory component of the original signal and will be represented as the first intrinsic mode function. This process is repeated, further decomposing each intrinsic mode until a final function or residual is reached. A simplified example of EEMD signal decomposition is represented in Figure 9.

In environmental applications such as water level analysis, EEMD has been utilized to decompose complex signals into principal hydrologic drivers (Chen et al. 2013; Gong et al. 2018; Alizadeh et al. 2020; Seidu et al. 2022). This approach has proven useful for forecasting river discharge as the quantification of a hydrologic driver's impact on the observed signal can be easily identified. In the context of coastal hydrogeology, the influence of tidal forces and precipitation on the water table elevation were the desired outcomes of decomposition. The EEMD algorithm was applied to cleaned groundwater elevation datasets using the PyEMD library in Python (Laszuk 2017). eIMF-specific frequencies were compared to those of the classic tidal constituents to identify which eIMF functions operate on tidal frequencies. A similar frequency

analysis was computed for the precipitation record. Computing a variance ratio for each eIMF relative to the original signal determined how much each eIMF, and associated hydrologic driver contributed to the original signal. To prepare water table elevation levels for EEMD analysis, gaps in the data were filled with a simple linear interpolation. In the maritime forest well (MF), data quality issues resulted in the removal of 38% of timeseries measurements. As a result, the data was subdivided into the longest two consecutive periods of reliable measurement for analysis and are referred to as MF – Subset 1 and MF – Subset 2.

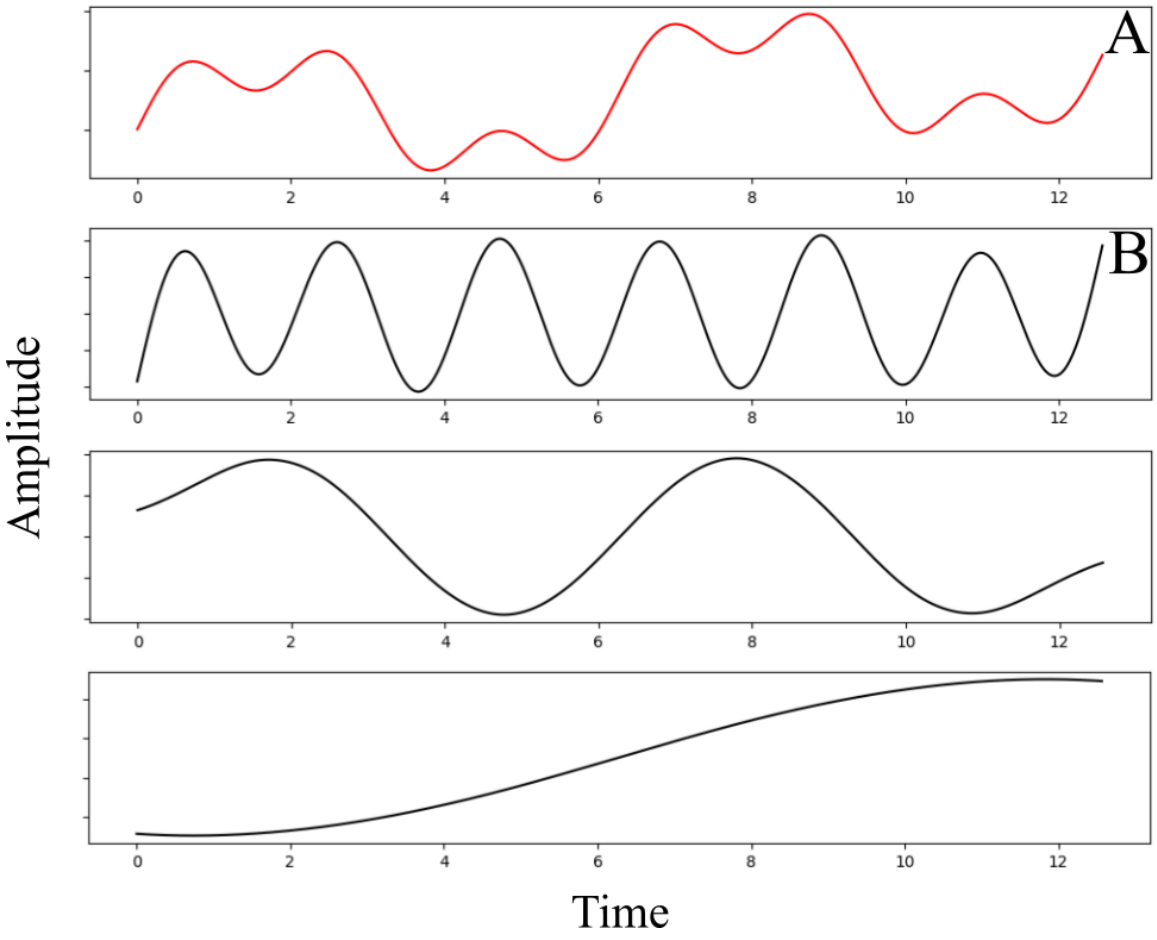


Figure 9. A visual example of EEMD signal decomposition. A) A simple two-function signal represents the original signal. B) Repeated decomposition of the original signal yields oscillatory components or intrinsic mode function.

3.5 Estimations of Darcy Flow

Estimations of groundwater flow rates were calculated utilizing Darcy's Law (Equation 3) as described by Guimond and Tamborski (2021).

$$Q = -KA\left(\frac{dH}{dL}\right) \quad 3)$$

Here (Q) represented the instantaneous flow ($cm^3\ d^{-1}$) of groundwater along the sediment facies present at the screened portion of the groundwater wells. (K), hydraulic conductivity ($cm\ s^{-1}$), was obtained utilizing a constant head permeameter using methods described in ASTM 2019 and by equations set forth in Klute and Dirksen 1986, and Rocha et al. 2005. Hydraulic head gradient is calculated as, the observed water table elevation difference in two wells (*dH*) divided by the horizontal distance between (*dL*) two wells. The head gradient is multiplied by the two-dimensional area, A, of the groundwater well screen, and the hydraulic conductivity, *K*. To account for the effect of salinity and temperature on fluid density and specific viscosity, the equation for hydraulic conductivity (*K*) is described below.

$$K = \ kg\rho/\mu \quad 4)$$

Hydraulic conductivity (*K*) can be calculated from permeability (*k*), a standardized dimension for how difficult the movement of fluid is through a material. For each water table elevation measurement acceleration due to gravity (*g*), fluid density (ρ), and dynamic viscosity (μ) were calculated using the average of corresponding groundwater salinity and temperature. Equations from Libes 2009, and Riley and Skirrow

1975 were used for the calculation of fluid density and dynamic viscosity, respectively. This created a specific *K* for each measurement that accounted for the effects of environmental conditions on the fluid. Two sets of flow rates were calculated for 24,329 groundwater measurements. The first set, DF1, represented flow between the maritime forest and the high marsh (wells MF and HM), while DF2 represented flow between the high marsh and the low marsh (wells HM and LM). Darcy flow rates were modified for comparison to other studies, the two-dimensional area of the well screen was removed from the calculated volumetric discharge to standardize the units to $cm^3\ cm^{-2}\ day^{-1}$ which is also equivalent to liters $cm^{-2}\ day^{-1}$.

3.6 Sediment Description and Analysis

Five vibracores collected adjacent to well locations provided a basis for the description of sediment texture, color, and any unique features such as fossils or biogeochemical markers for shallow geologic horizons. The four cores along transect Z were subsampled at 15-centimeter intervals, while the core along transect Y was subsampled at a 10-centimeter interval. Subsamples were subjected to analyses for percent water, fraction of organics, and laser grain size analysis. Grain sizes obtained using a CILAS 1190 (Anton Paar, Graz, Austria) were analyzed in GRADISTAT v9.1 (Blott and Pye 2001) providing a qualitative geologic description. Constant head permeameter tests (Klute and Dirksen 1986) were performed on the textural group present at the screened interval of the wells.

4. Results

4.1 Geologic Description

Cores C1 through C4, located along transect Z, contained a surficial sand deposit with increasing fines upward into the salt marsh (Figure 11). Core C4, located in the maritime forest, contained primarily clean fine sands with a thin mat of organics and root material at the top of the core. At the surface of the water table, yellowish-brown staining from iron precipitation was observed (Figure 10, 15). A similar unit of clean sands stained at the water table elevation was observed in core C3 at the forest-marsh boundary to a depth of 1.2 meters. With increasing depth, fines increased and transitioned the sand into a muddy sand texture. Fossils of *Crassostrea sp*. and *Uca sp*. were observed in this horizon indicating low marsh depositional conditions (Figure 14). Cores C2 and C1 (low marsh) were varied with numerous horizons beneath a sandy deposit approximately 0.95 - 1.1 meters thick. Beneath this sandy unit, a horizon of sandy mud and muddy sediments containing fossils of *Crassostrea sp*. and *Littorina sp*. were observed in both cores. Multiple narrow interjections of clean sand approximately 2 centimeters in thickness were observed in core C2, located at the transition from high marsh to low marsh, between 268-310 centimeters depth (Figure 13). These interjections of clean sand were not observed in the core furthest in low marsh (core C1), rather sediments became increasingly muddy to depth (Figure 12). Stratigraphic trends in core C5, located in the high marsh along transect Y, were similar to high marsh core C3, with a surficial deposit

of sand, increasing in fines to a muddy layer containing shell fragments and fossils of *Crassostrea sp*. (Figure 16).

In summary, sediment grain size analysis revealed four textural groups, sand, muddy sand, sandy mud, and mud. The sand group was present at each of the monitoring well's screened intervals. The permeability of this unit averaged 8.6×10-8 cm^2 with an average hydraulic conductivity of 0.01 cm s^{-1}. Textures with increased fines (sandy mud and mud) were determined to be impermeable with the constant head permeameter methodology.

Table 2. Description and hydraulic conductivity of sediment at each well point along transect Z.

Well Name	Well Point Elevation (m)	Corresponding Sediment	Corresponding Texture	Permeability, k (cm^2)	Hydraulic Conductivity, K (cm/s)
LM	-0.16	Well Sorted Fine Sand	Sand	$8.6x10^{-8}$	0.01
HM	0.49	Well Sorted Fine Sand	Sand	$8.6x10^{-8}$	0.01
MF	0.96	Well Sorted Fine Sand	Sand	$8.6x10^{-8}$	0.01

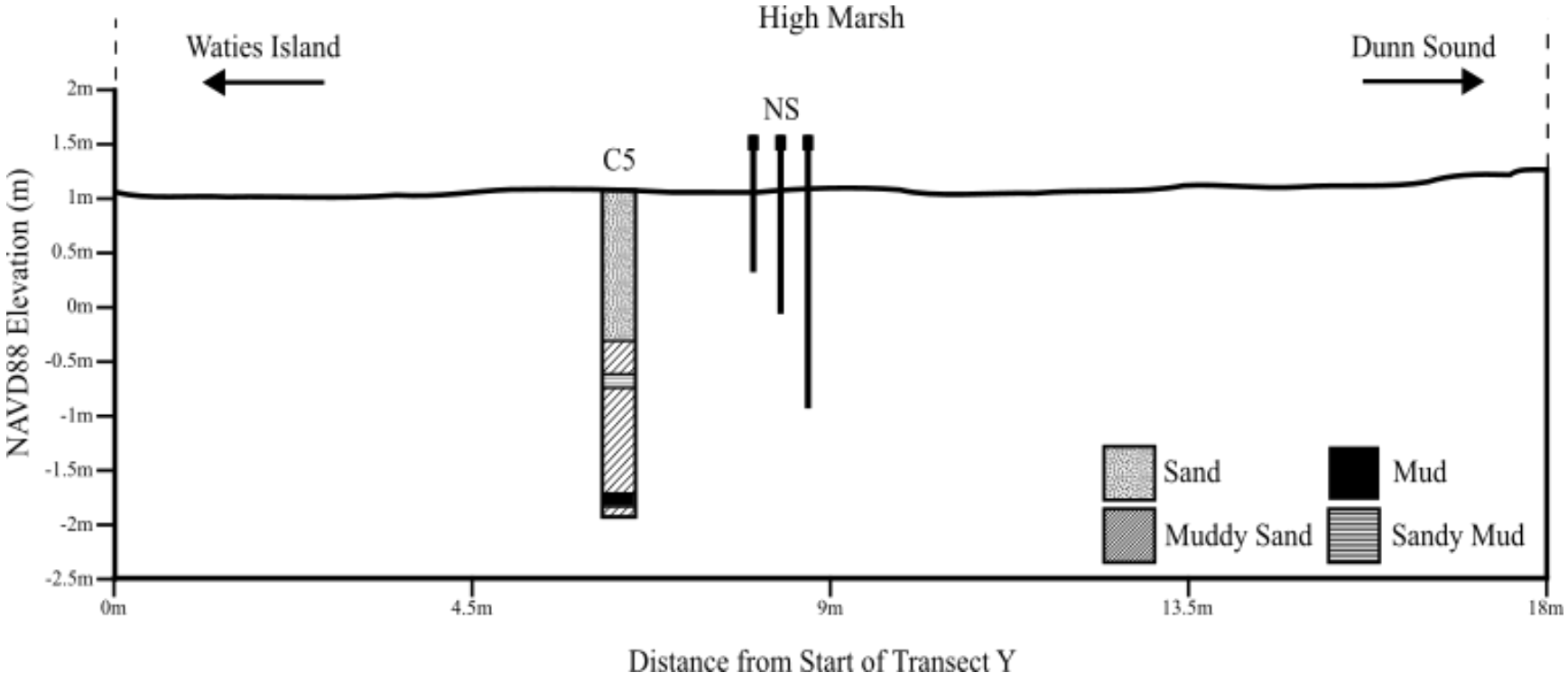


Figure 10. Geologic cross-sectional diagram of transect Y. Surface derived from topo-bathy LiDAR elevation.

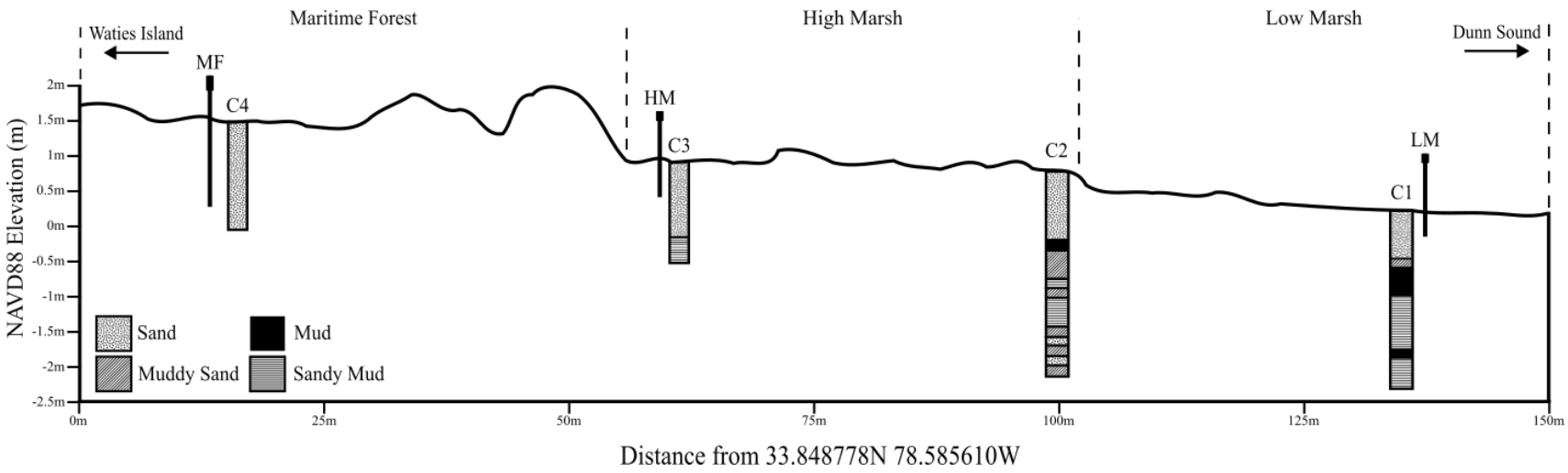


Figure 11. Geologic cross-sectional diagram of transect Z and wells LM and MF. Surface derived from topo-bathy LiDAR elevation.

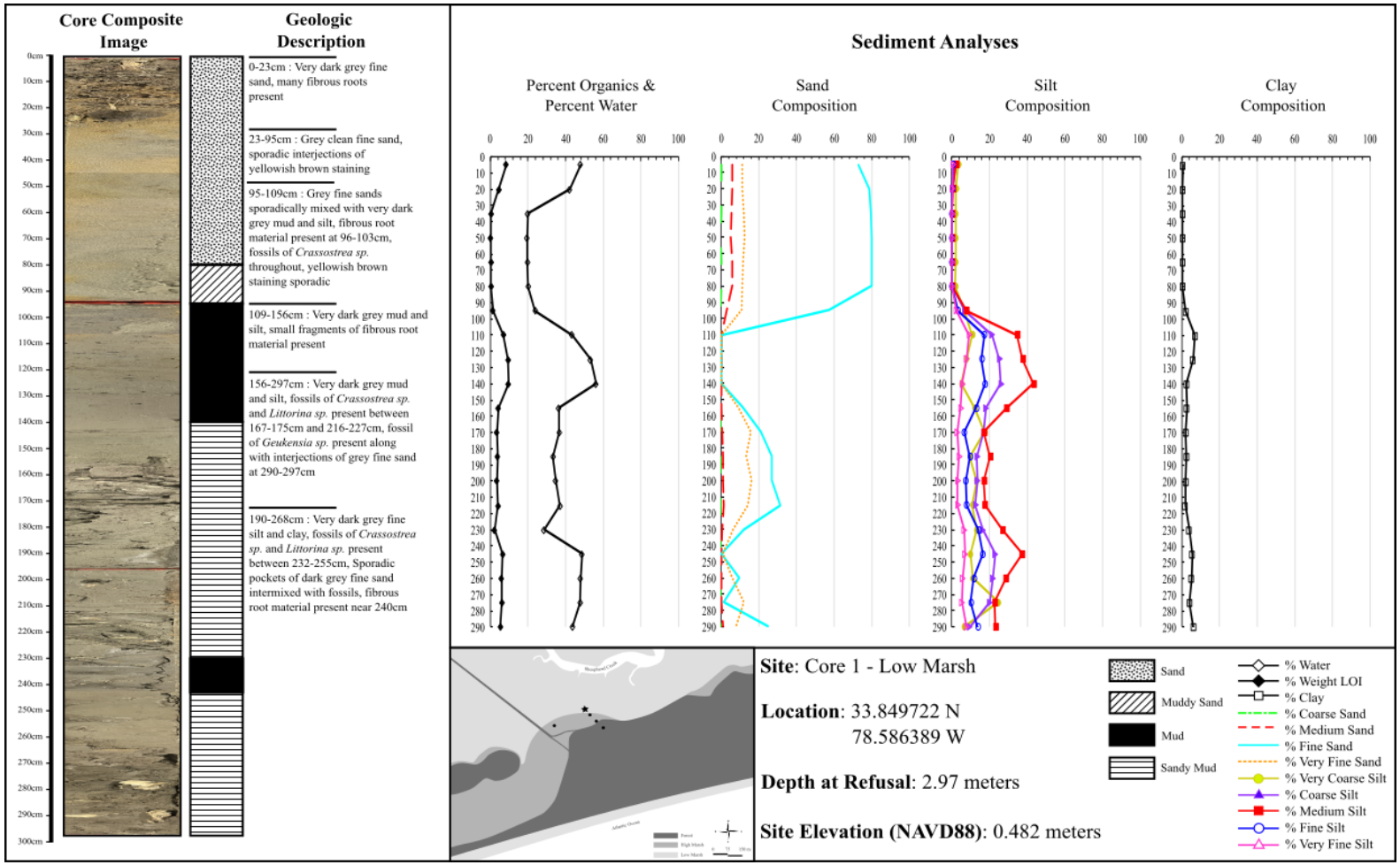


Figure 12. Geologic description and sedimentary analysis of Core 1, taken from the low marsh.

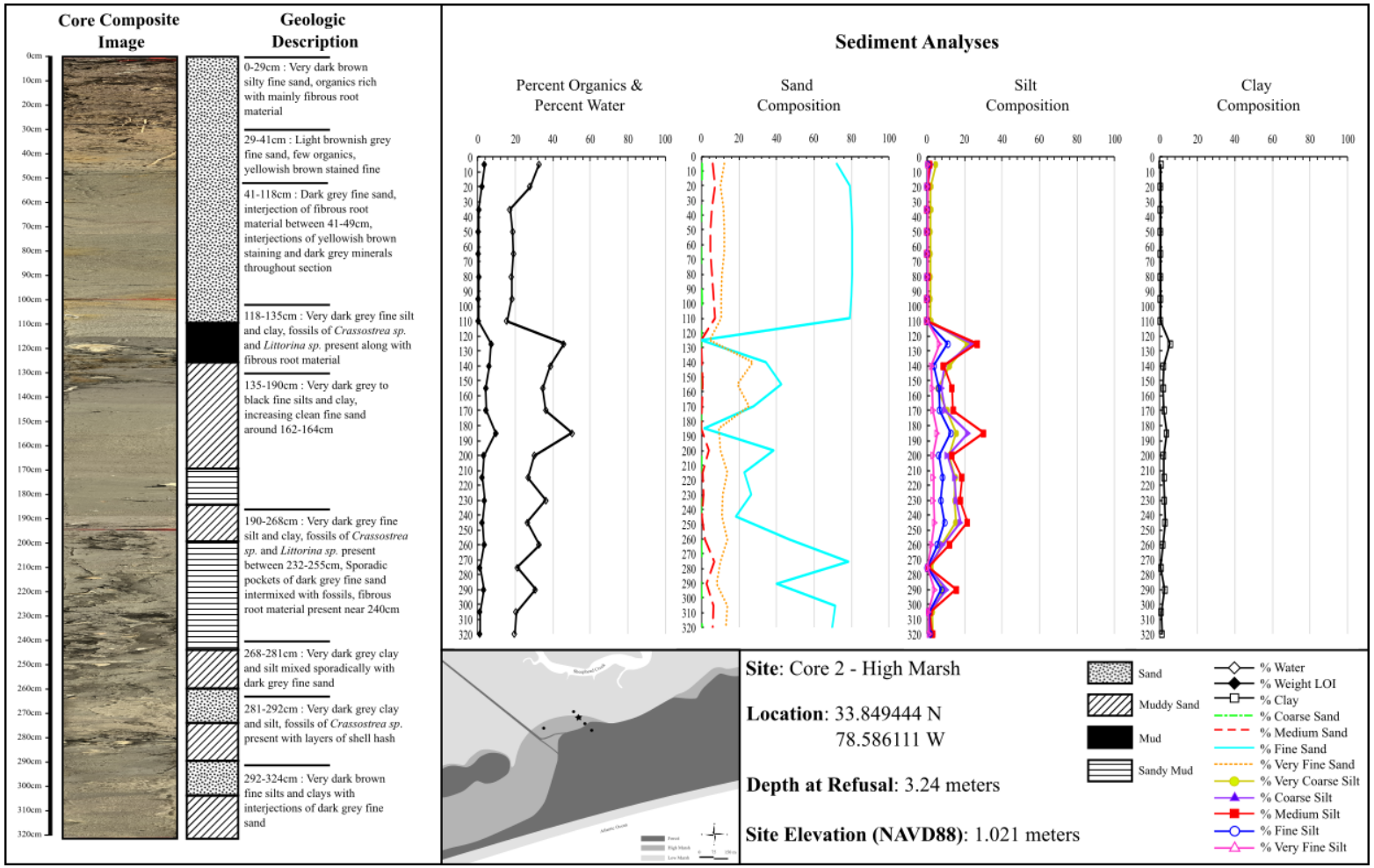


Figure 13. Geologic description and sedimentary analysis of Core 2, taken from the low marsh, high marsh transition.

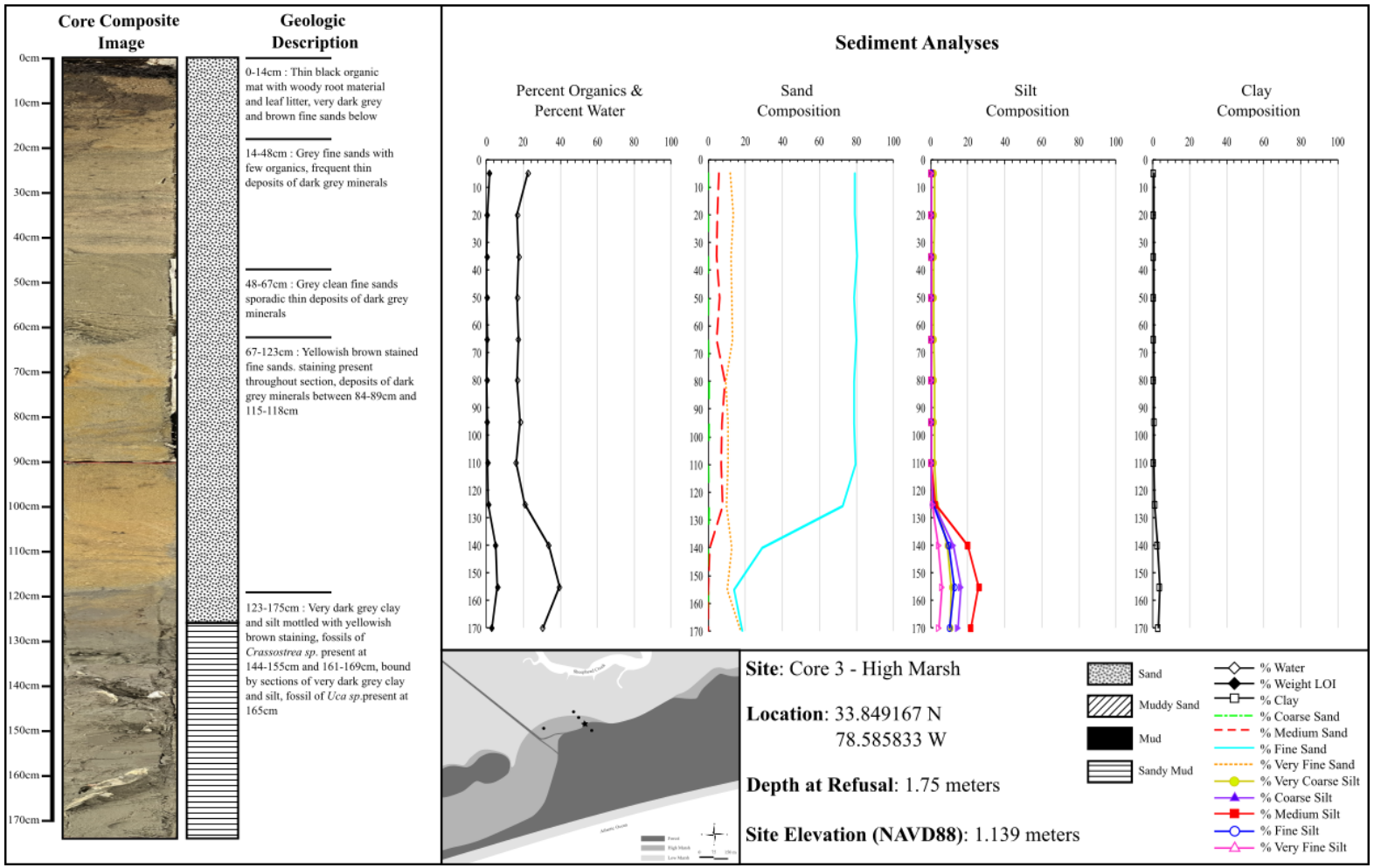


Figure 14. Geologic description and sedimentary analysis of Core 3, taken adjacent to well HM.

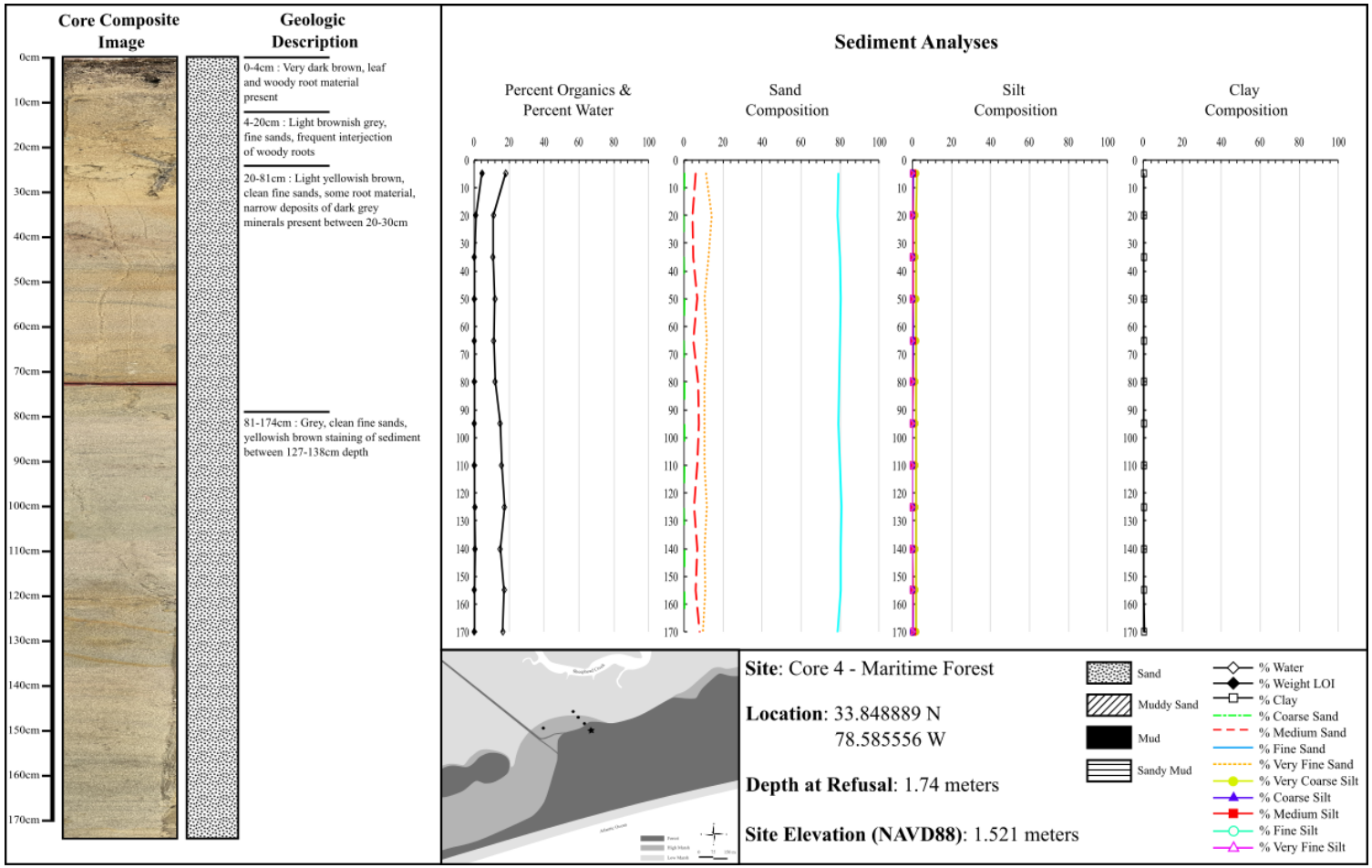


Figure 15. Geologic description and sedimentary analysis of Core 4, taken adjacent to well MF.

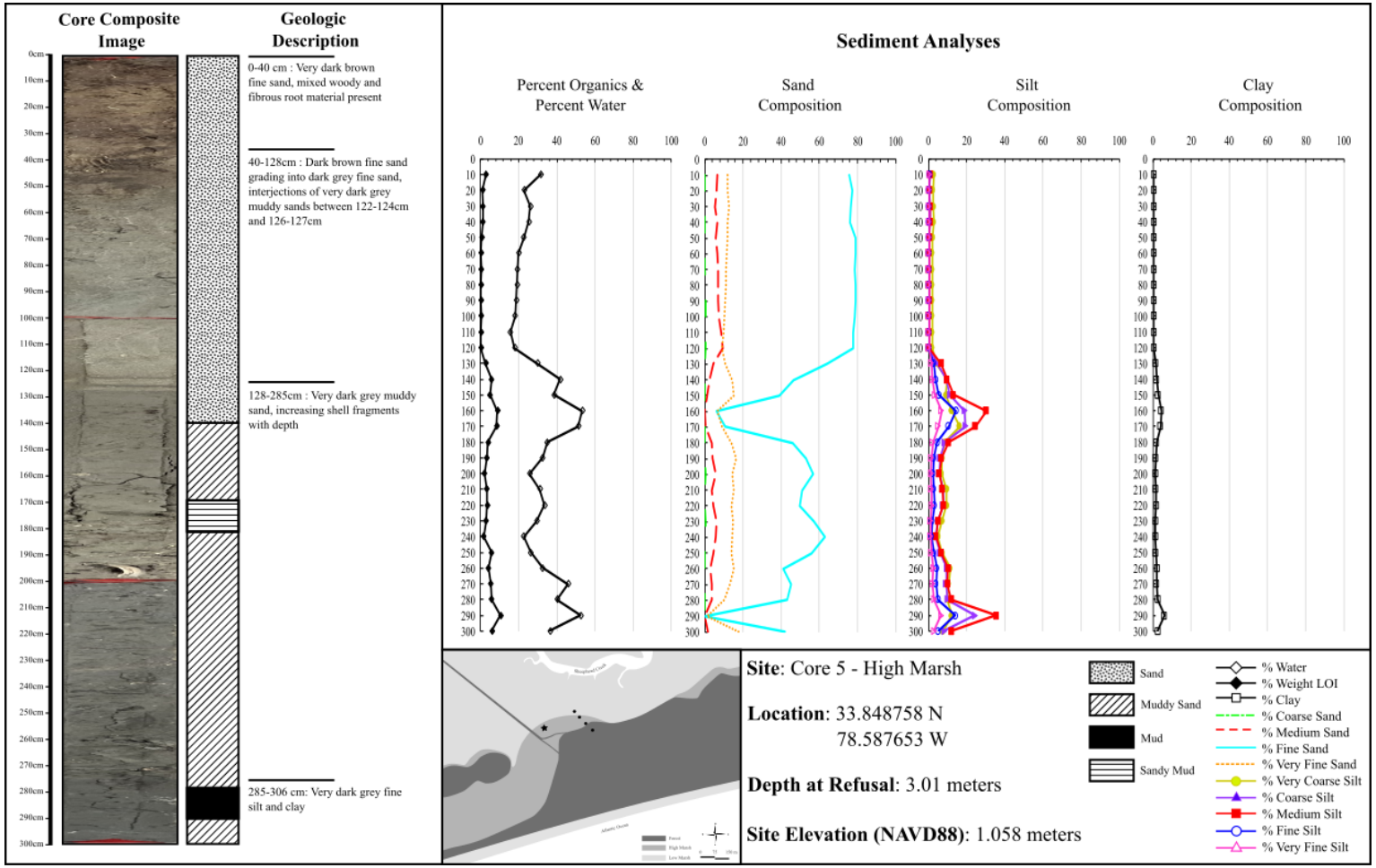


Figure 16. Geologic description and sedimentary analysis of Core 5, taken from the high marsh adjacent to the nested wells series.

4.2 Electrical Resistivity

Resistivity trends along transect X remained constant throughout the time-series (April 2021 – January 2022). A region of increased resistivity was observed at approximately 5 meters depth, and showed no lateral or vertical change despite seasonal, tidal, and meteorological variation (Figure 17). Little change in soil resistivity was observed beneath this perceived aquitard. Seasonal and meteorological trends were observed in the co-located shallower transect Y. Here, the highest soil resistivity was observed in March, April, and May where 48-hour precipitation totals prior to the survey were near or at zero. Overall, soil resistivity decreased into the summer months, with the lowest resistivities recorded in September of 2021. Precipitation totaled 4.88 centimeters prior to the August 2021 survey, which showed elevated soil resistivity within the 0.2 – 1-meter-deep band extending approximately 6 meters off the island (Figure 18). Similar patterns of resistivity were observed in transect Z, where regions of elevated electrical resistivity were located directly adjacent to the island (Figure 19).

Table 3. Soil resistivity extrema observed throughout the ER surveys. 48-hour precipitation prior to the survey indicates the general saturation of the system before measurement.

Survey Date	Transect	Max. Resistivity (Ω-m)	Min. Resistivity (Ω-m)	48 Hr. Prior Precipitation (cm)
2021-03-26	Y	3.70	1.20	0.25
2021-04-23	Y	5.33	1.19	0.00
	X	2.83	0.82	
2021-05-24	Y	4.19	0.84	0.00
	X	2.81	0.81	
2021-06-21	Y	2.51	0.83	3.23
	X	2.75	0.76	
2021-07-19	Y	2.71	0.82	1.07
	X	2.76	0.74	
2021-08-04	Y	5.14	0.83	4.88
	X	2.81	0.73	
2021-09-17	Y	2.19	0.62	0.00
	X	2.72	0.73	
2021-10-22	Y	2.32	0.85	0.00
	X	2.70	0.74	
2021-11-19	Y	2.27	0.75	0.00
	X	2.62	0.84	
2021-12-15	Y	2.52	0.88	0.00
	X	2.67	0.89	
2022-01-24	Y	3.18	1.02	0.89
	X	2.74	0.94	
2023-08-11	Z	3.84	0.83	0.00
2023-09-15	Z	9.01	0.96	2.18
2023-10-13	Z	2.50	0.96	3.07
2023-11-17	Z	2.78	0.61	0.00
2023-12-20	Z	3.58	1.12	7.95
2024-01-18	Z	4.01	1.06	0.152
2024-02-08	Z	3.60	1.32	0.00
2024-03-14	Z	3.969	1.351	0.00

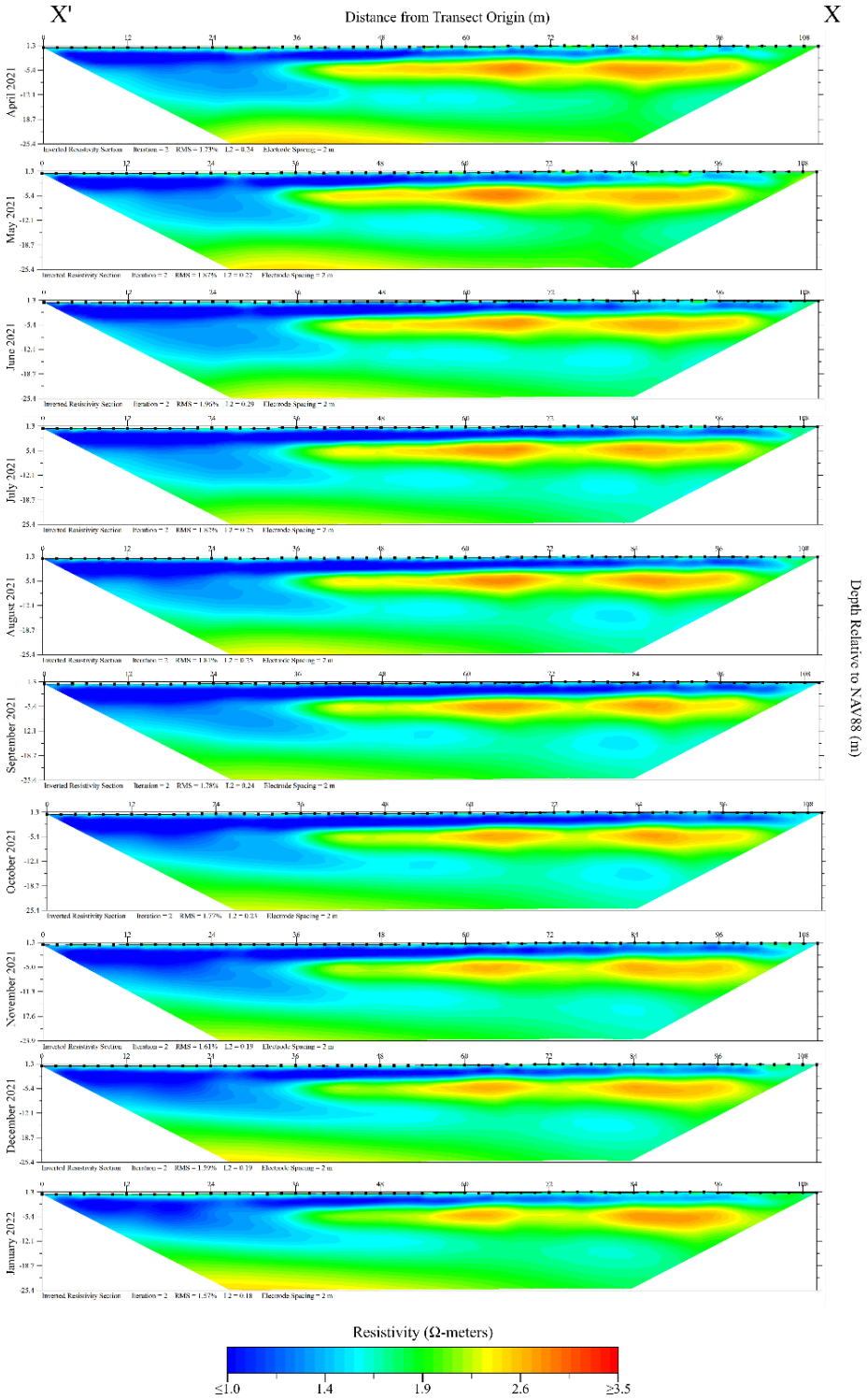


Figure 17. ER tomograms from transect X, Waties Island's headlands are towards the right of each tomogram while Dunn Sound is towards the left.

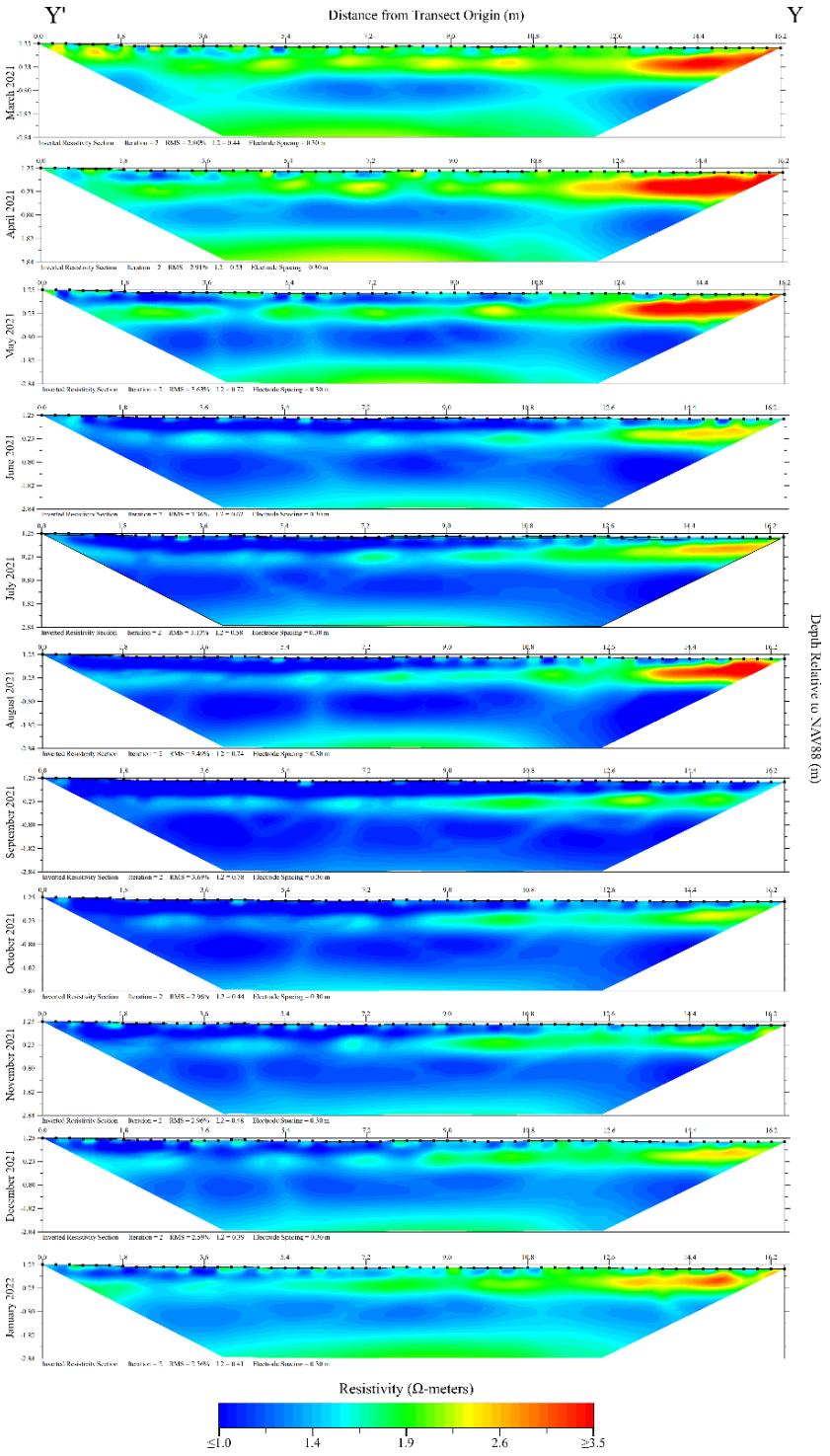


Figure 18. ER tomograms from transect Y, Waties Island's headlands are towards the right of each tomogram while Dunn Sound is towards the left.

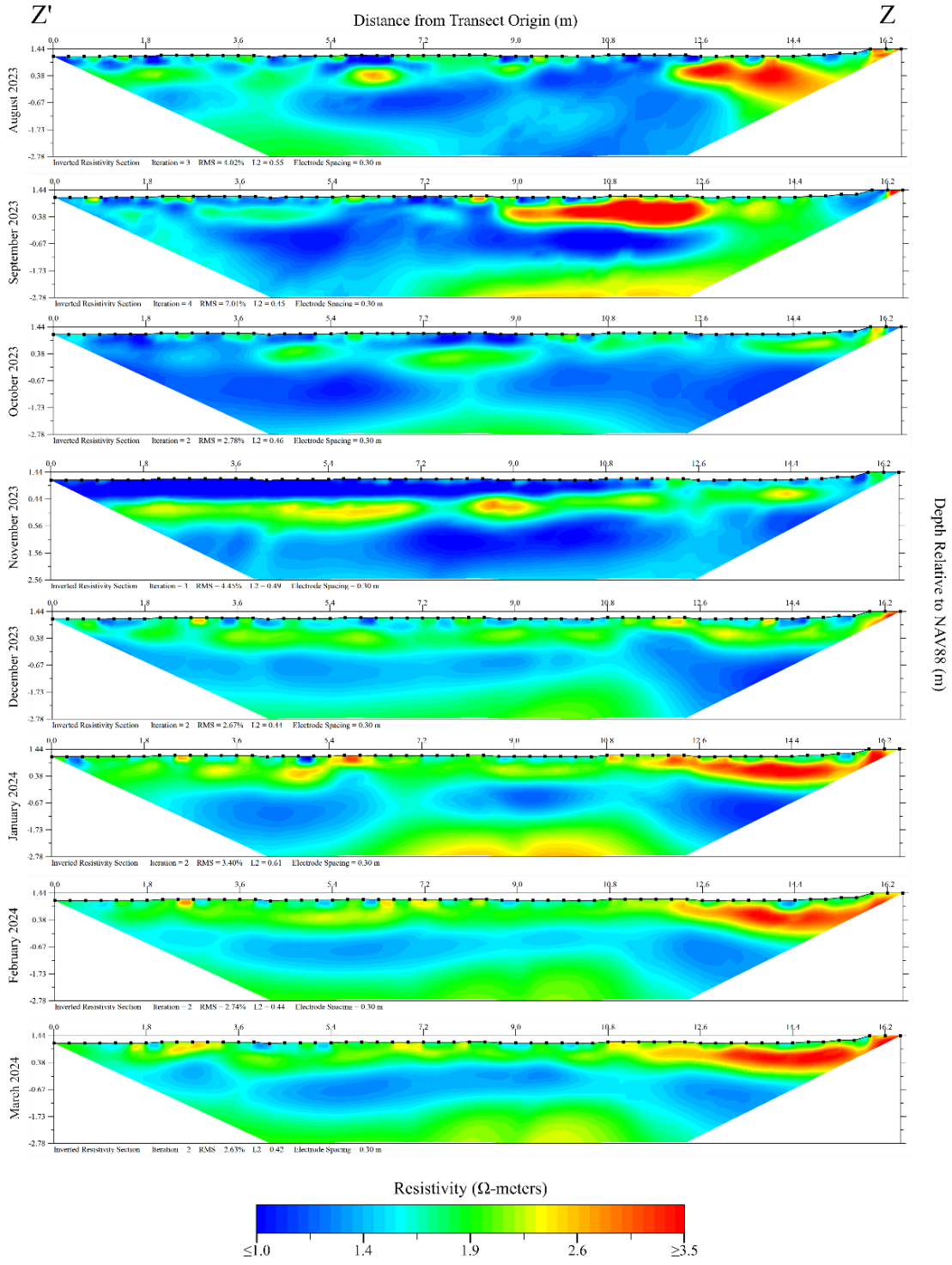


Figure 19. ER tomograms from Transect Z, Waties Island's headlands are towards the right of each tomogram while Dunn Sound is towards the left.

4.3 Groundwater Level, Temperature, and Salinity

Measurements (n = 24,332) were recorded from wells MF, HM, and LM over the 338-day period. In the maritime forest (well MF) salinity values ranged between 0.24-8.08 parts per thousand, with an average of 2.86 parts per thousand. Groundwater temperature in the forest ranged from 12.6 to 24.3 degrees Celsius. The temperature in all groundwater wells (MF, HM, and LM) followed seasonal variation (Figures 20-22). Water table elevations in the maritime forest were observed within a range of 95.6 and 173.7 centimeters above NAVD88 0. During deployment, the pressure transducer in this well was observed to record with a fixed error of 38 millibars, and this correction was applied in preprocessing. During periods of drought, water table elevations fell, surpassing the depth of the well installation, resulting in a dry monitoring well. These periods were identified when conductivity approached zero and recorded temperature reflected air temperature with diurnal fluctuation. Data associated with drought periods were removed from the timeseries. Water table elevation in the forest responded rapidly to precipitation events.

Groundwater salinity in the high marsh (well HM) averaged 14.8 parts per thousand. The widest range of groundwater salinity was observed in the high marsh varying from 10.1 to 24.5 parts per thousand. Water table elevations at this well averaged 98.8 centimeters above NAVD88 0, with maximum and minimum observations of 183.1 and 60.3 centimeters respectively.

Low marsh groundwater salinity (well LM) averaged 25.6 with excursions to 23.7 and 27.0 parts per thousand throughout the time-series. A malfunction occurred with this levelogger during the first deployment where recorded salinities were 15 parts per

thousand lower than verified YSI measurements. This salinity data was removed from the timeseries. Water table elevations ranged from 29.5 to 187.3 centimeters above NAVD88 0 with an average elevation of 54.6 centimeters.

Of the nested well series, the shallowest well (NS 0.75 meters depth) had the greatest observed range in salinity and temperature, with observations between 16.7-19 parts per thousand and 6.3-24.9 degrees Celsius respectively. The deepest nested well (NS 2 meters depth) maintained the smallest variation in groundwater salinity with an average of 16.4 while the median depth well (NS 1.2 meters depth) averaged a groundwater salinity of 15.9 parts per thousand.

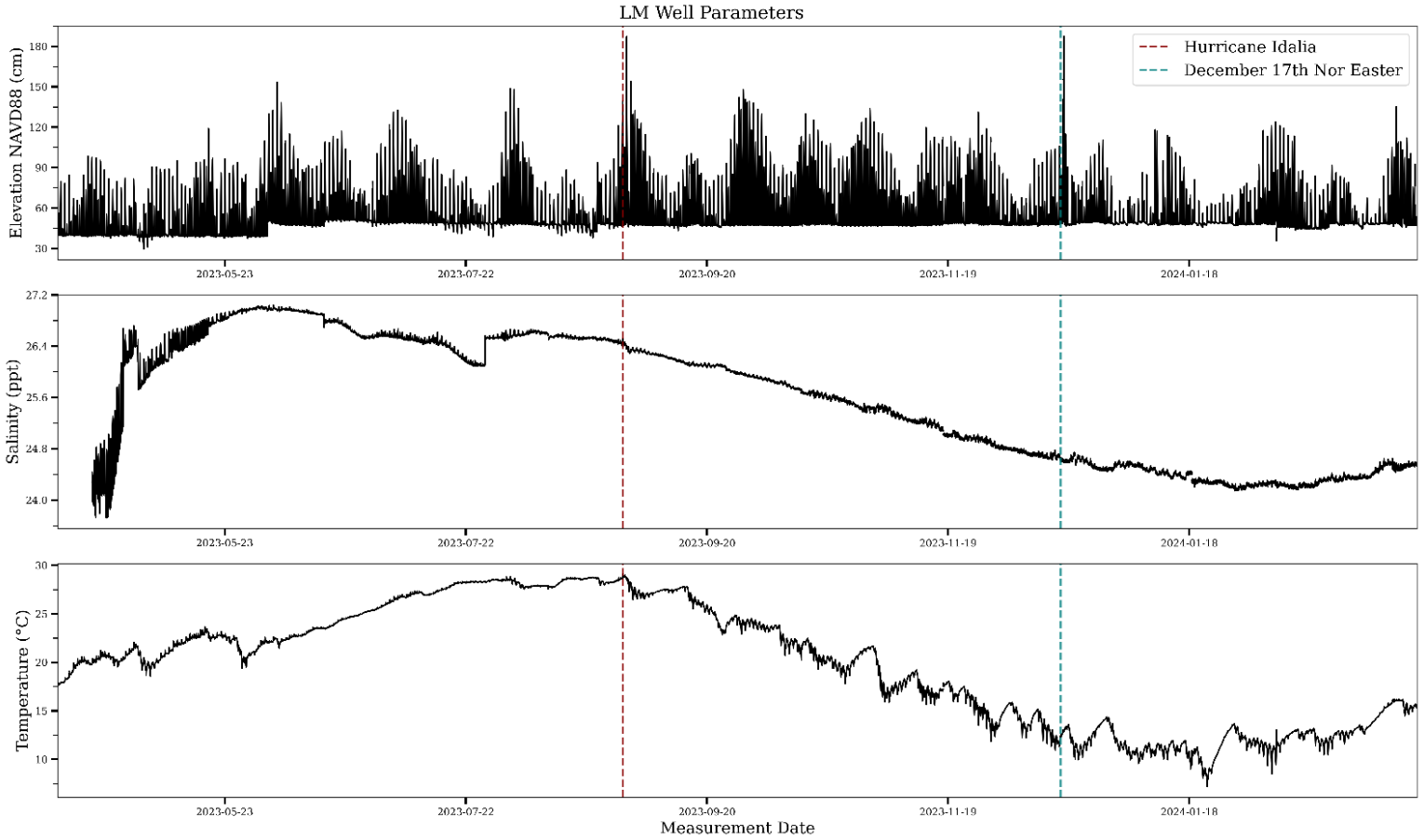


Figure 20. Groundwater level, temperature, and salinity from well LM, water table elevations are tightly coupled with tidal fluctuations.

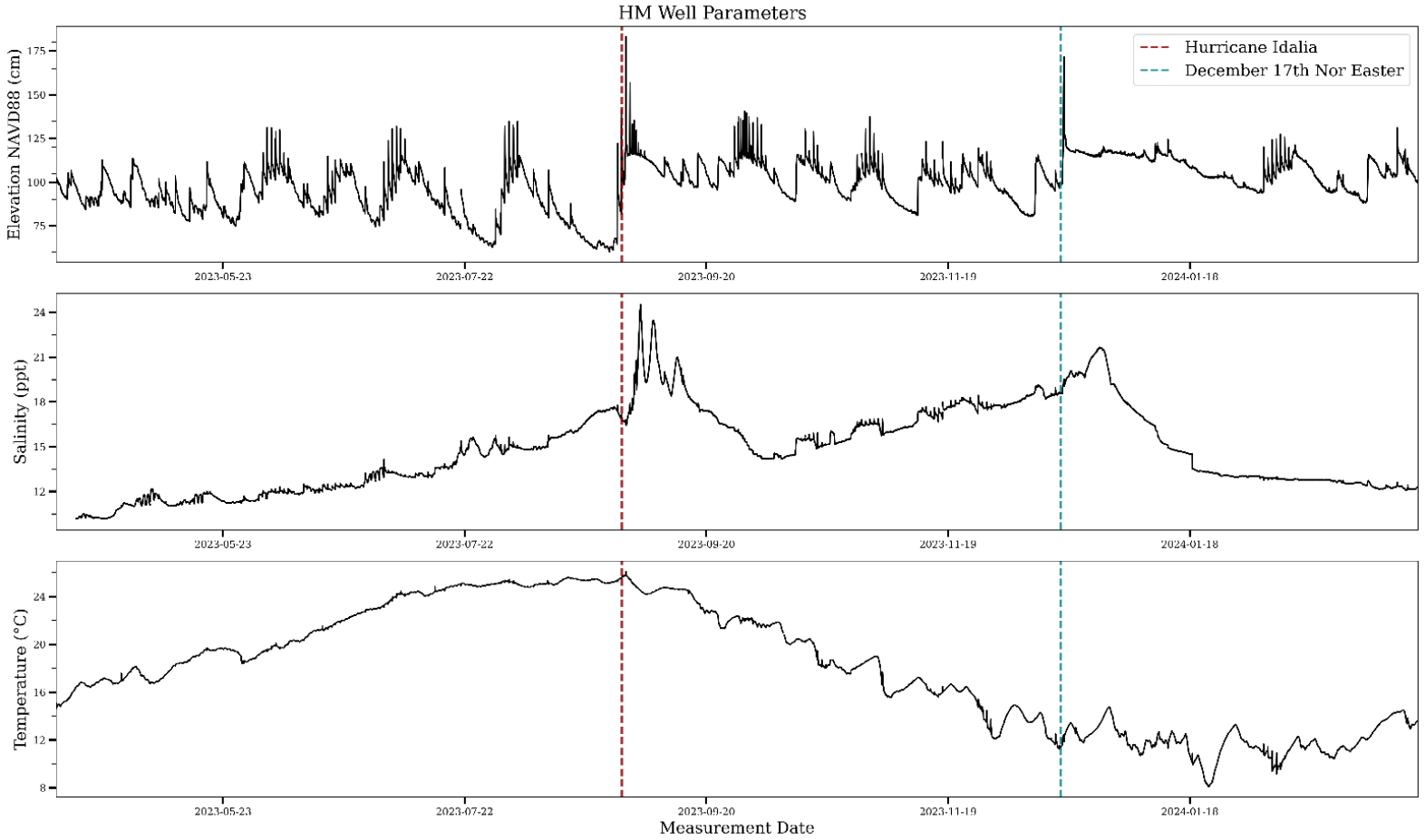


Figure 21. Groundwater level, temperature, and salinity from well HM, water table elevations are driven primarily by major precipitation events and periodically by spring tides.

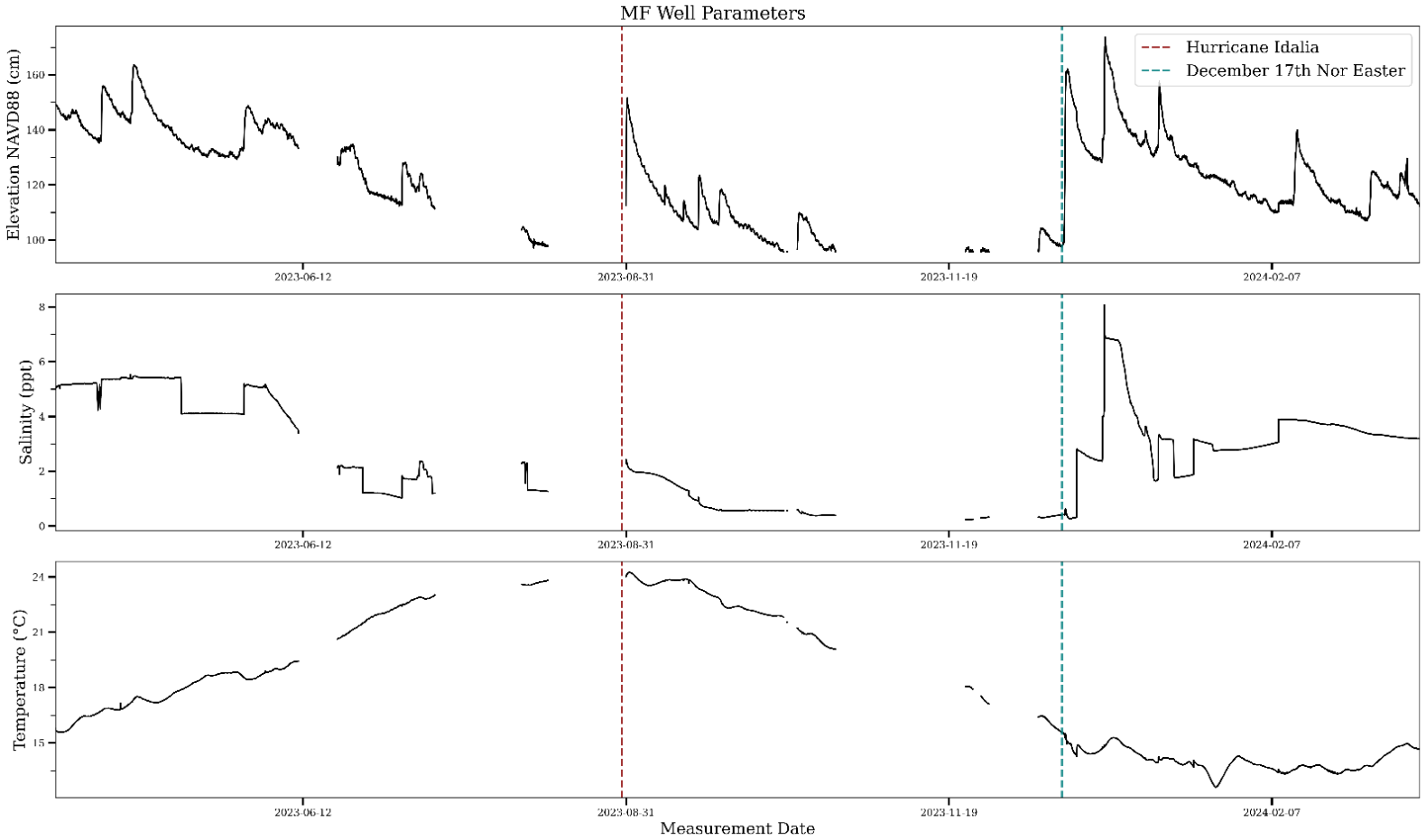


Figure 22. Groundwater level, temperature, and salinity from well MF, water table elevations reflect recharge from precipitation events.

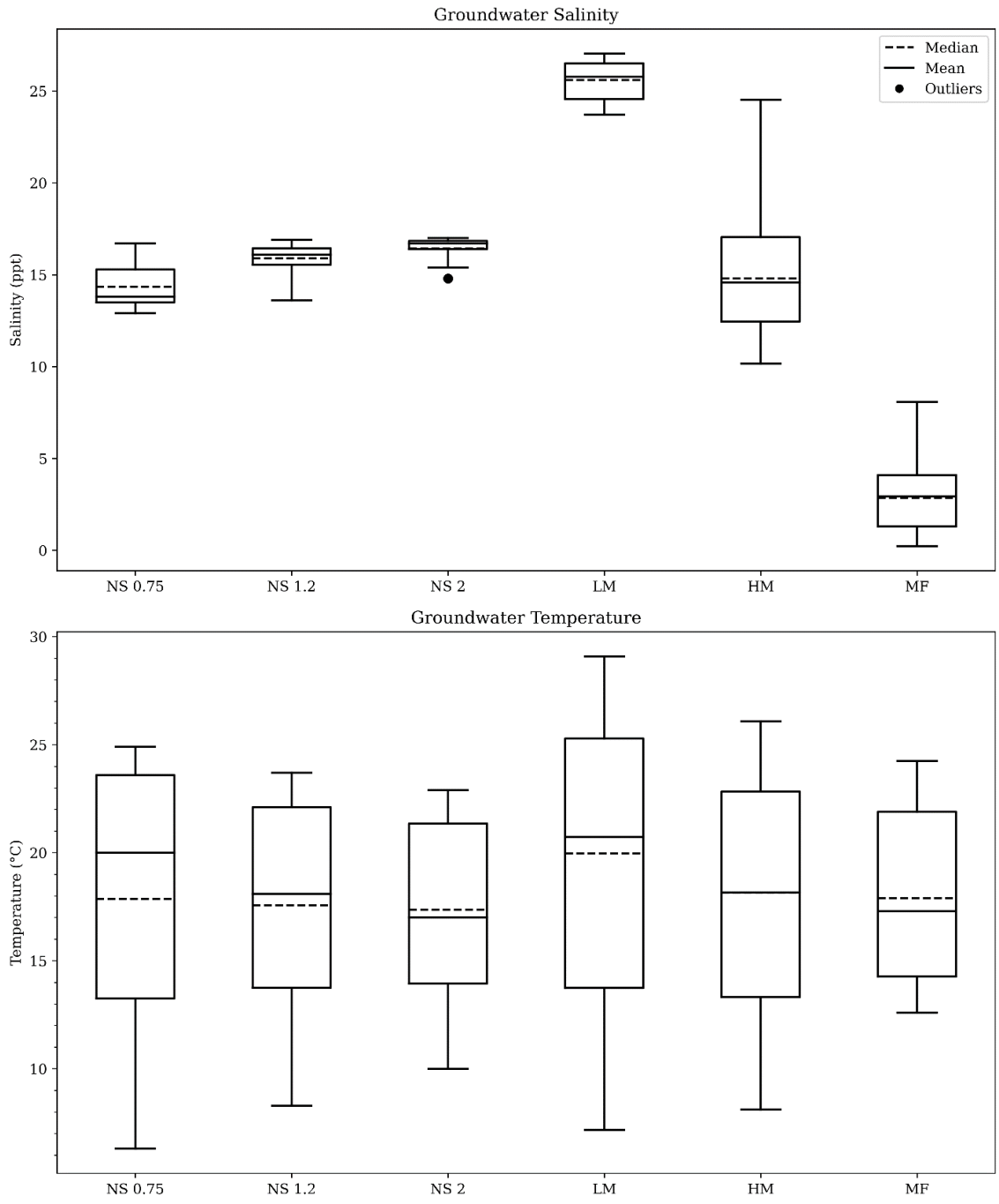


Figure 23. Boxplots of groundwater salinity and temperature observed in study wells. Whiskers represent data extents three standard deviations from the median.

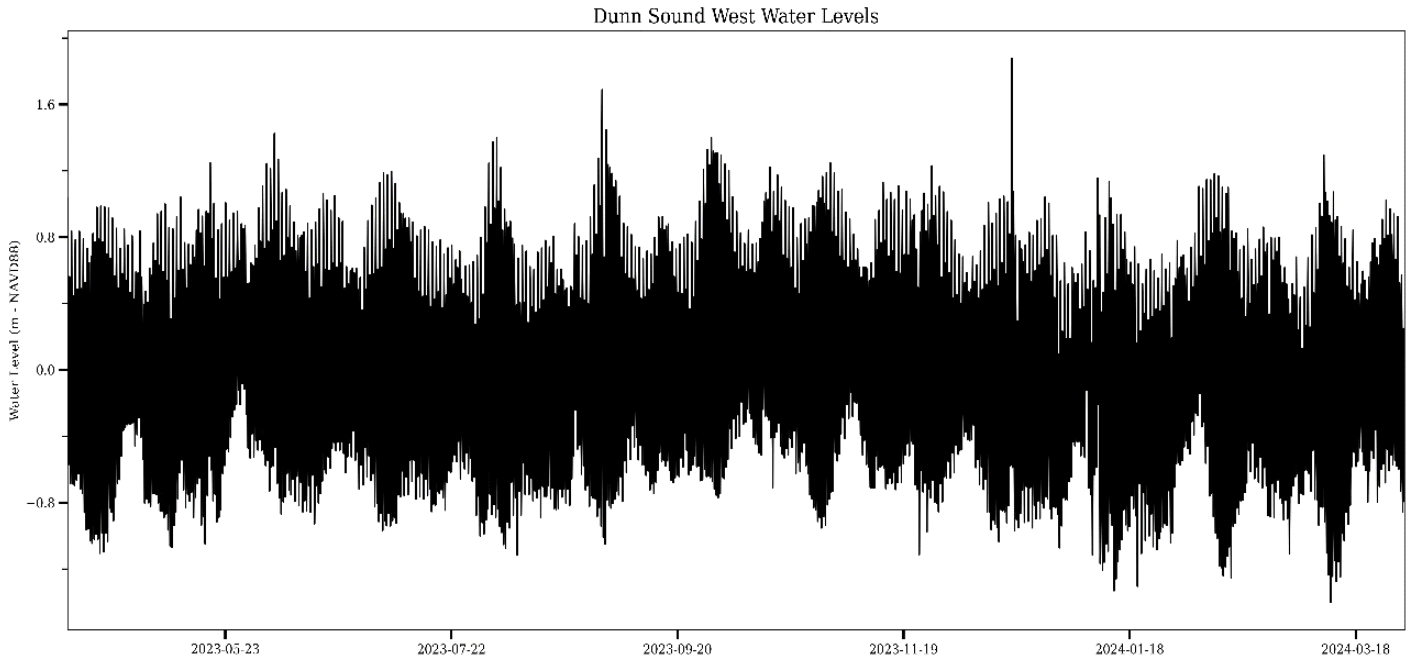


Figure 24. Tide predictions at Dunn Sound West, station 8660195, derived from water levels at the NOAA Springmaid Pier station 8661070 by applying high-low offsets and time corrections. Mean tidal range is 1.53 meters.

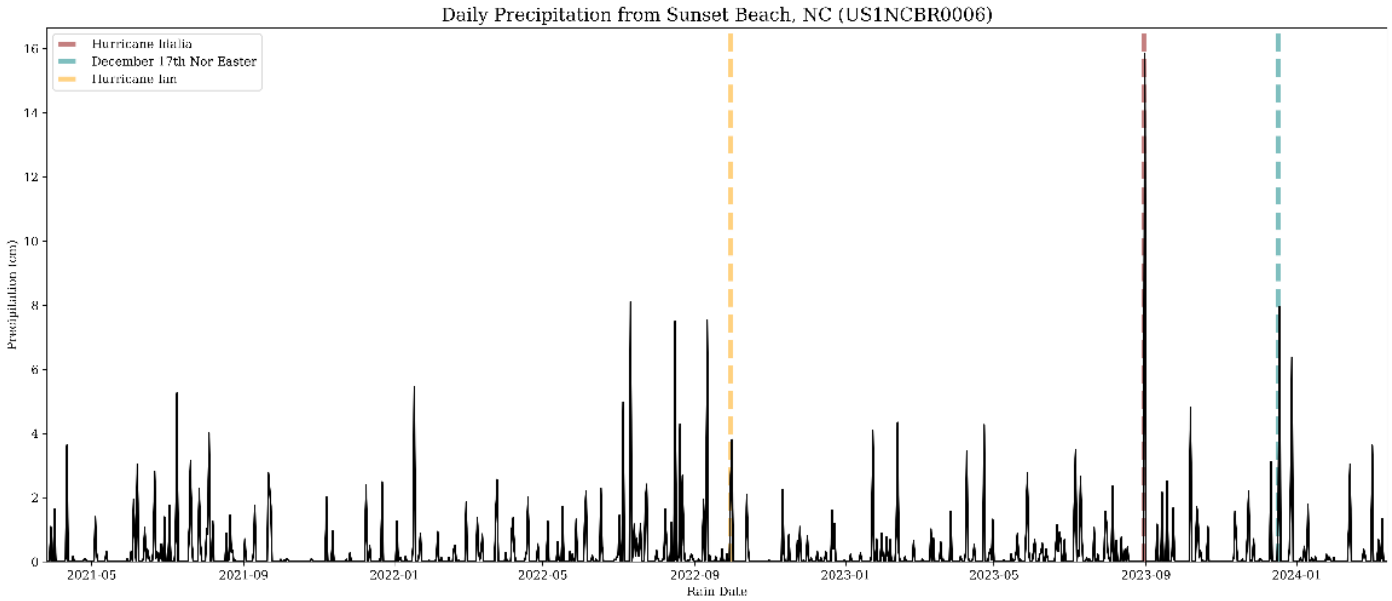


Figure 25. Daily precipitation totals from CoCoRaHS station US1NCBR0006, Sunset Beach. Local station precipitation totals verified against daily precipitation data from NOAA Springmaid Pier station and NWS North Myrtle Beach Airport station. Major meteorological events highlighted.

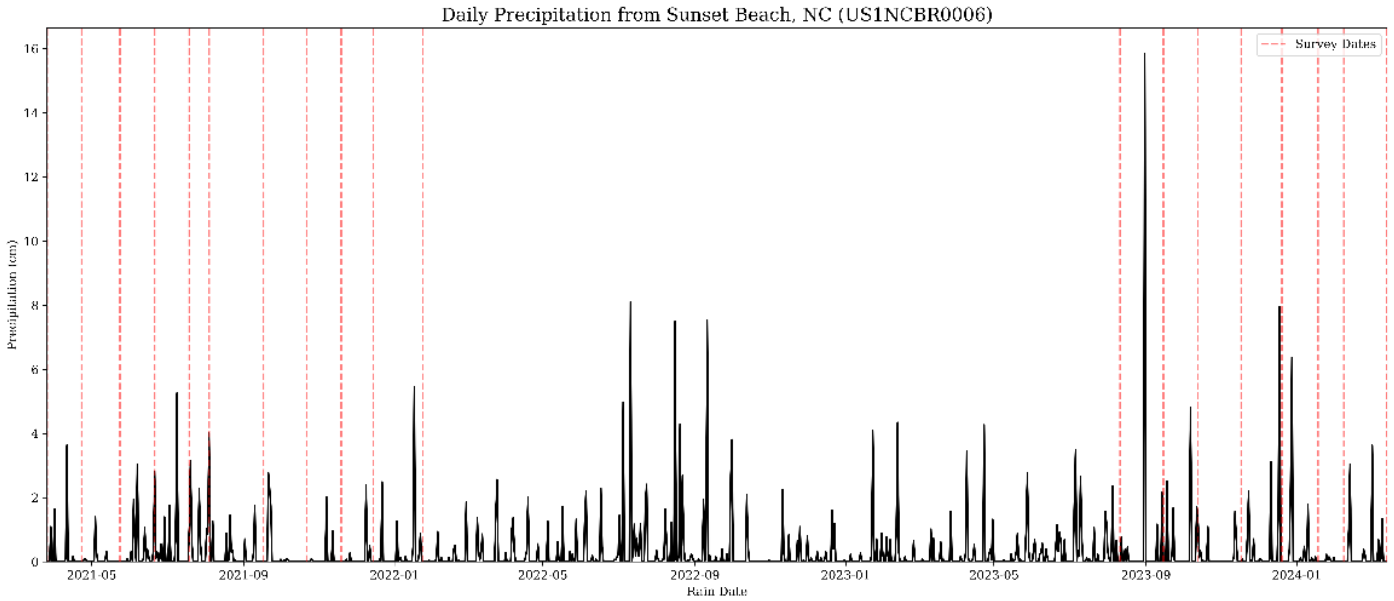


Figure 26. Daily precipitation totals from Sunset Beach. Dates of ER surveys are indicated with vertical red lines.

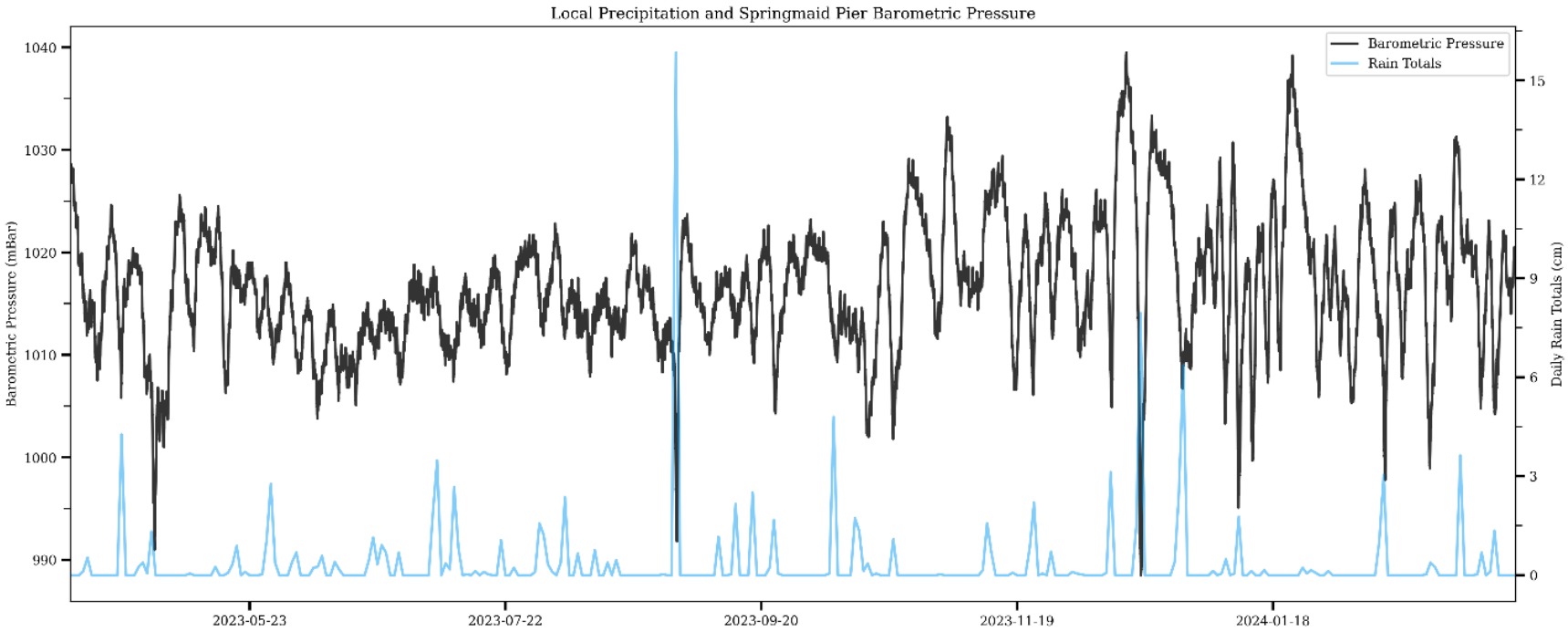


Figure 27. Sunset Beach, NC daily precipitation totals and atmospheric pressure from Springmaid Pier, SC. Major meteorological events corresponding with high precipitation totals are well correlated with drops in barometric pressure.

4.4 Groundwater Level Signal Analysis

In the low marsh water table elevation was decomposed into fourteen eIMFs (Figure 28). eIMF 5 had a frequency of 0.017 with a cycle completing every 5.84 hours (Table 5). This eIMF had the highest variance ratio (0.31) and aligned with the frequency of the M4 overtidal harmonic (Table 4). Decomposition of water table elevations from the high marsh resulted in 14 eIMFs. eIMF 10 contained the highest variance ratio with a frequency (0.005) similar to that of the precipitation events on the island exceeding 1 centimeter accumulation (0.004). In both maritime forest (MF) subsets high variance ratio eIMFs had frequencies aligning with precipitation events on the island of 0.003 and 0.005 respectively (Figures 30 and 31).

Table 4. Principal harmonic constituents in tidal signals, adapted from Chen et al. 2013

Tide Type	Term Name	Term	Hours/Cycle	Frequency
Semi-diurnal	Lunisolar diurnal constituent	K_2	11.9672	0.0836
	Principal solar semidiurnal constituent	S_2	12.000	0.0833
	Principle lunar semidiurnal constituent	M_2	12.4206	0.0805
	Large lunar elliptic semidiurnal constituent	N_2	12.6583	0.0775
	Second large lunar elliptic semidiurnal constituent	$2N_2$	12.9054	0.0790
Diurnal	Lunisolar diurnal constituent	K_1	23.9345	0.0418
	Principal solar diurnal constituent	P_1	24.0695	0.0416
	Principal lunar diurnal constituent	O_1	25.8193	0.0387
	Large lunar elliptic constituent	Q_1	26.8684	0.0372
Overtides	Solar quarter constituent	S_4	6.0000	0.1667
	Large lunar quarter constituent	M_4	6.2103	0.1610

Table 5. eIMF periodicity, frequencies, and variance ratios from EEMD analysis on well LM water table elevation.

Well - LM	Hours/Cycle	Frequency	Variance Ratio
eIMF 1	0.46	2.16	0.03
eIMF 2	0.81	1.23	0.01
eIMF 3	1.73	0.58	0.06
eIMF 4	2.99	0.33	0.12
eIMF 5	5.84	0.17	0.31
eIMF 6	9.81	0.10	0.12
eIMF 7	15.14	0.07	0.01
eIMF 8	31.81	0.03	0.01
eIMF 9	72.43	0.01	0.02
eIMF 10	169.01	0.006	0.03
eIMF 11	386.31	0.003	0.01
eIMF 12	1014.07	0.001	0.01
eIMF 13	2704.18	0.0004	0.03

Table 6. eIMF periodicity, frequencies, and variance ratios from EEMD analysis on well HM water table elevation.

Well - HM	Hours/Cycle	Frequency	Variance Ratio
eIMF 1	0.46	2.17	0.02
eIMF 2	0.80	1.26	0.01
eIMF 3	1.41	0.71	0.01
eIMF 4	2.49	0.40	0.01
eIMF 5	4.65	0.22	0.01
eIMF 6	9.14	0.11	0.02
eIMF 7	16.23	0.06	0.01
eIMF 8	35.27	0.03	0.03
eIMF 9	84.51	0.01	0.10
eIMF 10	208.01	0.005	0.25
eIMF 11	368.75	0.003	0.10
eIMF 12	1014.07	0.0009	0.06
eIMF 13	2028.14	0.0005	0.07
eIMF 14	8112.55	0.0001	0.12

Table 7. eIMF periodicity, frequencies, and variance ratios from EEMD analysis on water table elevation subset 1 from the MF well.

MF – Subset 1	Hours/Cycle	Frequency	Variance Ratio
eIMF 1	0.47	2.14	0.006
eIMF 2	0.87	1.15	0.002
eIMF 3	1.73	0.58	0.002
eIMF 4	3.51	0.28	0.002
eIMF 5	8.60	0.12	0.006
eIMF 6	19.51	0.05	0.02
eIMF 7	55.54	0.02	0.16
eIMF 8	180.51	0.006	0.11
eIMF 9	361.02	0.003	0.37
eIMF 10	1444.07	0.0007	0.26

Table 8. eIMF periodicity, frequencies, and variance ratios from EEMD analysis on water table elevation subset 2 from the MF well.

MF – Subset 2	Hours/Cycle	Frequency	Variance Ratio
eIMF 1	0.47	2.15	0.009
eIMF 2	0.84	1.18	0.003
eIMF 3	1.61	0.62	0.002
eIMF 4	3.18	0.31	0.002
eIMF 5	6.27	0.16	0.005
eIMF 6	14.99	0.07	0.02
eIMF 7	38.38	0.03	0.06
eIMF 8	94.35	0.01	0.15
eIMF 9	226.43	0.004	0.28
eIMF 10	566.08	0.0018	0.13
eIMF 11	1132.16	0.0009	0.21

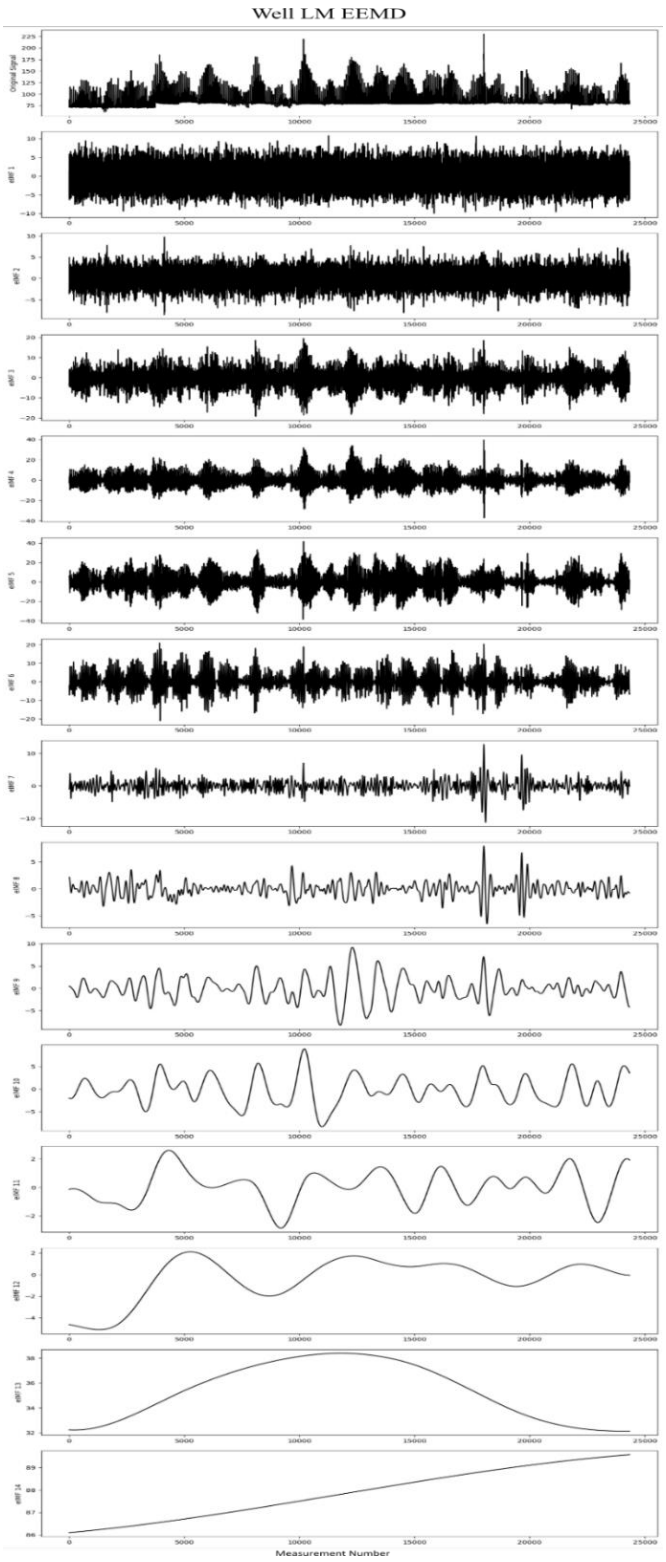


Figure 28. Water table elevation and eIMFs from the low marsh, well LM.

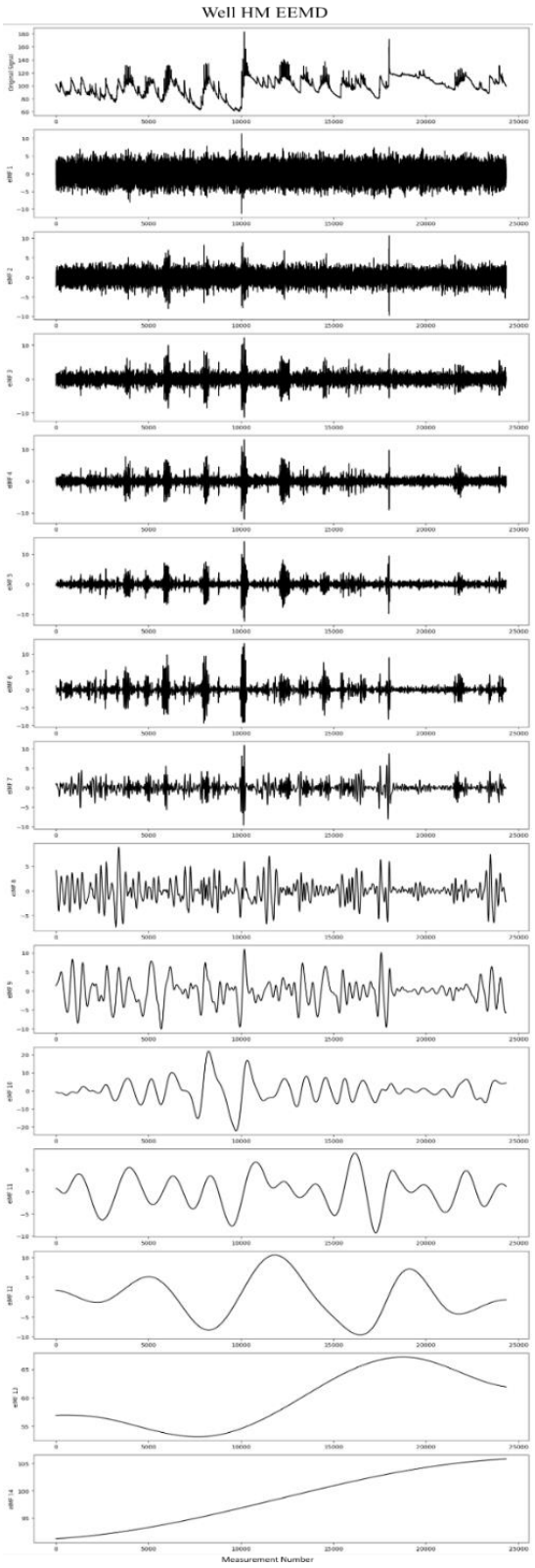


Figure 29. Water table elevation and eIMFs from the high marsh, well HM.

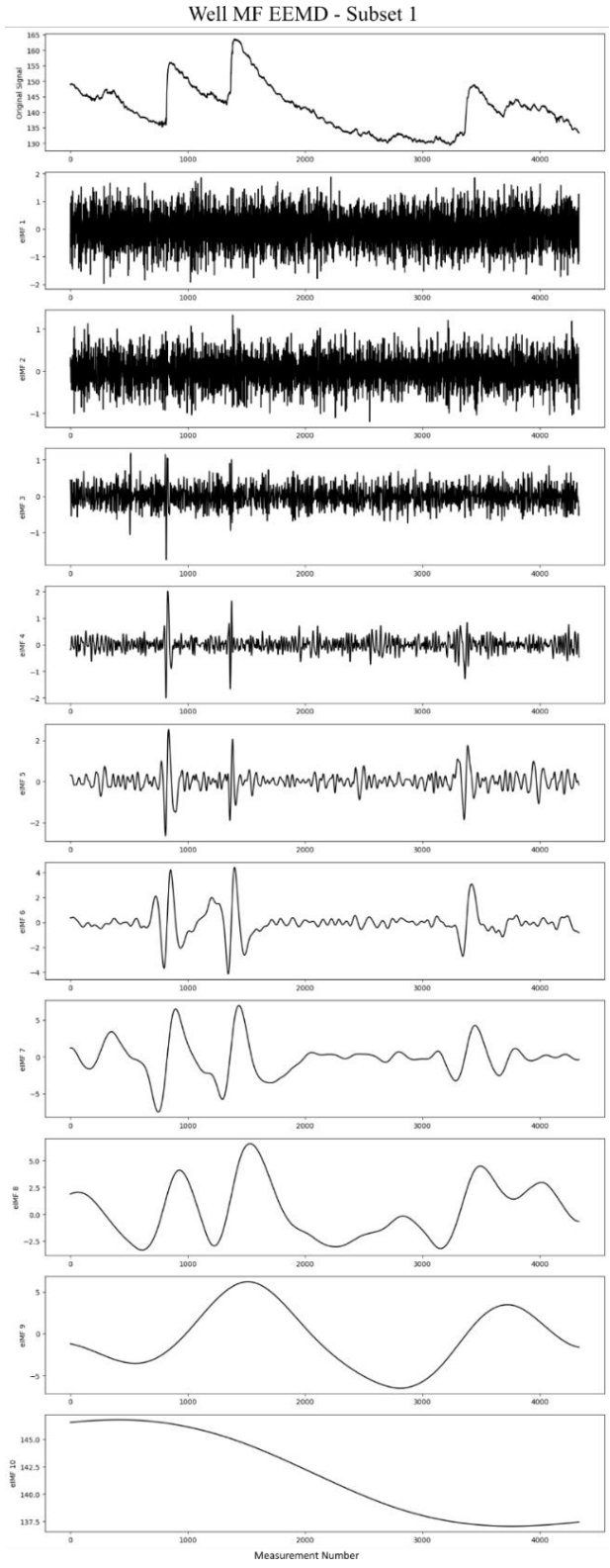


Figure 30. Water table elevation and eIMFs from the maritime forest, well MF, subset 1.

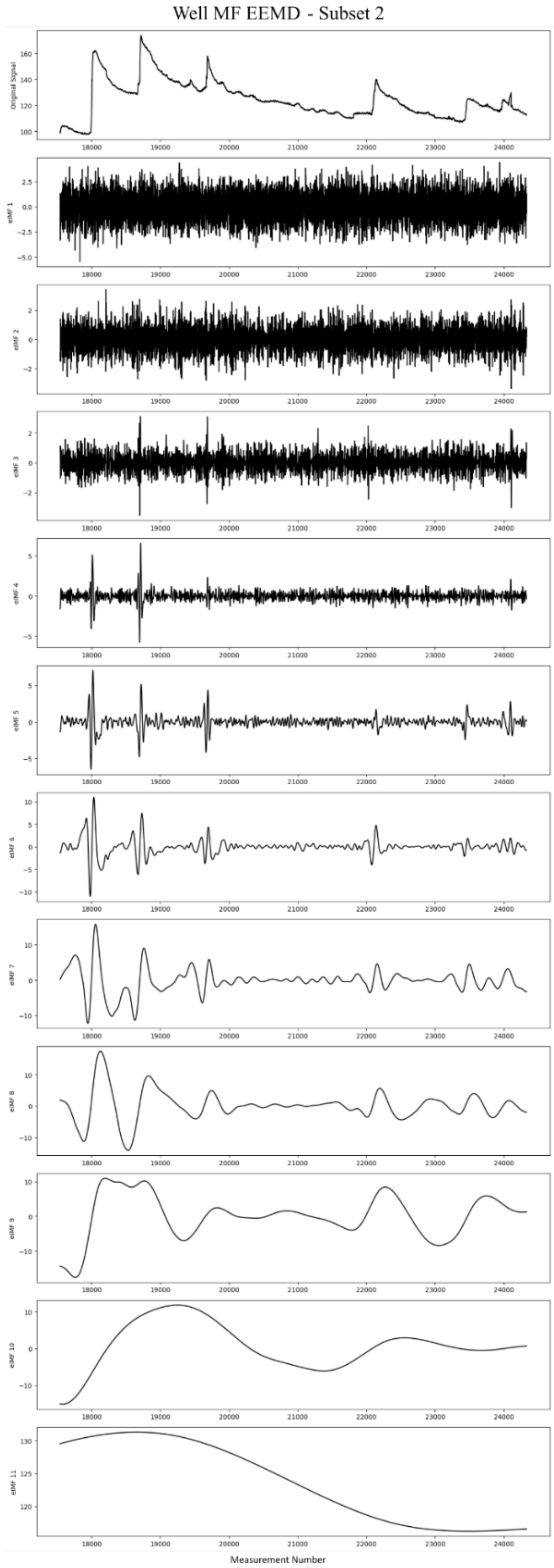


Figure 31. Water table elevation and eIMFs from the maritime forest, well MF, subset 2.

4.5 Cross-Correlation Analysis

Six cross-correlation analyses assessed the time relationships between the major hydrologic drivers at the study site and the observed water table elevation at each well. The low marsh showed a strong correlation between water table elevation and tide (Figure 32). The strongest correlation was observed when water levels in Dunn Sound preceded the water table elevation in the well by one sampling period (20 minutes). Tidal correlation between the low marsh and maritime forest varied. Maximum correlation coefficients were observed at a lag of 93.6 and 34.7 days in each well. All three wells (LM, HM, and MF) displayed strong correlation with precipitation at a lag time of zero (Figures 32-34).

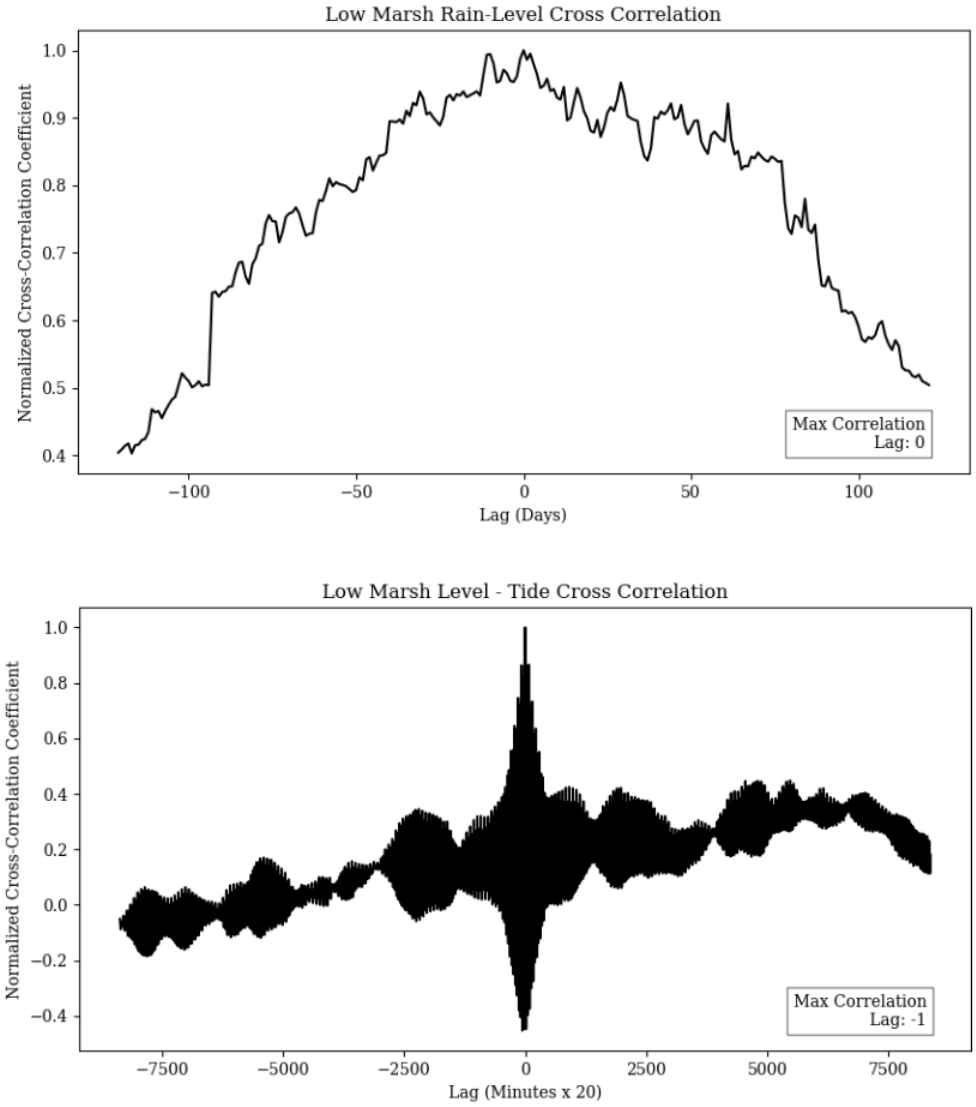


Figure 32. Cross correlation of Dunn Sound West tides and daily precipitation with low marsh groundwater level.

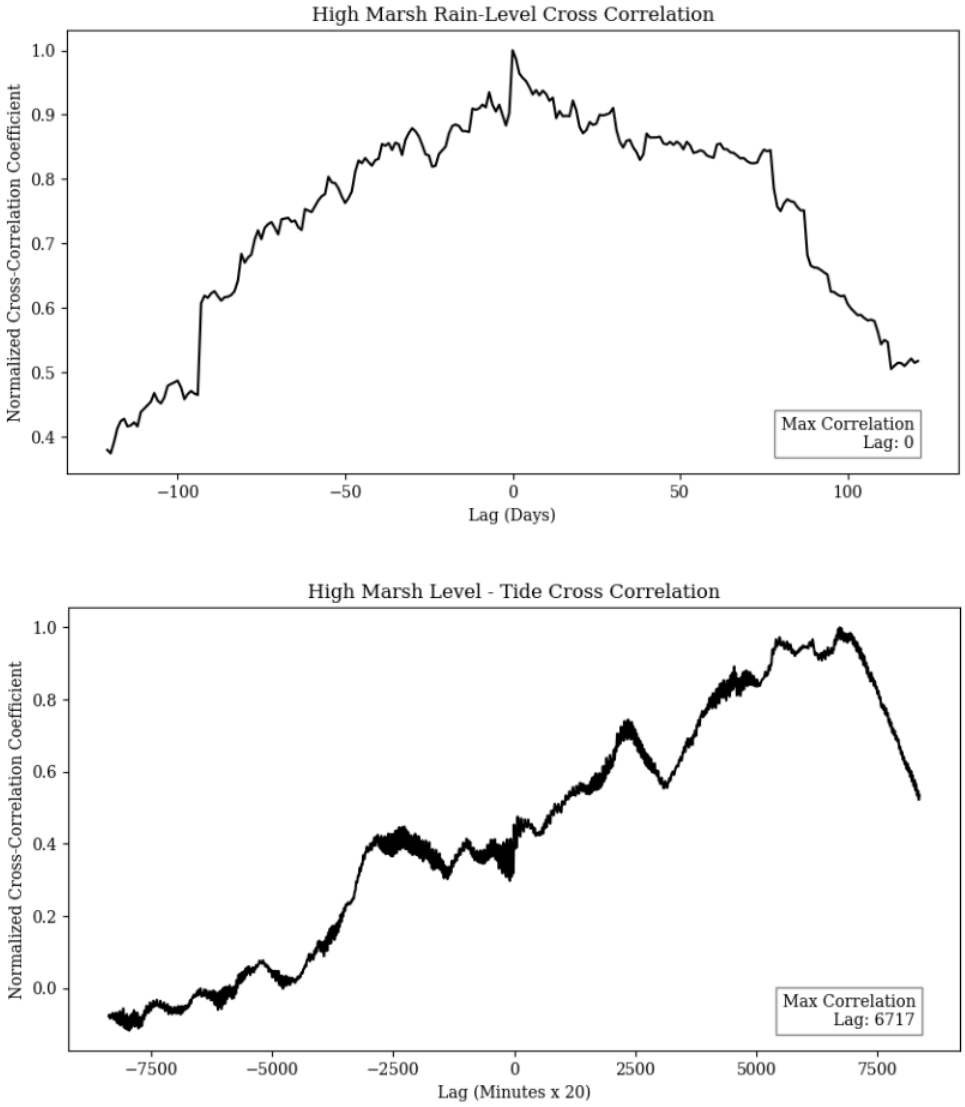


Figure 33. Cross correlation of Dunn Sound West tides and daily precipitation with high marsh groundwater level.

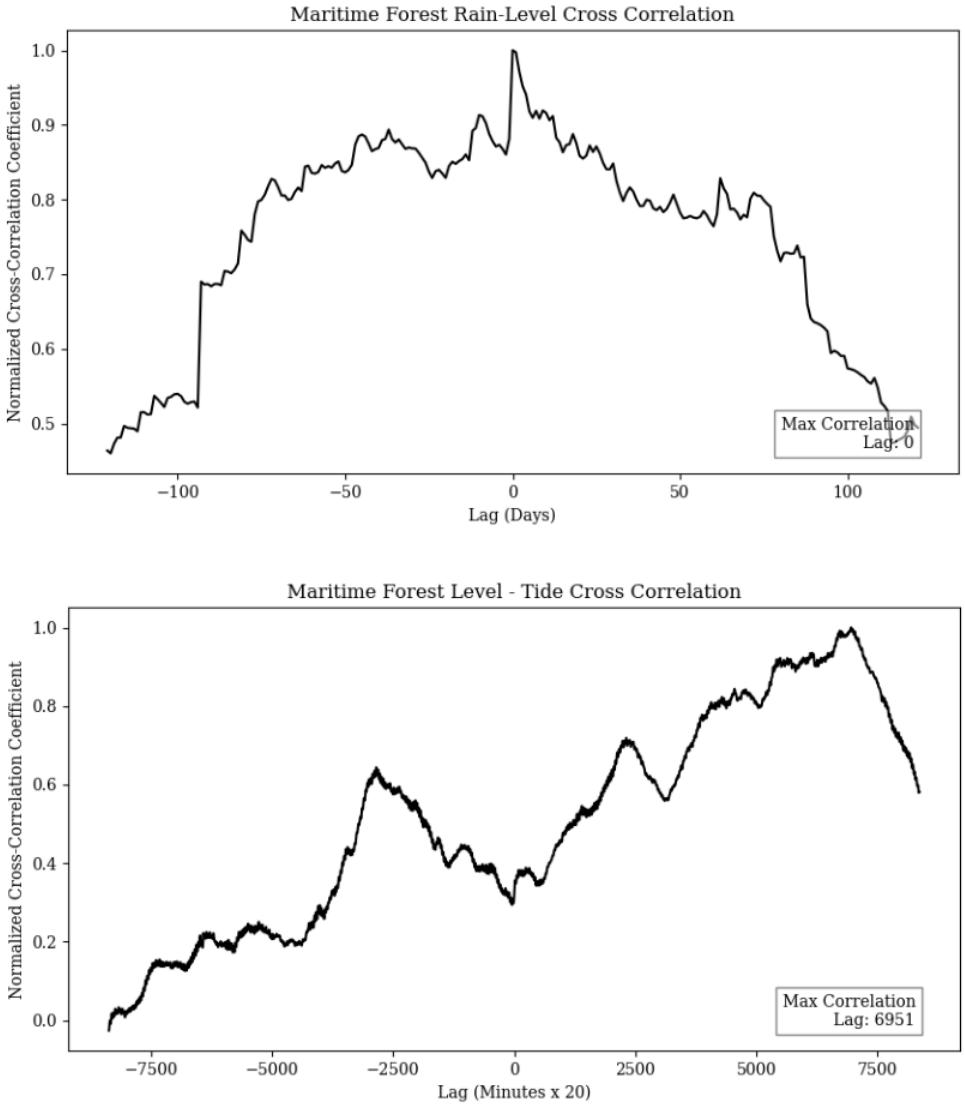


Figure 34. Cross correlation of Dunn Sound West tides and daily precipitation with maritime forest groundwater level.

4.6 Darcy Flow Calculations

Estimations of groundwater flow from the maritime forest to the low marsh were determined in two subsets. The first calculation estimated the flow between the maritime forest and the high marsh. The second between high marsh and low marsh. Due to inconsistencies within the maritime forest well timeseries, only the continuous and reliable water table elevations were utilized.

Between the high marsh and low marsh, the influence of tides was evident. Spring tides amplified the transport between the low and high marsh (Figure 36). Instances of negative Q values, representing a hydraulic gradient reversal back towards the island, were observed during these periods of enhanced tidal amplitude. An average flow rate of 11.45 cm^3 cm^{-2} day^{-1} was calculated for this section. Flow rates were varied between the maritime forest and high marsh. A pattern of increased flow with precipitation events was observed (Figure 35). Reversals of the hydraulic head were less frequent and were observed only during spring tidal cycles and storm-driven tides. Large precipitation events and the associated storm tides amplified the volume of estimated exchange between the island and the salt marsh. The average flow of groundwaters between maritime forest and high marsh well was calculated to be 12.50 cm^3 cm^{-2} day^{-1}.

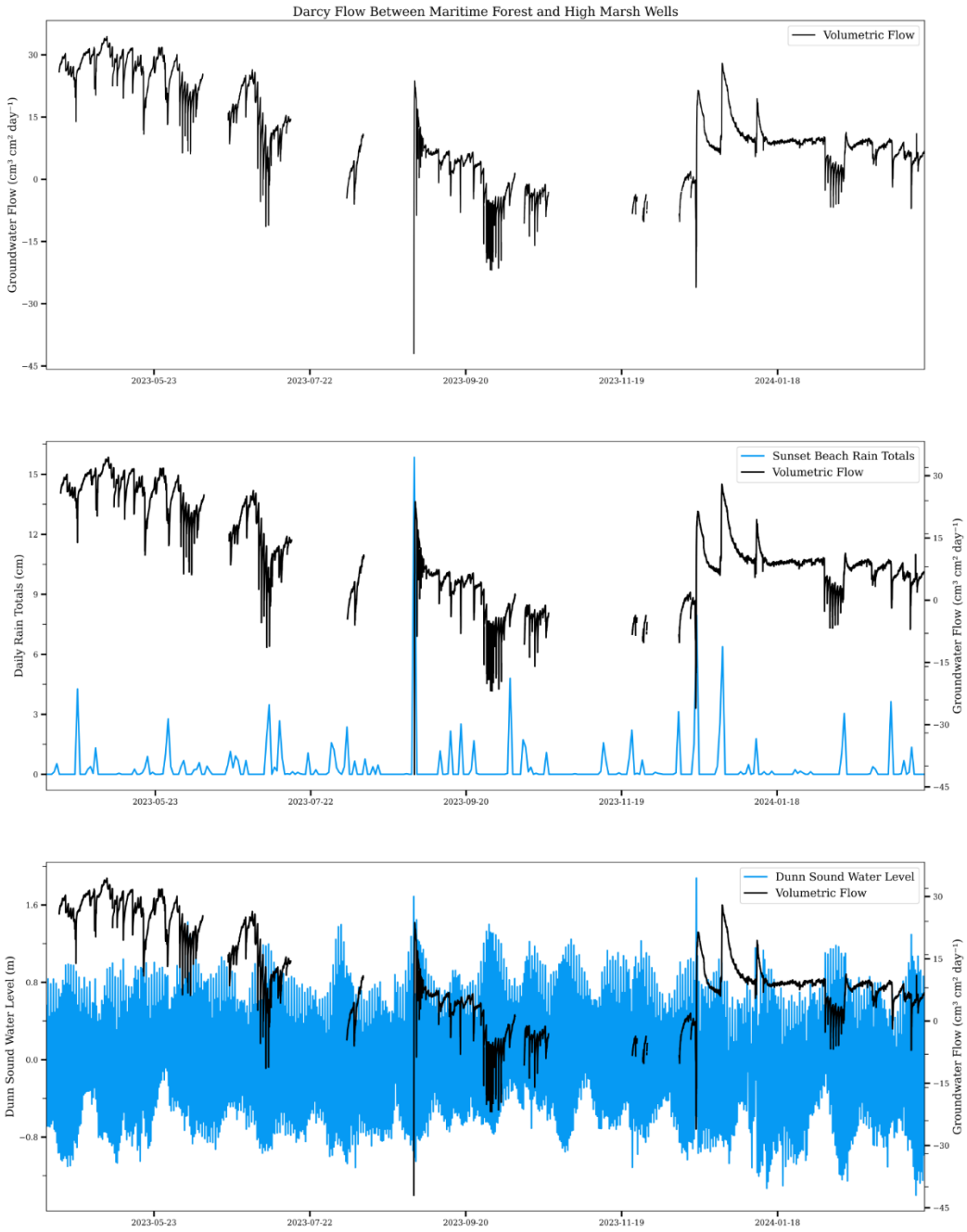


Figure 35. Calculated groundwater flow between wells MF and HM. Large precipitation enhanced the transport of waters off the island, while spring tides and storm tides reversed transport, pushing salt marsh porewaters towards the island.

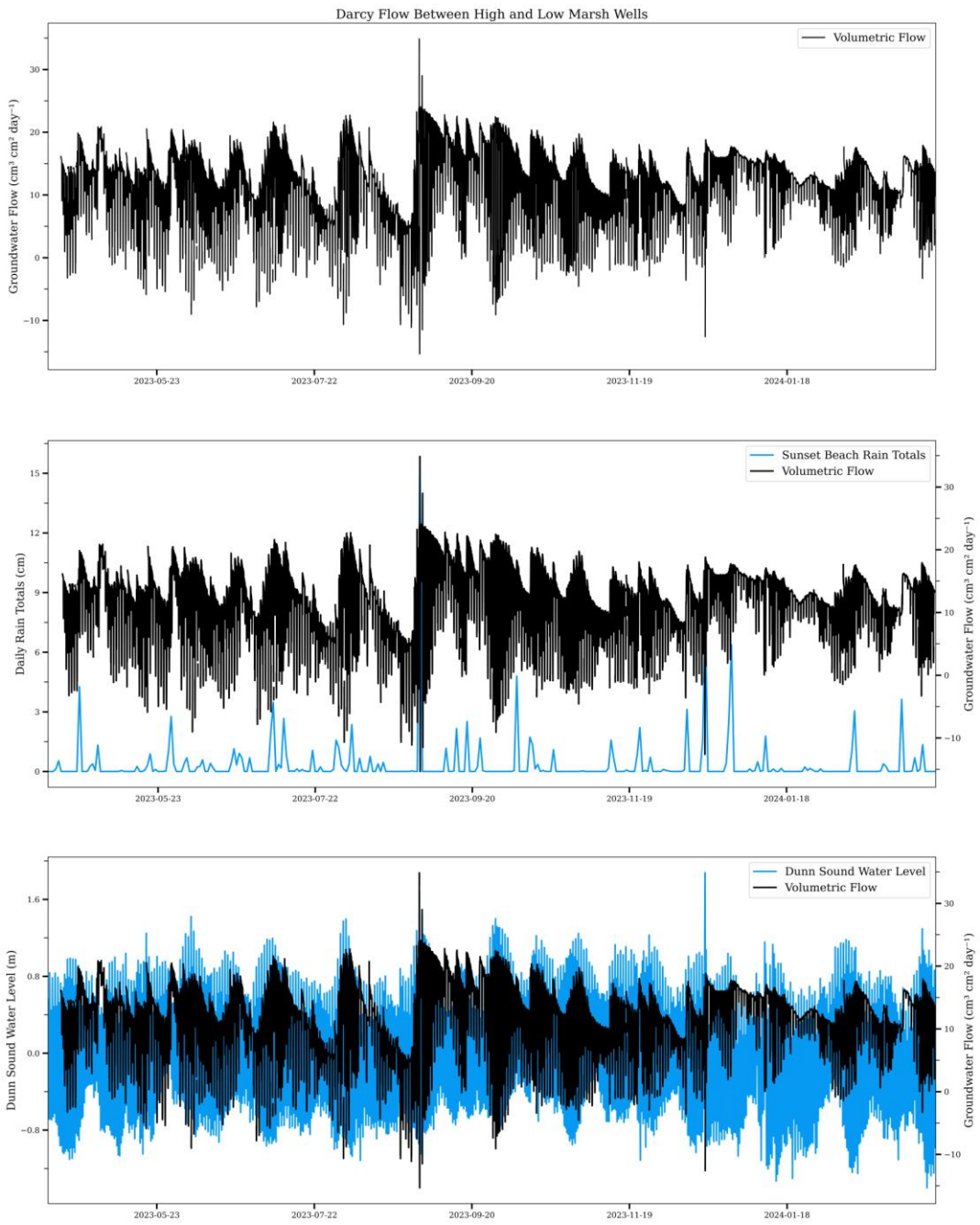


Figure 36. Calculated groundwater flow between wells LM and HM. Precipitation exerted less influence on groundwater transport between wells. Frequent excursions of flow rates to negative values indicate the tidal nature of transport between these wells.

5. Discussion

5.1 Electrical Resistivity

A horizon of high electrical resistivity was consistently observed between 0.2 - 1 meters below the marsh surface in transects Y and Z. This unit correlates with deposits of permeable, clean sands observed in the cores adjacent to these transects, C3 and C5 (Figures 37 and 38). Therefore, any changes in the observed resistivity of this unit are interpreted as changes in the salinity of water mass. In this regard the time series resistivity surveys from transect Y and Z support the conclusion that clean sand deposits within the marsh platform act as conduits for waters from the freshwater lens to penetrate into the marsh. This conclusion is also evidenced by the August 2021 transect Y survey where, despite a large precipitation event saturating the environment, the dispersion of higher resistivity porewater remained constricted to the highly permeable sand layer adjacent to the island, suggesting horizontal mixing between island-derived freshwater and marsh-derived saltwater is the dominant process, not vertical infiltration. These data support the conclusion that clean sand deposits left from coastal processes such as overwashing and relic beach ridges buried by modern salt marshes, act as preferential pathways for island-derived groundwater to enter the shallow salt marsh platform.

Winter months were characterized by higher overall resistivities than summer months, suggesting a greater fraction of freshwater within the marsh platform when ecological productivity is low. This trend is consistent with salt concentrating processes

including increased evapotranspiration rates, and ecological demand terms in the overall water budget – when these processes are maximum, freshwater consumption is maximum and resistivity rises. The continuity of the horizontal, high resistivity band in transect Y tomograms, further supports the conclusion that vertical infiltration and percolation of overlaying waters into the marsh platform is not as significant as horizontal flow. Personal observations made in the field corroborate this finding as neither tidal floodwaters nor fresher stormwaters penetrated the marsh platform even several days past an event. Direct random measurements of these pooled waters revealed salinities that were not consistent with well waters at the same time. This suggests the anisotropic nature of fines such as mud and silt are clogging pore spaces within sandy surficial sediments, greatly reducing vertical flow. Tidal pumping was not observed in the ER data despite conducting surveys at various tidal stages. However, evidence of the tidal signal propagating into the high marsh at well HM, suggests groundwaters could be tidally modulated within the ER tomograms.

While the interpretation of ER time series herein are corroborated by the geologic description of the site, it is necessary to recognize the limitations of electrical resistance methods for discerning hydrogeologic processes within each timeseries. While the assumption of a saturated marsh environment is valid, the presence and varying degree of chloride ions in porewater creates difficulty interpreting discrete resistance measurements as unique parcels of groundwater (Table 9). It was also observed that throughout each timeseries, despite varying tidal stages, pre-survey precipitation, and groundwater well salinities, no discernable relationship between average survey resistivity and these factors that should affect the electrical resistance could be found (Figures 39-41). ERT has

proved to be a valuable method for low impact mapping of subsoil structures within the saltmarsh, provided interpretation focuses on the variety of permeability characteristics associated with the stratigraphy and how the conceptual freshwater lens model would interact in such conditions. The data provided reveals the limits of interpretation with this method suggesting postulations concerning residence time and flushing of the system between the barrier island and high marsh are not founded given the low soil resistivities observed. Subtle changes in porewater salinity associated with tidal pumping may not be detectable with the ER method.

Table 9. Water samples of various salinity and representative electrical resistance at 25 °C. Table adapted from Wiater 2012.

Water Sample	Resistivity (Ω-m)	Salinity (ppt)
Distilled Water	5000	0
Rain Water	200	0.013
Tap Water	30	0.15
River Water	25	0.2
Brackish Water	2	2.7
Coastal Sea Water	0.3	20.6
Oceanic Sea Water	0.2	25.5

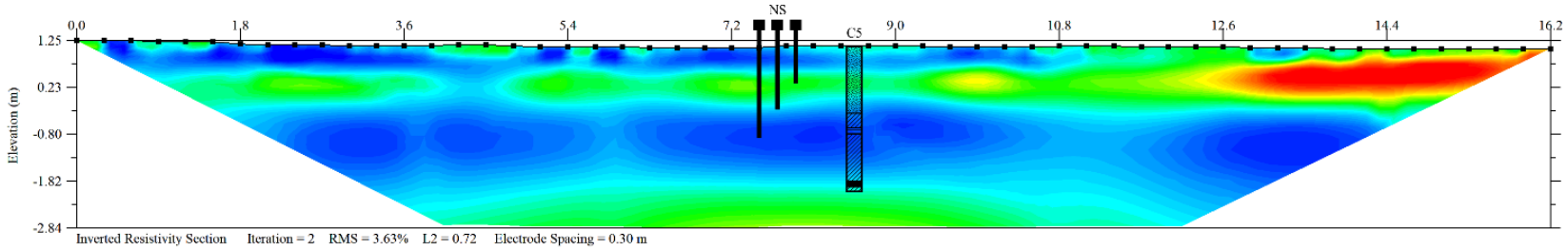


Figure 37. ER tomogram from transect Y with nested well series and core C5 imposed to show relative depths.

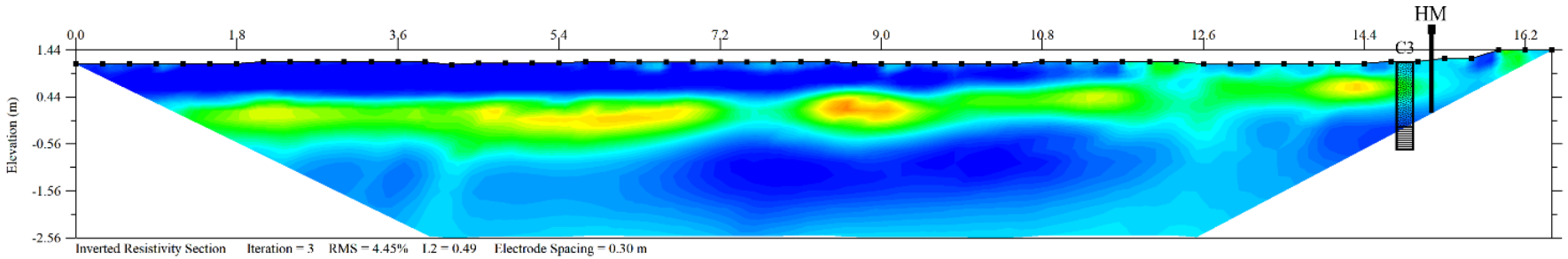


Figure 38. ER tomogram from transect Z with well HM and core C3 imposed to show relative depths.

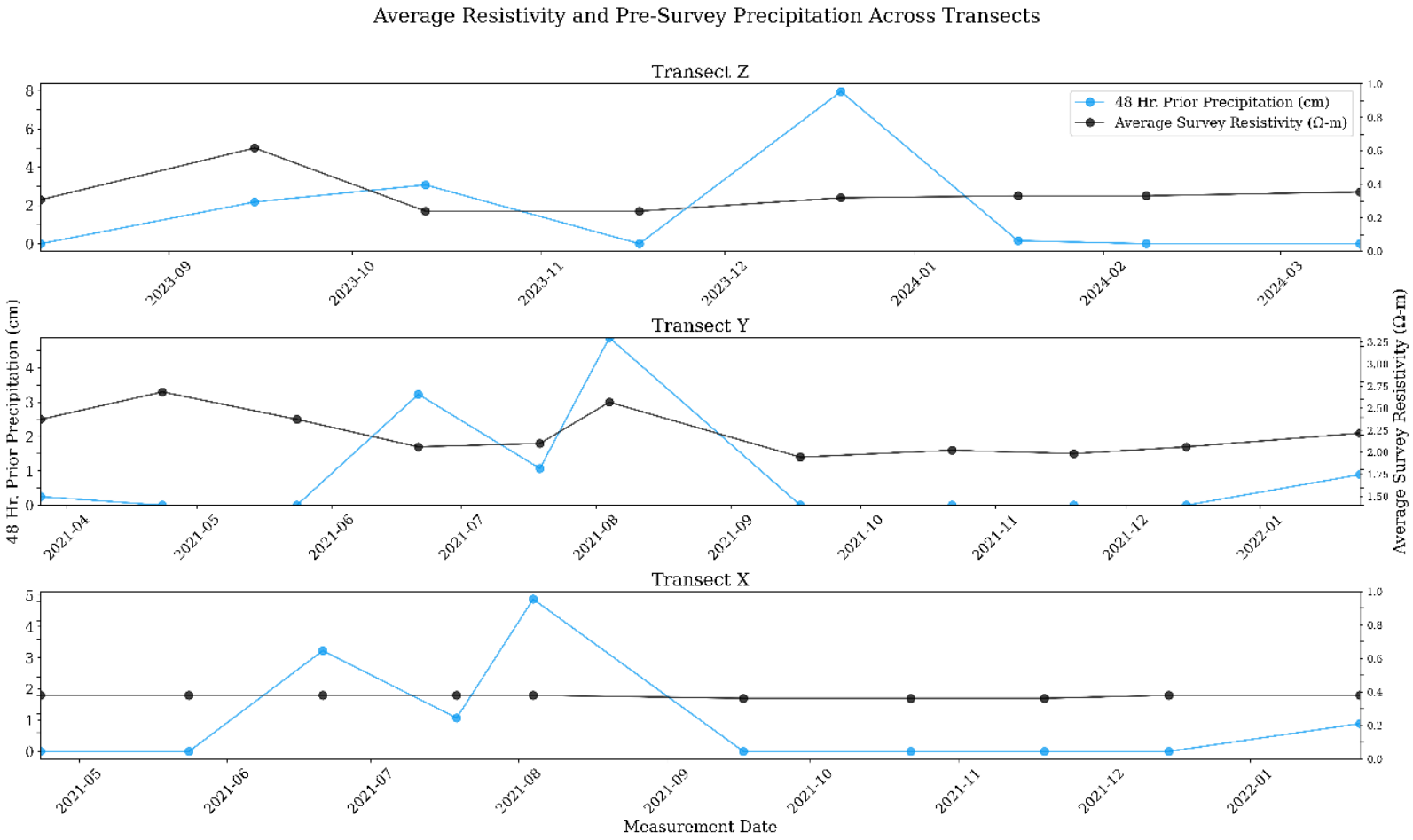


Figure 39. Timeseries comparison of average electrical resistance across all ER surveys with precipitation totals from Sunset Beach, NC 48 hours prior to surveying date.

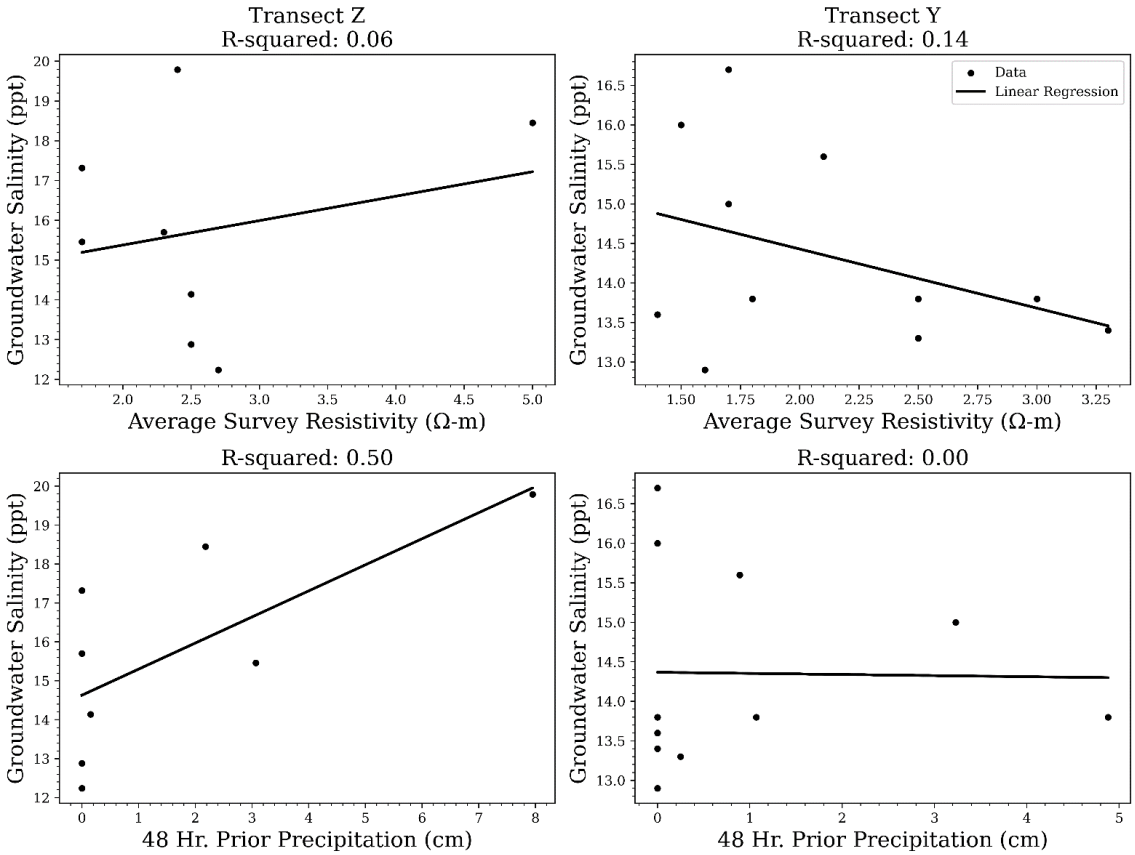


Figure 40. Linear regression results between precipitation, average survey resisitivty, and observed groundwater salinity on transects X and Y.

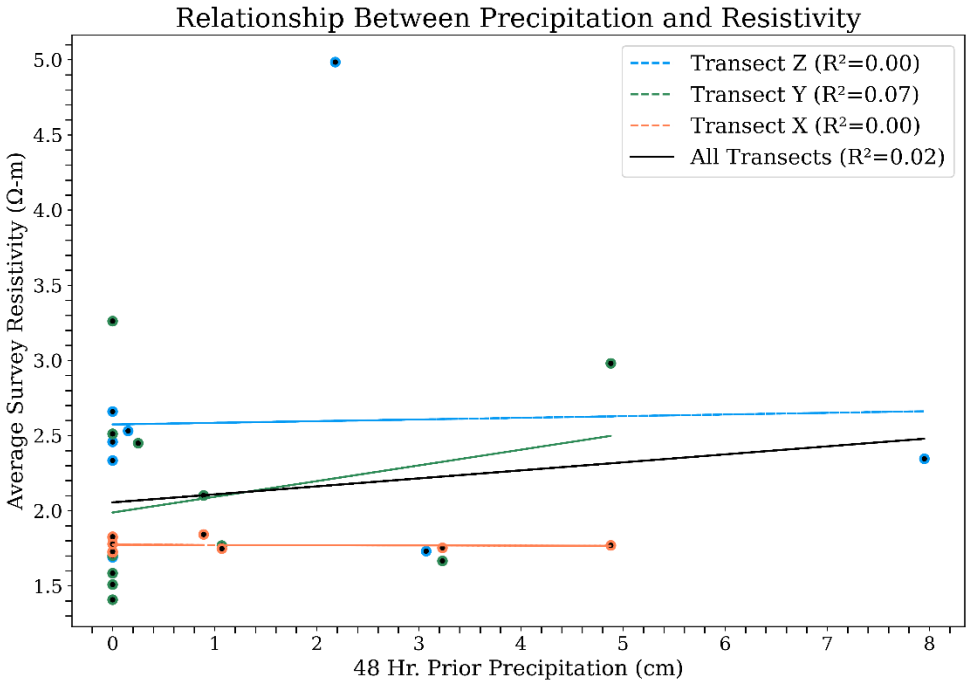


Figure 41. Linear regression results of average tomogram resistivity and precipitation totals from Sunset Beach, NC 48 hours prior to survey date. Results indicate the saturation of back barrier sediments is not resolvable by comparing soil resistance.

5.2 Groundwater Level Signal Analysis

All wells displayed the expected seasonal variation of groundwater temperature. Water table elevations in the low marsh are controlled by the tidal water level in Dunn Sound with a lag time between surface waters and groundwaters of approximately 20 minutes or less. The strong correlation between water table height and tidal stage in addition to eIMF 5 containing the largest variance ratio and a tidal frequency supports this conclusion. Further evidence of tidal control of groundwaters at this well was observed in salinity values at the low marsh. A constant saline environment was measured throughout the time-series with no major deviation during precipitation events. Water table elevations in the high marsh are influenced by a combination of tides and precipitation, with precipitation exerting a stronger influence. Modal decomposition revealed eIMF 10 which had the greatest influence on the signal, contains a frequency corresponding to the precipitation frequency of rainfalls greater than 1 cm on the island (Table 10). EEMD analysis did not reveal a tidal component in the high marsh, despite a fortnightly tide trend visible within the water level data. Further evidence of tidal influence was observed in the groundwater salinity record. During major storms, large tides raised groundwater salinity in the high marsh to observed maxima. Spring tides also appeared to spike salinity for a short duration. These smaller salinity spikes associated with fortnightly tides could be artifacts of stratified well fluid traversing the sensor face, yet the vertical movement of well fluid corresponding to the tides is also evidence of tidal modulation. The discrepancy between visual and statistical analyses of tidal components in the high marsh could indicate the limitations of the EEMD method for resolving groundwater signals. Discontinuous temporal and spatial propagation of the tidal force

through salt marsh sediment and associated lag times could be masking the signal. The periodic nature of observed tidal influence may not be consistent enough to appear as a modal function in decomposition. Observed water table elevations in the maritime forest were controlled by precipitation. High variance ratio eIMFs aligning with the precipitation frequency on the island in both subsets support this observation.

Table 10. Frequency and description of rainfall events from Sunset Beach, NC.

Event Description	Calculated Frequency
Any recorded precipitation accumulation	0.007
Precipitation exceeding 1cm in accumulation	0.004

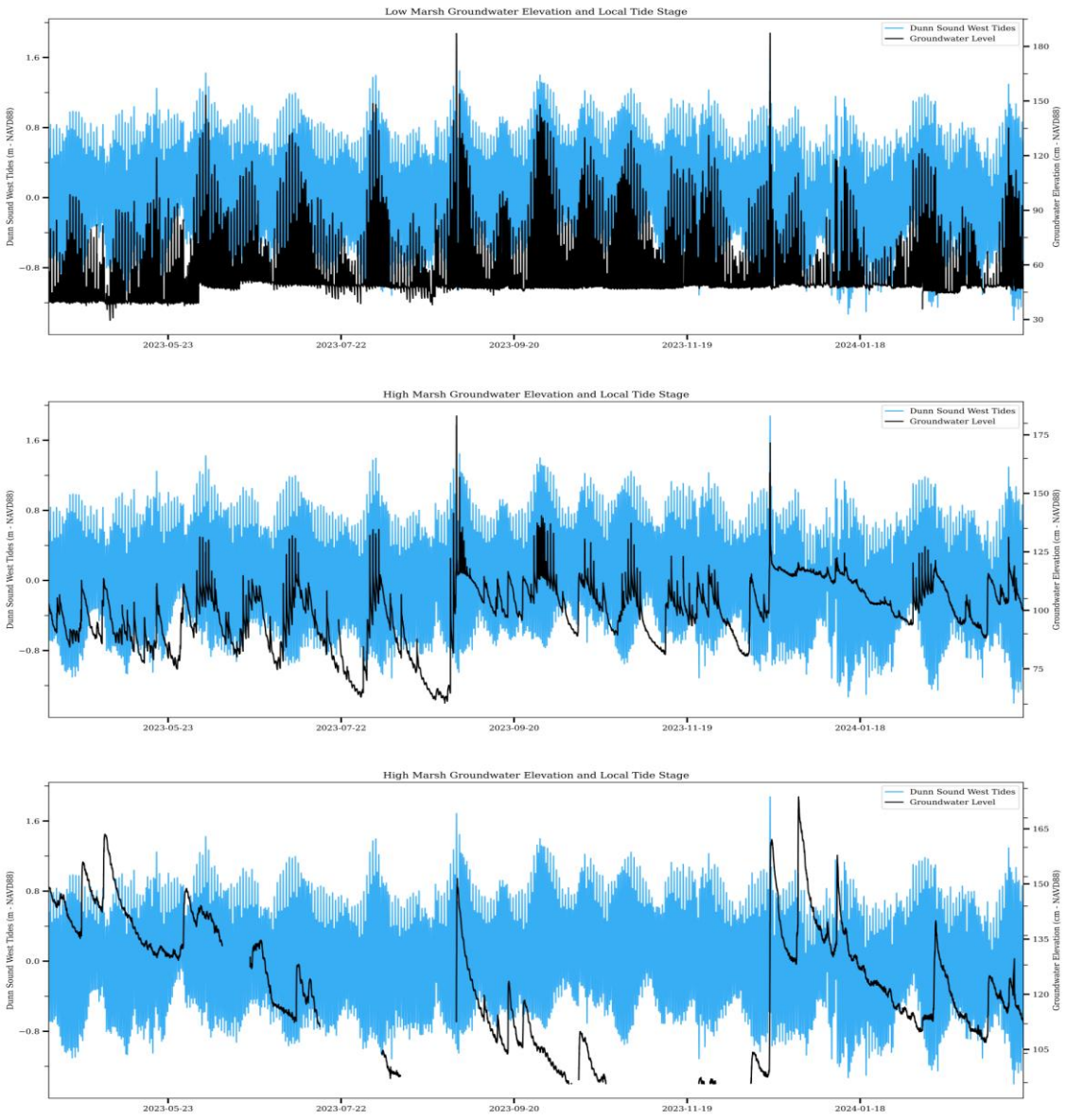


Figure 42. Water table elevation in wells LM, HM, MF, and water levels in Dunn Sound West. Correlation with tidal water level decreases with increasing distance from the sound.

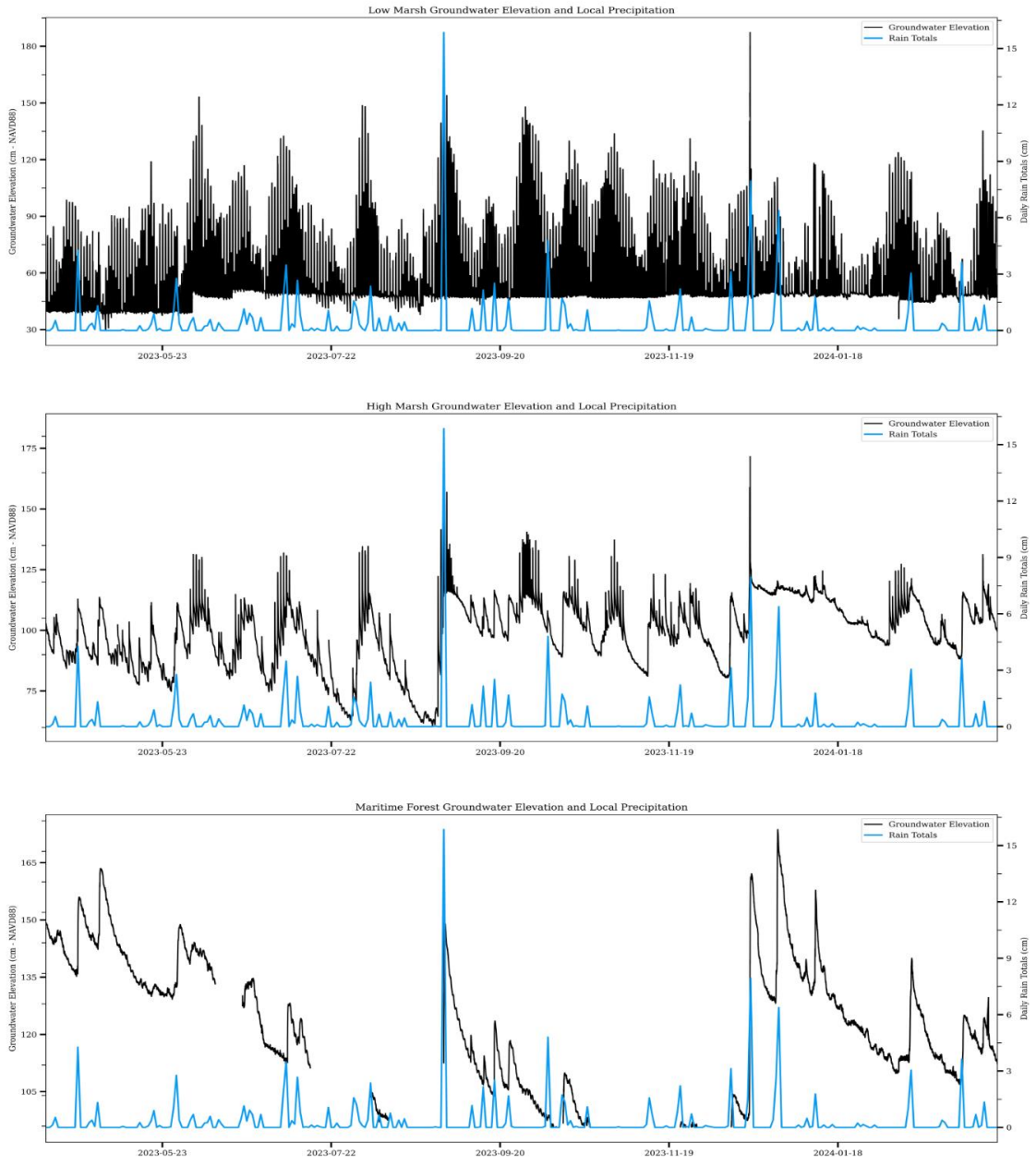


Figure 43. Water table elevation in wells LM, HM, MF, and daily precipitation totals from Sunset Beach, NC. Major precipitation events were observed as pulses in water table elevation throughout each well.

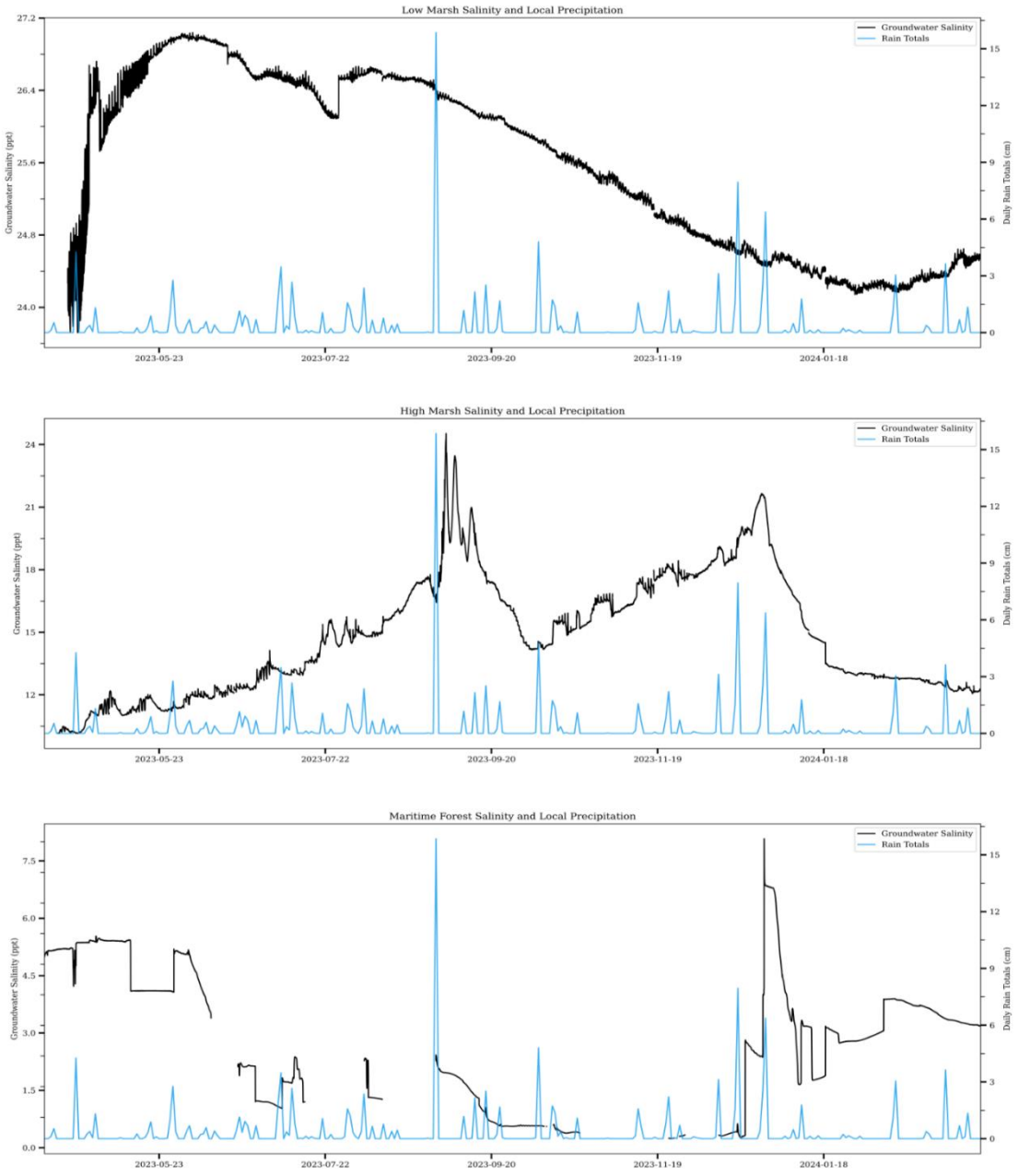


Figure 44. Groundwater salinity in wells LM, HM, MF and Sunset Beach, NC daily precipitation totals.

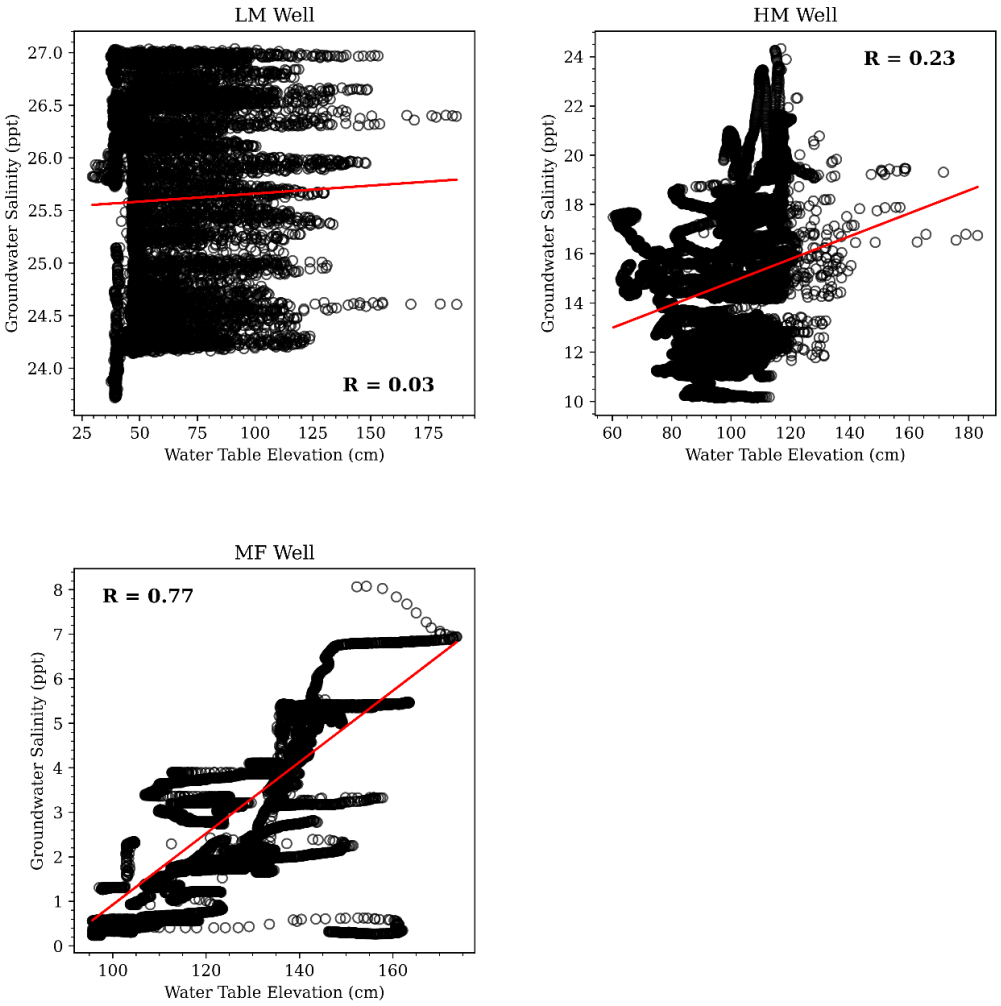


Figure 45. Linear regression models of groundwater level and salinity within each well located along transect Z. Rows containing missing values from either level or salinity were removed prior to analysis. The line of best fit is indicated in red and the Pearson correlation coefficient R is listed in each figure.

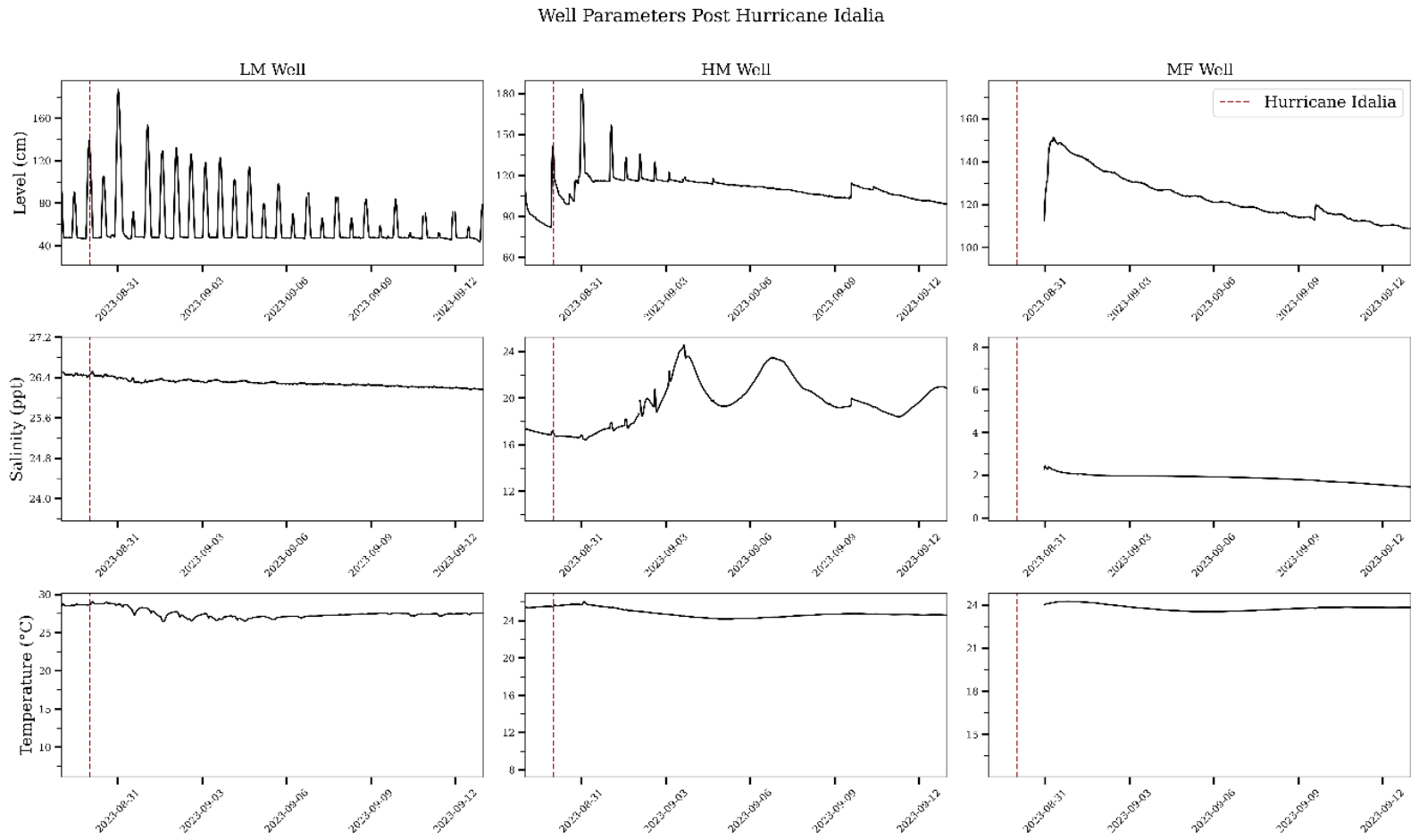


Figure 46. Recorded groundwater parameters following Hurricane Idalia, which passed approximately 25 nautical miles southeast of Waties Island, SC as a tropical storm on August 30th, 2023.

5.3 Sediment Analysis and Darcy Flow

Permeameter tests indicated that increasing the fraction of fines within an otherwise highly permeable sandy sediment drastically reduces the hydraulic conductivity of the unit. This result is consistent with the interpretation of the ER data that there are preferential pathways for fresh, island-derived groundwaters to enter the salt marsh.

Groundwater flow rates between the maritime forest and high marsh (wells MF and HM) reflected the periodicity of precipitation events on the island. Each precipitation event is represented by a pulse of increased discharge to the high marsh for a short duration following the initial event (Figure 43). However, spring tides significantly reduced or reversed freshwater transport to the high marsh back to the island, which suggests the freshwater lens experiences a squeezing effect during these higher tides. Flow rates between the high and low marsh (wells HM and LM) indicate the presence of horizontal tidal pumping. The hydraulic gradient is periodically reversed during spring tides forcing salty low marsh porewaters towards the island (Figure 36). Following the December 17th , 2023, nor'easter, tidal modulation of the water level within this salt marsh was notably low despite the elevated tidal amplitude, which can be interpreted as enhanced runoff from the freshwater lens dampening the tidal pumping in the marsh platform.

Estimations of groundwater transport along a two-dimensional transect are difficult and perhaps represent an oversimplification of the system. However, these estimations verify and model the perceived drivers of subterranean flow. Xin et al. (2022) outlined the limitations of such well arrays and the results here can be interpreted as

maximum conceptual flow rates between ecotones. Multiple methods have been utilized to quantify porewater transport within and from the salt marsh such as Darcy's Law calculations, seepage meters, isotope tracers, and numerical models (Harvey and Odum 1990; Tobias et al 2001; Dias et al. 2016; Guimond and Tamborski 2021). The variety of approaches attempting to describe groundwater exchange highlights the crucial role this physical process imparts on biogeochemistry, nutrient budgets in the coastal ocean, and the biology of estuarine and coastal ecosystems. Comparison of the average groundwater flow rates calculated along transect Z with those derived from other studies indicates that this simplistic model is suitable for rough estimations of porewater flux between points (Figure 47).

Table 11. Comparison of calculated groundwater fluxes from regional sites.

Location	Sediment Type	Hydraulic Conductivity (cm/s)	Observed Groundwater Flow (cm^3/cm^2 day)	Method	Reference
Waties Island, SC	Well Sorted Fine Sand	0.01	11.45 - 12.5	Darcy's Law	This Study
Lower Chesapeake Bay, VA	High Marsh Root Zone Sediments	0.0002 - 0.00126	0.2 - 1	Darcy's Law	Harvey and Odum 1990
Lower Chesapeake Bay, VA	High Marsh Sands	0.0002 - 0.00173	-8 - 80	Darcy's Law	Tobias et al. 2001
Lower Chesapeake Bay, VA	High Marsh Sands	-	0.6 - 22.6	Salt Balance	Tobias et al. 2001
Virginia Coast Reserve, VA	Low Marsh Root Zone Sediment	-	0.012	Darcy's Law	Chambers et al. 1992
Virginia Coast Reserve, VA	High Marsh Root Zone Sediment	-	2.8	Salt Balance	Nuttle and Harvey 1995
St. Jones NERR, DE	Sandy Creekbank Interface	-	22	Seepage Meter	Guimond and Tamborski 2021
Folly Beach, SC	Low Marsh Root Zone Sediment	-	54	Ra-224 | Th-228 Sediment Equilibrium	Dias et al. 2016
Pritchard's Island, SC	Upper 20 cm of High Marsh Sediment	0.007	109	Seepage Meter and Darcy's Law	Osgood 2000
Virginia Coast Reserve, VA	Upper 20 cm of High Marsh Sediment	0.021	102	Seepage Meter and Darcy's Law	Osgood 2000

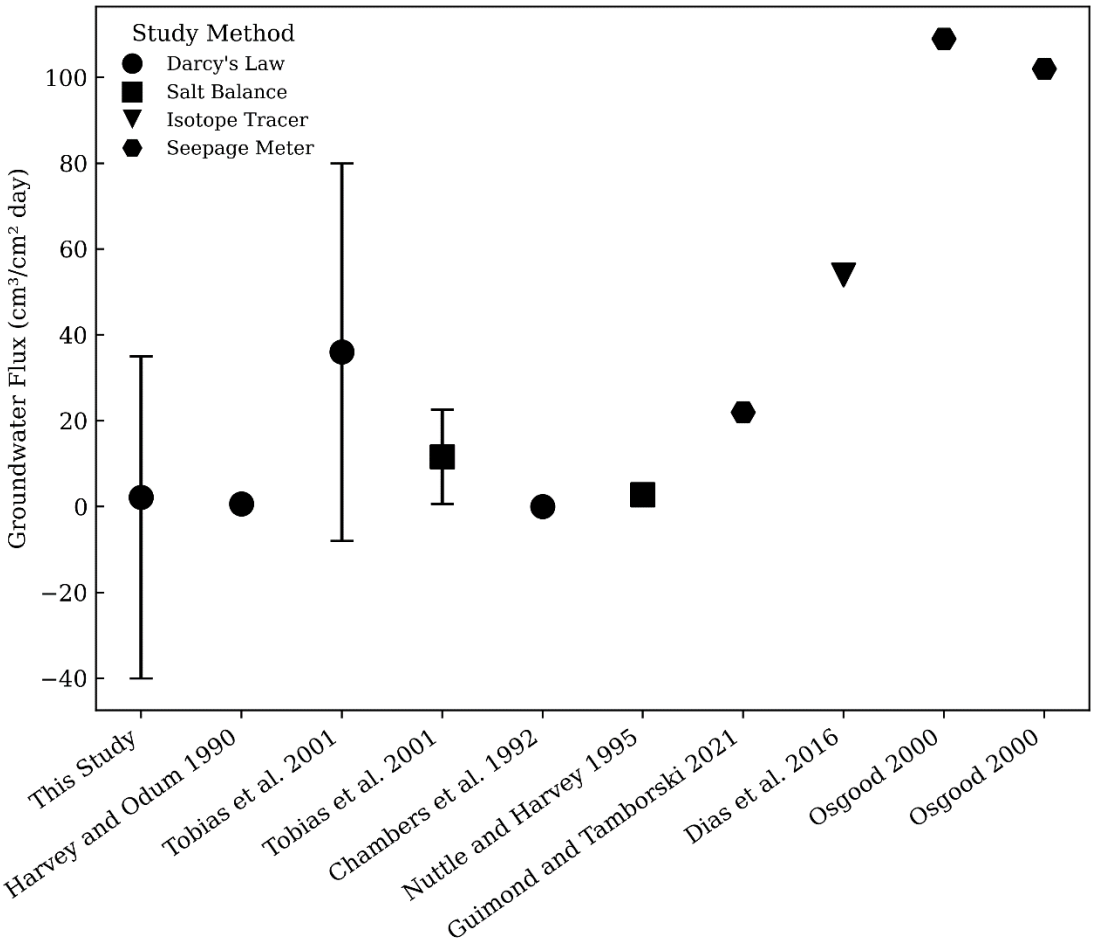


Figure 47. Comparison of groundwater flow rates within and between estuarine and upland systems. Markers represent average values or reported value of study, whiskers indicate total reported range.

6. Conclusion

The calculated rates of groundwater flow at Waties Island are similar to those observed on other barrier islands in the region, indicating the permeability characteristics present at the surface of the water table are comparable. Despite the island exhibiting the same foundational geology of Holocene barriers, the presence of spatially discontinuous layers of sand in the high and low marsh directly affected the observed mixing and transport of groundwaters between island and marsh environments.

Precipitation events were observed to be the main hydrologic driver at the high marsh well, with tidal modulation of the groundwaters here occurring during spring tide cycles. Water table elevations in the low marsh are directly linked to the surface water levels in the adjacent estuary. Increased tidal amplitude during spring and storm driven tides propagated the tidal signal far into the marsh platform, to the boundary between maritime forest and high marsh. During storm events, this surge of saline porewaters through the sediment package towards the island was counteracted by an elevated freshwater lens which increased transport of fresh porewaters towards the marsh. However, on spring tides and storm-associated tides that were not followed by rainfall on the island, an increase in groundwater salinity was observed at the high marsh, suggesting these events have the capacity to increase mixing and salinization at the fringes of the freshwater lens.

Time-series electrical resistivity tomography surveys have further solidified this technique as a method to map groundwater provinces in coastal environments in a relatively efficient, and non-invasive manner. Additionally, statistical decomposition of water table elevations has shown promise in delineating the core hydrologic drivers in these coastal aquifers. However, further refinement for this method is needed to account for the impedance of the signal propagating through the environment. While estimations of two-dimensional groundwater transport using Darcy's Law may appear to be simplistic and reductionist, they provide further insight as to how physical controls such as precipitation and tides interact with the freshwater lens system.

The results outlined here highlight the importance of tailored hydrogeologic studies on barrier island systems which recognize the system's unique parameters and susceptibility to environmental change. Waties Island is a unique structure, existing between tidally dominated barriers to the south and wave dominated barrier features to the north. These governing geomorphological processes undoubtedly affect freshwater lens hydrogeology by distributing over wash fans and shifting inlets and tidal creeks through the sediment package. Furthermore, human modification of the freshwater lens through the construction of roads, homesites, shallow wells, and seawalls may hold ramifications for freshwater and nutrient transport between the island and back barrier environment. Although it is not believed that the freshwater lens system on Waties Island is linked to larger aquifer units below, the presence of Little River Inlet, an regularly maintained and dredged channel to the north, raises the risk of saltwater intrusion into freshwater resources if confining units are breached or significantly thinned (Peters et al., 2022).

This study has elucidated the complex relationship between coastal geomorphic processes, foundational geology of barrier islands, and the hydrogeologic cycle, particularly in the transport and mixing of groundwaters between the island and back-barrier environments. Identifying the preferential pathways created by overwash fans and barrier island morphology in the salt marsh sediment package emphasizes the importance of mapping local geology to properly parameterize model-based studies to characterize the freshwater lens on these barrier systems. Continuing efforts studying this hydrogeologic interface should focus on event scale effects on the freshwater lens. We observed a period of "recharge" in well HM where hydrologic parameters seemed to return to a steady state following a large tidal or precipitation event. This finding underscores the sensitivity of this system to hydrologic events, which could shift in frequency and intensity in a changing climactic future. Understanding how the freshwater lens will respond to these pressures is essential to forecasting the response of the subterranean estuary, determining whether the range of biogeochemical interaction will grow or shrink in magnitude and spatial range. Finally, rapid shifts in the hydrogeologic regime associated with these events have the potential to shift ecological baselines, jeopardizing the ecological and societal value these islands provide.

7. References

Anderson Jr, W.P.A., 2002. Aquifer Salinization from Storm Overwash. Journal of Coastal Research 18, 413–420.

ASTM International, 2019. D2434 − 19 Standard Test Method for Permeability of Granular Soils (Constant Head).

Blott, S.J., Pye, K., 2001. GRADISTAT: a grain size distribution and statistics package for the analysis of unconsolidated sediments. Earth Surface Processes and Landforms 26, 1237–1248. https://doi.org/10.1002/esp.261

Carter, M., 2015. Characterization of Groundwater Discharge in a Back Barrier Tidal Creek. Electronic Theses and Dissertations https://digitalcommons.coastal.edu/etd/7/

Chambers, R., Harvey, J., Odum, W., 1992. Ammonium and Phosphate Dynamics in a Virginia Salt Marsh. Estuaries and Coasts 15, 349–359. https://doi.org/10.2307/1352782

Chen, Y.-C., Kao, S.-P., Chiang, H.-W., 2013. Defining an estuary using the Hilbert-Huang transform. Hydrological Sciences Journal 58, 841–853. https://doi.org/10.1080/02626667.2013.779776

Crain, C., Silliman, B., Bertness, S., Bertness, M., 2004. Physical and biotic drivers of plant distribution across estuarine salinity gradients. Ecology 85, 2539–2549. https://doi.org/10.1890/03-0745

Crosset, K., Ache, B., Pacheco, P., Haber, K., 2013. National Coastal Population Report: Population Trends from 1970 to 2020. NOAA: National Oceanic and Atmospheric Administration.

D18 Committee, n.d. Test Method for Permeability of Granular Soils (Constant Head). https://doi.org/10.1520/D2434-19

Dias, D.M.C., Copeland, J.M., Milliken, C.L., Shi, X., Ferry, J.L., Shaw, T.J., 2016. Production of Reactive Oxygen Species in the Rhizosphere of a Spartina-Dominated Salt Marsh Systems. Aquatic Geochemistry 22, 573–591. https://doi.org/10.1007/s10498-016-9307-1

Farhad Alizadeh, Gharamaleki, A.F., Jalilzadeh, M., Akhoundzadeh, A., 2020. Prediction of River Stage-Discharge Process Based on a Conceptual Model Using EEMD-WT-LSSVM Approach. Water Resources 47, 41–53. https://doi.org/10.1134/S0097807820010066

Gardner, L.R., 2009. Assessing the accuracy of monitoring wells in tidal wetlands. Water Resources Research 45. https://doi.org/10.1029/2008WR007626

Gardner, L.R., 2007. Role of stratigraphy in governing pore water seepage from salt marsh sediments. Water Resources Research 43. https://doi.org/10.1029/2006WR005338

Gardner, L.R., 2005. Role of geomorphic and hydraulic parameters in governing pore water seepage from salt marsh sediments. Water Resources Research 41. https://doi.org/10.1029/2004WR003671

Gardner, L.R., Porter, D.E., 2001. Stratigraphy and geologic history of a southeastern salt marsh basin, North Inlet, South Carolina, USA. Wetlands Ecology and Management 9. https://doi.org/10.1023/A:1012060408387

Gardner, Leonard R, Reeves, H.W., 2002. Spatial patterns in soil water fluxes along a forest-marsh transect in the southeastern United States. Aquatic Sciences 64. https://doi.org/10.1007/s00027-002-8062-0

Gardner, Leonard R., Reeves, H.W., 2002. Seasonal patterns in the soil water balance of a Spartina marsh site at North Inlet, South Carolina, USA. Wetlands 22, 467–477. https://doi.org/10.1672/0277-5212(2002)022[0467:SPITSW]2.0.CO;2

Gong, Y., Wang, Z., Xu, G., Zhang, Z., 2018. A Comparative Study of Groundwater Level Forecasting Using Data-Driven Models Based on Ensemble Empirical Mode Decomposition. Water 10, 730. https://doi.org/10.3390/w10060730

Griffiths, D.H., Barker, R.D., 1993. Two-dimensional resistivity imaging and modelling in areas of complex geology. Journal of Applied Geophysics 29, 211–226. https://doi.org/10.1016/0926-9851(93)90005-J

Guimond, J., Tamborski, J., 2021. Salt Marsh Hydrogeology: A Review. Water 13, 543. https://doi.org/10.3390/w13040543

Harvey, J.W., Odum, W.E., 1990. The influence of tidal marshes on upland groundwater discharge to estuaries. Biogeochemistry 10, 217–236. https://doi.org/10.1007/BF00003145

Holt, T., Greskowiak, J., Seibert, S.L., Massmann, G., 2019. Modeling the Evolution of a Freshwater Lens under Highly Dynamic Conditions on a Currently Developing Barrier Island. Geofluids 2019, e9484657. https://doi.org/10.1155/2019/9484657

Holt, T., Seibert, S.L., Greskowiak, J., Freund, H., Massmann, G., 2017. Impact of storm tides and inundation frequency on water table salinity and vegetation on a juvenile barrier island. Journal of Hydrology 554, 666–679. https://doi.org/10.1016/j.jhydrol.2017.09.014

Huang, N., Shen, Z., Long, S., Wu, M.L.C., Shih, H., Zheng, Q., Yen, N.-C., Tung, C.-C., Liu, H., 1998. The empirical mode decomposition and the Hilbert spectrum for nonlinear and non-stationary time series analysis. Proceedings of the Royal Society of London. Series A: Mathematical, Physical and Engineering Sciences 454, 903–995. https://doi.org/10.1098/rspa.1998.0193

Klute, A., Dirksen, C., 1986b. Hydraulic conductivity and diffusivity: laboratory methods, in: Klute, A. (Ed.), Methods of Soil Analysis, Part 1: Physical and Mineralogical Methods. American Society of Agronomy - Soil Science Society of America, Madison, Wisconsin, U.S.A., pp. 687–734.

Krumbein, W.C., Monk, G.D., 1943. Permeability as a function of the size parameters of unconsolidated sand. Transactions of the American Institute of Mining, Metallurgical and Petroleum Engineers. 151, 153–163.

Ledoux, J., Alexander, C., Meile, C., 2013. Delineating the drivers of groundwater flow at a back barrier island – marsh transect in coastal Georgia. Electronic Theses and Dissertations. https://esploro.libs.uga.edu/esploro/outputs/graduate/Drivers-of-groundwater-flow-at-a-back-barrier-island-marsh-transect-in-coastal-Georgia/9949333740602959

Liang, B.-X., Hu, J.-P., Liu, C., Hong, B., 2020. Data pre-processing and artificial neural networks for tidal level prediction at the Pearl River Estuary. Journal of Hydroinformatics 23, 368–382. https://doi.org/10.2166/hydro.2020.055

Libes, S., 2011. Introduction to Marine Biogeochemistry. Academic Press.

Luken, J.O., 2012. Relative Stability of Plant Communities in a South Carolina High Salt Marsh. Castanea 77, 327–334. https://doi.org/10.2179/12-007

Moffett, K., Robinson, D., Gorelick, S., 2010. Relationship of Salt Marsh Vegetation Zonation to Spatial Patterns in Soil Moisture, Salinity, and Topography. Ecosystems 13, 1287–1302. https://doi.org/10.1007/s10021-010-9385-7

Moffett, K.B., Gorelick, S.M., McLaren, R.G., Sudicky, E.A., 2012. Salt marsh ecohydrological zonation due to heterogeneous vegetation–groundwater–surface water interactions. Water Resources Research 48. https://doi.org/10.1029/2011WR010874

Moore, W.S., 1999. The subterranean estuary: a reaction zone of ground water and sea. Marine Chemistry 65. https://doi.org/10.1016/S0304-4203(99)00014-6

Nuttle, W.K., Harvey, J.W., 1995. Fluxes of water and solute in a coastal wetland sediment. l. The contribution of regional groundwater discharge. Journal of Hydrology 164, 89–107. https://doi.org/10.1016/0022-1694(94)02561-O

Osgood, D.T., 2000. Subsurface hydrology and nutrient export from barrier island marshes at different tidal ranges. Wetlands Ecology and Management 8, 133–146. https://doi.org/10.1023/A:1008488317880

Payne, D., 2010. Effects of Sea-Level Rise and Pumpage Elimination on Saltwater Intrusion in the Hilton Head Island Area, South Carolina, 2004—2104. United States Geological Survey Technical Report.

Pennings, S., Grant, M.-B., Bertness, M., 2004. Plant zonation in low-latitude salt marshes: Disentangling the roles of flooding, salinity and competition. Journal of Ecology 93, 159–167. https://doi.org/10.1111/j.1365-2745.2004.00959.x

Peters, C.N., Kimsal, C., Frederiks, R.S., Paldor, A., McQuiggan, R., Michael, H.A., 2022. Groundwater pumping causes salinization of coastal streams due to baseflow depletion: Analytical framework and application to Savannah River, GA. Journal of Hydrology 604, 127238. https://doi.org/10.1016/j.jhydrol.2021.127238

Riggs, S.R., Cleary, W.J., Snyder, S.W., 1995. Influence of inherited geologic framework on barrier shoreface morphology and dynamics. Marine Geology 126, 213–234. https://doi.org/10.1016/0025-3227(95)00079-E

Rocha, Carlos, Forster, S., Koning, E., Epping, E., 2005. High-resolution permeability determination and two-dimensional porewater flow in sandy sediment. Limnology and Oceanography: Methods 3, 10–23. https://doi.org/10.4319/lom.2005.3.10

Seidu, J., Ewusi, A., Kuma, J.S.Y., Ziggah, Y.Y., Voigt, H.-J., 2022. A hybrid groundwater level prediction model using signal decomposition and optimised extreme learning machine. Modeling Earth Systems Environment 8, 3607–3624. https://doi.org/10.1007/s40808-021-01319-w

Seyfferth, A.L., Bothfeld, F., Vargas, R., Stuckey, J.W., Wang, J., Kearns, K., Michael, H.A., Guimond, J., Yu, X., Sparks, D.L., 2020. Spatial and temporal

heterogeneity of geochemical controls on carbon cycling in a tidal salt marsh. Geochimica et Cosmochimica Acta 282, 1–18. https://doi.org/10.1016/j.gca.2020.05.013

Thibodeau, P.M., Gardner, L.R., Reeves, H.W., 1998. The role of groundwater flow in controlling the spatial distribution of soil salinity and rooted macrophytes in a southeastern salt marsh, USA. Mangroves and Salt Marshes 2, 1–13. https://doi.org/10.1023/A:1009910712539

Tobias, C.R., Harvey, J.W., Anderson, I.C., 2001. Quantifying groundwater discharge through fringing wetlands to estuaries: Seasonal variability, methods comparison, and implications for wetland-estuary exchange. Limnology and Oceanography 46, 604–615. https://doi.org/10.4319/lo.2001.46.3.0604

Valiela, I., Teal, J.M., Volkmann, S., Shafer, D., Carpenter, E.J., 1978. Nutrient and particulate fluxes in a salt marsh ecosystem: Tidal exchanges and inputs by precipitation and groundwater 1. Limnology and Oceanography 23, 798–812. https://doi.org/10.4319/lo.1978.23.4.0798

Wiater, J., 2012. Electric shock hazard limitation in water during lightning strike. Przeglad Elektrotechniczny 88.

Wilson, A., Moore, W., Joye, S., Anderson, J., Schutte, C., 2011. Storm-driven groundwater flow in a salt marsh. Water Resources Research - Water Resources Research 47. https://doi.org/10.1029/2010WR009496

Wilson, A.M., Evans, T., Moore, W., Schutte, C.A., Joye, S.B., Hughes, A.H., Anderson, J.L., 2015a. Groundwater controls ecological zonation of salt marsh macrophytes. Ecology 96, 840–849. https://doi.org/10.1890/13-2183.1

Wilson, A.M., Evans, T.B., Moore, W.S., Schutte, C.A., Joye, S.B., 2015b. What time scales are important for monitoring tidally influenced submarine groundwater discharge? Insights from a salt marsh. Water Resources Research 51, 4198–4207. https://doi.org/10.1002/2014WR015984

Wilson, A.M., Morris, J.T., 2012b. The influence of tidal forcing on groundwater flow and nutrient exchange in a salt marsh-dominated estuary. Biogeochemistry 108, 27–38. https://doi.org/10.1007/s10533-010-9570-y

Wu, Z., Huang, N.E., 2009. Ensemble empirical mode decomposition: a noise-assisted data analysis method. Advances in Adaptive Data Analysis. 01, 1–41. https://doi.org/10.1142/S1793536909000047

Xia, Y.Q., Li, H.L., 2012. A combined field and modeling study of groundwater flow in a tidal marsh. Hydrology and Earth System Sciences 16, 741–759. https://doi.org/10.5194/hess-16-741-2012

Xin, P., Wilson, A., Shen, C., Ge, Z., Moffett, K.B., Santos, I.R., Chen, X., Xu, X., Yau, Y.Y.Y., Moore, W., Li, L., Barry, D.A., 2022. Surface Water and Groundwater Interactions in Salt Marshes and Their Impact on Plant Ecology and Coastal Biogeochemistry. Reviews of Geophysics 60, e2021RG000740. https://doi.org/10.1029/2021RG000740